

**UNIVERSIDADE FEDERAL DE SANTA CATARINA
PROGRAMA DE PÓS-GRADUAÇÃO EM ENGENHARIA
DE AUTOMAÇÃO E SISTEMAS**

Tiago Jackson May Dezuo

**DESIGN OF SWITCHING STRATEGIES WITH
APPLICATIONS IN PHOTOVOLTAIC ENERGY
GENERATION**

Florianópolis

2014

Tiago Jackson May Dezuo

**DESIGN OF SWITCHING STRATEGIES WITH
APPLICATIONS IN PHOTOVOLTAIC ENERGY
GENERATION**

Thesis submitted to the *Universidade Federal de Santa Catarina* as part of the requirements for obtaining the degree of Doctor in Automation and Systems Engineering.

Advisor: Prof. Dr. Alexandre Trofino Neto

Florianópolis

2014

Ficha de identificação da obra elaborada pelo autor,
através do Programa de Geração Automática da Biblioteca Universitária da UFSC.

Dezuo, Tiago Jackson May

Design of switching strategies with applications in photovoltaic energy generation / Tiago Jackson May Dezuo ; orientador, Alexandre Trofino Neto - Florianópolis, SC, 2014.

199 p.

Tese (doutorado) - Universidade Federal de Santa Catarina, Centro Tecnológico. Programa de Pós-Graduação em Engenharia de Automação e Sistemas.

Inclui referências

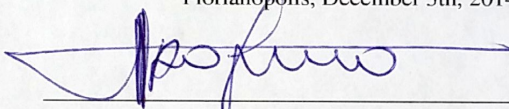
1. Engenharia de Automação e Sistemas. 2. Switching rule. 3. Photovoltaic generation. 4. LMI. 5. MPPT. I. Neto, Alexandre Trofino. II. Universidade Federal de Santa Catarina. Programa de Pós-Graduação em Engenharia de Automação e Sistemas. III. Título.

DESIGN OF SWITCHING STRATEGIES WITH APPLICATIONS IN PHOTOVOLTAIC ENERGY GENERATION

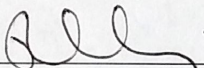
TIAGO JACKSON MAY DEZUO

This Thesis was deemed sufficient for obtaining the title of Doctor in Automation and Systems Engineering, Area of Concentration *Control, Automation and Systems*, and approved in its final form by the *Programa de Pós-Graduação em Engenharia de Automação e Sistemas* of the *Universidade Federal de Santa Catarina*.

Florianópolis, December 5th, 2014



Alexandre Trofino Neto, Dr.
Supervisor

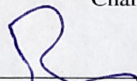


Rômulo Silva de Oliveira, Dr.
Coordinator of the *Programa de Pós-Graduação em Engenharia de Automação e Sistemas*

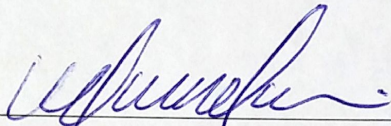
Examining Committee:



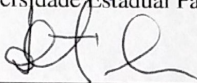
Alexandre Trofino Neto, Dr.
Chairman



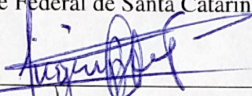
Pierre-Alexandre Jacques Bliman, Dr.
Fundação Getúlio Vargas (FGV)



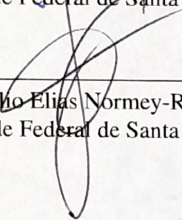
Marcelo Carvalho Minhoto Teixeira, Dr.
Universidade Estadual Paulista (UNESP)



Daniel Ferreira Coutinho, Dr.
Universidade Federal de Santa Catarina (UFSC)



Eugênio de Bona Castelan Neto, Dr.
Universidade Federal de Santa Catarina (UFSC)



Julio Elias Normey-Rico, Dr.
Universidade Federal de Santa Catarina (UFSC)

To my family.

ACKNOWLEDGMENTS

First and foremost, I would like to express my gratitude for my family, for the constant support, comprehension and tenderness. In special, my mother Deolinda and my sister Elisângela.

I am also grateful to Professor Alexandre Trofino for being an extraordinary advisor for both my M.Sc. and Ph.D. degrees who showed me the road and helped to get me started on the path to these degrees. His enthusiasm, encouragement and faith in me throughout the last six years have been extremely helpful, always giving generously of his time and vast knowledge. I am also thankful to Professor Luis Rodrigues for being my supervisor during my internship abroad. He always knew where to look for the answers to obstacles while leading me to the right source, theory and perspective.

I also would like to express my appreciation for the friends from all over the world I made during this journey, specially in Florianópolis and in Montreal. Not to mention that the life experience in these two places was overwhelming! Also my friends from before, who were always there for me and understood my times of absence. Special thanks to César Scharlau for the dedication in our team work, essencial for achieving the results of this thesis, to Miad Moarref and Azita Malek for the company in the lab at Concordia University, to Veronique Talbot for receiving me in Montreal and introducing me to the Canadian lifestyle and to all the people that somehow contributed to this achievement. You all represent a great part of this, thank you very much!

I must express my sincere thanks to the committee members, Dr. Pierre-Alexandre Jacques Blieman, Dr. Marcelo Carvalho Minhoto Teixeira, Dr. Daniel Ferreira Coutinho, Dr. Eugênio de Bona Castelan Neto and Dr. Julio Elias Normey-Rico, for their valuable comments and contributions to the consistency, accuracy and improvement of this document.

I also would like to thank CNPq (*Conselho Nacional de Desenvolvimento Científico e Tecnológico*) for funding this work in the form of a national doctoral scholarship, edict MCT/CNPq 70/2009, process number 558642/2010-1, and a doctoral internship abroad, edict RN029-2012 (SWE/CsF), process number 246392/2012-6.

*Somewhere, something incredible is waiting to
be known.*

Carl Sagan

ABSTRACT

Abstract of Thesis presented to UFSC as a partial fulfillment of the requirements for the degree of Doctor in Automation and Systems Engineering.

DESIGN OF SWITCHING STRATEGIES WITH APPLICATIONS IN PHOTOVOLTAIC ENERGY GENERATION

Tiago Jackson May Dezuo

December / 2014

Advisor: Alexandre Trofino Neto, Dr..

Area of Concentration: Control, Automation and Systems.

Number of pages: 199

This work presents control strategies and stability analysis for switched systems with a proposed application to photovoltaic energy generation systems. The conditions are based on Linear Matrix Inequalities (LMIs).

Initially, a general description of the photovoltaic systems is presented covering the following aspects: the modeling of a photovoltaic array, some common connection topologies, the main objectives, techniques for maximizing the generated power, among other informations. This content is necessary for the control design method proposed in this work.

Next, a design technique for the stabilization of affine switched systems is shown. The methodology used is based on the Lyapunov's theory for stability of systems, describing sufficient conditions for the proposed switching rule design in the form of LMIs and solving them using existing software packages. In the sequel, the switching strategy is extended for a class of nonlinear systems of great interest, especially for the control of photovoltaic systems. This class is composed of systems containing sector-bounded nonlinearities. Furthermore, a method for stability analysis of switched systems is proposed, extending the class of switched systems analyzed by the current literature. Numerical examples illustrate all the approaches developed.

At the end, the application of the nonlinear control techniques to photovoltaic generation systems is presented. The main objectives considered are the tracking of the maximum power generation, with robustness to variations of the input parameters of the photovoltaic array, and the delivery of only active power to the grid. Finally, simulation results demonstrate the applicability

of the methodology for the control of this type of system, evidencing the compliance of the stated objectives.

Keywords: Switching rule. LMI. Photovoltaic generation. MPPT.

RESUMO EXPANDIDO

Resumo expandido da Tese apresentada à UFSC como parte dos requisitos necessários para a obtenção do grau de Doutor em Engenharia de Automação e Sistemas.

PROJETO DE ESTRATÉGIAS DE CHAVEAMENTO COM APLICAÇÕES NA GERAÇÃO DE ENERGIA FOTOVOLTAICA

Tiago Jackson May Dezuo

Dezembro / 2014

Orientador: Alexandre Trofino Neto, Dr..

Área de Concentração: Controle, Automação e Sistemas.

Número de Páginas: 199

Durante a última década, a tecnologia de sistemas fotovoltaicos tem mostrado potencial para se tornar uma das principais fontes de energia para o mundo, com crescimento contínuo e robusto, mesmo em tempos de crise econômica e financeira. Visando ampliar o aproveitamento da energia gerada e até mesmo reduzir os custos do sistema, o projeto de técnicas de controle eficientes apresenta grande importância para este tipo de sistema. Em sistemas fotovoltaicos o controle é realizado através de conversores de potência, que são sistemas chaveados. Por este motivo, o foco principal deste trabalho é a apresentação de estratégias de controle e análise de estabilidade para sistemas chaveados com uma proposta de aplicação para sistemas de geração de energia fotovoltaica. As condições de projeto e análise são todas baseadas em desigualdades matriciais lineares (LMIs).

Inicialmente, uma descrição geral dos sistemas fotovoltaicos é apresentada, contendo a modelagem de um arranjo fotovoltaico, algumas topologias comuns de conexão, os principais objetivos, técnicas para a maximização da potência gerada, dentre outras informações necessárias para o projeto da técnica de controle proposta para este sistema.

Na sequência é mostrada uma técnica de projeto de estratégias de chaveamento, cujo objetivo principal é garantir estabilidade e desempenho de sistemas comutados. A metodologia usada é baseada na teoria de estabilidade de Lyapunov, de modo a descrever condições suficientes para o projeto

da lei de chaveamento em forma de LMIs e resolvê-las usando pacotes computacionais existentes. O método se aplica à classe de sistemas chaveados onde cada subsistema tem um campo vetorial afim e considera-se uma lei de chaveamento baseada no máximo entre funções auxiliares. A estabilidade do sistema em malha fechada é garantida mesmo se modos deslizantes ocorram em qualquer superfície de chaveamento resultante do projeto. Os resultados são apresentados para os casos de realimentação completa e realimentação parcial dos estados do sistema.

Em seguida, uma das principais contribuições da tese, a proposta de uma extensão da lei de chaveamento para uma classe de sistemas chaveados não lineares é apresentada. O sistema pode conter não linearidades dependentes do estado limitadas em setor, como é o caso da não linearidade existente no modelo de painéis fotovoltaicos. As funções não lineares podem conter também parâmetros incertos, contanto que a função permaneça dentro dos limites do setor dado para toda a faixa de valores de interesse do parâmetro. Além disso, condições de projeto de leis de chaveamento independentes do equilíbrio são fornecidas e, portanto, neste caso a técnica se torna robusta a mudanças no ponto de operação desejado. Por fim, considerações sobre limitar a frequência de chaveamento são discutidas.

A aplicação das técnicas descritas anteriormente para topologias comuns de conexão de sistemas fotovoltaicos é apresentada em seguida. Alguns dos desafios superados são a presença de referências variáveis, não linearidades limitadas em setor e medição parcial de estados no mesmo sistema. A aplicabilidade da metodologia para controlar o sistema fotovoltaico é ilustrada através de simulações baseadas em um exemplo numérico usando parâmetros de um sistema real. Como resultado requisitos importantes são satisfeitos, como o rastreamento do ponto de máxima potência e robustez com relação aos parâmetros incertos do painel fotovoltaico. Para a obtenção da robustez foram derivadas equações para determinar um setor que contém a não linearidade para quaisquer valores dos parâmetros. As dificuldades e perspectivas para o caso mais complexo (conexão com a rede elétrica) também são apresentadas.

Motivado pela falta de técnicas de análise de estabilidade de sistemas seccionalmente afins contendo modos deslizantes na literatura atual, condições LMI suficientes para resolver este problema são propostas, resultando em outra importante contribuição da tese. As condições são baseadas em uma

função de Lyapunov composta pela combinação convexa de funções quadráticas diferentes para cada região do sistema. As condições propostas incluem o importante caso onde o ponto de equilíbrio está localizado na fronteira entre subsistemas afim. Adicionalmente, condições suficientes para análise independentemente da parametrização das superfícies de chaveamento são derivadas, isto é, a superfície de chaveamento pode ser desconhecida neste caso. A nova técnica leva a uma metodologia unificada para a análise de estabilidade de sistemas seccionalmente afins e de sistemas chaveados afins com uma superfície de chaveamento previamente projetada.

Esta tese é organizada em sete capítulos, quatro apêndices e referências. O Capítulo 1 tem o objetivo de contextualizar e motivar de forma breve o assunto da tese. O conhecimento básico sobre sistemas fotovoltaicos necessário para a aplicação proposta no documento é concentrado no Capítulo 2. O Capítulo 3 apresenta uma técnica de projeto de uma lei de chaveamento para o controle de sistemas chaveados com campos vetoriais afim. Esta técnica serve de base para as principais contribuições teóricas desta tese, apresentadas nos Capítulos 4, 5 e 6. No Capítulo 4, é apresentado o projeto de leis de chaveamento para sistemas chaveados contendo não linearidades limitadas em um setor, enquanto o Capítulo 5 apresenta a aplicação desta técnica para o controle de sistemas fotovoltaicos. No Capítulo 6, um método para análise de estabilidade de sistemas seccionalmente afins é introduzida. Exemplos numéricos são utilizados para ilustrar todas as contribuições da tese em seus respectivos capítulos. Algumas conclusões são discutidas no Capítulo 7, incluindo uma lista de sugestões para trabalhos futuros. Por fim, três apêndices demonstram o equacionamento de ferramentas de circuitos elétricos trifásicos utilizadas na tese e um apêndice apresenta resumos das publicações geradas pelo autor durante o período de doutorado.

Palavras-chave: Estratégia de chaveamento. LMI. Geração fotovoltaica. MPPT.

CONTENTS

1	GENERAL INTRODUCTION	37
1.1	Presentation	37
1.2	Objectives	41
1.3	Description of chapters	42
2	PHOTOVOLTAIC GENERATION SYSTEMS	45
2.1	Introduction	45
2.2	PV system	45
2.2.1	<i>I-V</i> characteristic	49
2.2.2	Architectures of photovoltaic systems	49
2.2.2.1	Local topology without converters	51
2.2.2.2	Local topology with a DC/DC converter	53
2.2.2.3	Grid-connected topology without a DC/DC converter	55
2.2.2.4	Grid-connected topology with a DC/DC converter	56
2.2.3	MPPT techniques	56
2.2.3.1	Voltage P&O algorithm	57
2.2.3.2	Current P&O algorithm	59
2.2.4	Grid model	59
2.2.5	Coordinate transformations and reference frames	61
2.2.5.1	Coordinate transformation from three-phase to two-phase	61
2.2.5.2	Reference frame transformation from stationary to synchronous	62
2.2.6	Grid synchronization	63
2.3	Switched systems	64
2.3.1	Classification according to the type of commutation	66
2.3.2	Sliding modes	67
2.3.3	Control structure	68
2.4	Additional mathematical background	70
2.5	Concluding remarks	72
3	CONTROL OF AFFINE SWITCHED SYSTEMS	75
3.1	Introduction	75
3.2	Preliminaries	75

3.3	Related methods	78
3.4	Switching rule design	79
3.4.1	Partial state measurement	86
3.5	Numerical examples	87
3.6	Concluding remarks	92
4	CONTROL OF SWITCHED SYSTEMS WITH SECTOR-BOUNDED NONLINEARITIES	95
4.1	Introduction	95
4.2	Preliminaries	96
4.2.1	Switching rule using a max composition	98
4.2.2	Sector-bounded nonlinearity	98
4.3	Switching rule design	99
4.3.1	Partial state measurement	106
4.3.2	LMIs independent of the equilibrium point	107
4.4	Limited switching frequency	108
4.5	Numerical examples	113
4.6	Concluding remarks	119
5	CONTROL OF PHOTOVOLTAIC SYSTEMS	123
5.1	Introduction	123
5.2	Stand-alone PV system	123
5.2.1	Mathematical model of the PV-Boost system	123
5.2.2	References generation for MPPT	125
5.2.3	Robust sector bounds for PV systems	126
5.2.4	Switching rule design for the PV-Boost system	128
5.2.5	Results and simulations	129
5.3	Grid-connected PV system	132
5.4	Stage 2: inverter-grid	133
5.4.1	Model	134
5.4.2	References generation	139
5.4.3	Perspectives for the switching rule design for the stage 2	141
5.4.4	Analysis of the complete system	142
5.5	Concluding remarks	143
6	STABILITY ANALYSIS OF PIECEWISE AFFINE SYSTEMS WITH SLIDING MODES	147
6.1	Introduction	147
6.2	Preliminaries	148

6.3	Main results	149
6.4	Numerical examples	157
6.5	Concluding remarks	163
7	CONCLUSIONS AND PROSPECTS	165
7.1	General concluding remarks	165
7.2	Prospects	167
7.3	Activities abroad	167
7.4	Publications related to the work	168
	Appendix A – Input/output voltages relation in a three-phase inverter . . .	187
	Appendix B – Clarke’s transformation	189
	Appendix C – Park’s transformation	193
	Appendix D – Abstracts of published papers	195

LIST OF FIGURES

1	Evolution of global cumulative installed capacity 2000-2013. Source: EPIA (EUROPEAN PHOTOVOLTAIC INDUSTRY ASSOCIATION (EPIA), 2014b).	39
2	Equivalent circuit of a photovoltaic cell.	46
3	Illustrative diagram of a photovoltaic array.	48
4	Equivalent circuit of a photovoltaic array.	49
5	(a) I - V characteristic curve. (b) P - V curve. In both cases, the data of the Table 1 was used with only 1 photovoltaic module.	50
6	(a) I - V curves for several levels of solar radiation G ($T = T_r = 25^\circ\text{C}$). (b) I - V curves for different temperatures T ($G = G_r = 1000 \text{ W/m}^2$). The MPP of each curve is indicated by the symbol \bullet	52
7	Local topology without converters.	53
8	I - V characteristic curve (blue) and load line (red). The data of the Table 1 was used with only 1 photovoltaic module and the load considered was $R = 2\Omega$. The operating point is denoted by the symbol \bullet	54
9	Local topology with a DC/DC converter.	54
10	Grid-connected topology with a DC/AC converter only.	55
11	Grid-connected topology with both DC/DC and DC/AC converters.	56
12	Flowchart of the P&O algorithm for voltage control.	58
13	Flowchart of the P&O algorithm for current control.	60
14	Vector synchronizer based on the utility grid voltage.	64
15	Example of trajectories of a bimodal switched system: (a) crossing the switching surface; (b) resulting in sliding mode. Source: (SCHARLAU, 2013).	68
16	Basic control scheme for switched system with a state-dependent switching rule.	69
17	Control scheme for a state-dependent switching rule with an interface to PWM controlled devices.	70
18	Buck-Boost converter used in the Example 3.1.	88
19	Buck-Boost converter operating as a Buck with $V_{out} = -9\text{V}$	89
20	Buck-Boost converter operating as a Boost with $V_{out} = -21\text{V}$	90
21	Buck-Boost converter operating as a Buck (left side curves) and as a Boost (right side curves) with a switching rule designed with an adequate choice of the parameters α_i	91

22	Stable subsystems ($\beta = 1$). Solid (black) curves are the error trajectories; dashed curves (in assorted colors) are switching surfaces.	92
23	Unstable subsystems ($\beta = -1$). Solid (black) curve is a error trajectory; dashed curves (in assorted colors) are switching surfaces.	93
24	Example of sector bounds (red lines) for a particular nonlinear function (blue curve).	99
25	Illustration of the piecewise-constant approximation \bar{x} for a variable reference $\bar{x}(t)$. The ideal $\bar{x}(t)$ is represented in black color and the approximate \bar{x} in red.	109
26	Voltage and current dynamics on a switch during switching transient.	111
27	A generic DC/AC converter leg with dead time introduced in the switching rule.	111
28	Deviation in the desired average value for a switching surface $x(t) = \bar{x}$. (a) Ideal sliding mode (no deviation); (b) dwell time with positive deviation; (c) dwell time with negative deviation.	112
29	Sector bounds (red dashed lines) for the nonlinear saturation function (4.63) (blue lines).	115
30	State trajectories for the given initial condition $x(0)$	116
31	(a) Auxiliary functions $v_i(e(t))$, $i \in \mathbb{I}_m$. (b) Active mode $\sigma(e(t))$	117
32	State trajectories for the given initial condition $x(0)$ with dwell time $\tau_s^{min} = 0.1s$	118
33	State trajectories for null initial conditions.	120
34	Sector bounds (red lines) for the nonlinear function (4.77) (blue curve).	121
35	Topology of the DC/DC converter stage.	124
36	Example of I - V characteristic curve (blue curve) and sector bounds (red lines).	127
37	(a) $P_{pv} = V_{pv}i_{pv}$ (black curve) and the MPP for each values of T and G (red lines). (b) i_{pv} (black curve) and its reference \bar{i}_{pv} (green lines). (c) V_{pv}	131
38	Topology considered for connection of the PV system with the grid.	132
39	Three-phase inverter feeding a three-phase load (grid) through an L filter.	135

40	Complete control structure. The highlighted blocks are: the measured variables (in yellow), reference generation blocks (in green) and blocks for calculation of the Lyapunov functions (in gray).	142
41	Some state trajectories for the system in Example 6.1 (solid black curves) and the switching surface (red dotted line). . .	158
42	Some state trajectories for the system in Example 6.2 with $\delta = 2$ (black solid curves), the switching surface (red dotted line) and trajectories that touch the surface only at the origin (blue dot-dashed curve).	159
43	Some state trajectories for the system in Example 6.3 for $\delta = 1$ (black solid curves) and the switching surface (red dotted line).	161
44	Structure of the Buck converter.	162
45	Three-phase inverter with output connected in a star configuration.	187
46	Transformation from abc to $\alpha\beta$	189
47	Transformation from $\alpha\beta$ to abc	191
48	Transformation from $\alpha\beta$ to dq	193
49	Transformation from dq to $\alpha\beta$	193

LIST OF TABLES

1	Data of the KC200GT photovoltaic module.	51
2	Data of the Buck-Boost converter used in the Example 3.1.	88
3	Power properties and switching speed of the controlled switches: MOSFET, IGBT e GTO.	110
4	Signal u_0 send to the switch s_0 of the Boost converter, where $u_0 = 1$ puts the switch in the “closed” state (conducting) and $u_0 = 0$ in the “open” state (not conducting).	124
5	Data of the PV system with a local load from Figure 35.	129
6	Signals u_1, u_2, u_3 send to the switches s_1, s_2, s_3 of the inverter, where $u_j = 1$ puts the switch s_j in the “closed” state (conducting) and $u_j = 0$ in the “open” state (not conducting). The commands for s_4, s_5, s_6 are the binary complements $\bar{u}_1, \bar{u}_2, \bar{u}_3$, respectively.	134
7	Magnitudes of the elements $U_{\alpha i}$ and $U_{\beta i}$ and of the module of the vector $U_{\alpha\beta}$ for each operation mode.	136
8	Parameters os the Buck converter from Figure 44.	162

LIST OF ABBREVIATIONS AND ACRONYMS

PV	Photovoltaic
ISS	International Space Station
ROW	Rest of the World
MEA	Middle East and Africa
APAC	Asia Pacific
MPP	Maximum Power Point
MPPT	Maximum Power Point Tracking
PWM	Pulse-Width Modulation
PWA	Piecewise Affine
PWQ	Piecewise Quadratic
PWL	Piecewise Linear
LMI	Linear Matrix Inequality
STC	Standard Test Conditions
DC	Direct Current
AC	Alternating Current
PF	Power Factor
THD	Total Harmonic Distortion
VSI	Voltage Source Inverter
CV	Constant Voltage
P&O	Perturb & Observe
LPF	Low-Pass Filter
NP-hard	Non-deterministic Polynomial-time hard
ZOH	Zero-Order Holder
MOSFET	Metal Oxide Semiconductor Field Effect Transistor
IGBT	Insulated Gate Bipolar Transistor
GTO	Gate Turn-Off
OCC	Opposed Current Converter
RMS	Root Mean Square

LIST OF SYMBOLS AND NOTATION

abc	Three-phase coordinates
$\alpha\beta$	Two-phase coordinates in the stationary reference frame
dq	Two-phase coordinates in the synchronous reference frame
f_{abc}	Quantity vector f in three-phase coordinates abc
$f_{\alpha\beta}$	Quantity vector f in two-phase coordinates $\alpha\beta$
f_{dq}	Quantity vector f in two-phase coordinates dq
f^{peak}	Peak value of the sinusoidal variable f
f^{rms}	RMS value of the sinusoidal variable f
\bar{f}	Constant equilibrium value of the variable f in steady state
\dot{f}	Derivative of f with respect to the time
∇f	Gradient of f
\mathbb{R}^n	Euclidean space with dimension n
$\mathbb{R}^{n \times m}$	Set of real matrices of dimension $n \times m$
\mathbb{I}_q	Denotes the set of integers $\{1, \dots, q\}$
\emptyset	Denotes an empty set
$\mathcal{P}(\mathbb{I}_m)$	Denotes the powerset of the set \mathbb{I}_m
$\overline{\mathcal{R}}$	Denotes the closure of a set \mathcal{R}
$\mathcal{U} \subset \mathcal{V}$	The set \mathcal{U} is a subset of the set \mathcal{V}
\cup	Operator for union of sets
\cap	Operator for intersection of sets
$\mathfrak{V}(\Theta)$	Set of all vertices of the polytope (or simplex) Θ
$\mathbf{Co}(f_i)$	Convex hull of the set f_i
M'	Transposed of the real matrix (or vector) M
M^{-1}	Inverse of the real matrix M
$M^\#$	Pseudo-inverse of the real matrix M (Moore-Penrose)
$M > 0$	Real matrix M is symmetric and positive-definite
$M < 0$	Real matrix M is symmetric and negative-definite
$\lambda_{min}(M)$	Minimum eigenvalue of a symmetric matrix M
$row_i(M)$	Represents the i -th row of a matrix M
\succ	Strict element-wise inequality
\preceq	Non-strict element-wise inequality
\star	Block matrix terms that can be deduced from symmetry
I_n	Identity matrix of dimension $n \times n$
0_n	Square matrix of zeros of dimension $n \times n$

$0_{n \times m}$	Matrix of zeros of dimension $n \times m$
$\ \cdot \ $	Euclidean norm of vectors and induced spectral norm of matrices
\otimes	Kronecker product
$\exp(\cdot)$	Exponential function of (\cdot)
σ	Index set defining the active subsystems
v_i	Auxiliary function for the i -th operation mode of the switched system
$V(e(t))$	Lyapunov function for the switched system
$\arg \max \{v_1, \dots, v_m\}$	Denotes the index $i \in \{1, \dots, m\}$ associated to the maximum element of the set $\{v_1, \dots, v_m\}$, where $v_i \in \mathbb{R}$
\mathcal{D}_h	Operator for the Dini's directional derivative in the direction h
i_{ph}	Photocurrent
i_r	Reverse saturation current of a photovoltaic cell
R_s	Series resistance of a photovoltaic cell
R_p	Parallel (shunt) resistance of a photovoltaic cell
ε	Electron charge (1.6×10^{-19} C)
η	Quality factor of the p-n junction
κ	Boltzmann constant (1.38×10^{-23} J/K)
T_r	Temperature of reference in Standard Test Conditions (298K)
G_r	Radiation intensity of reference in Standard Test Conditions (1000 W/m^2)
i_{sc}	Short circuit current
V_{oc}	Open circuit voltage
γ	Temperature coefficient of i_{sc}
i_{rr}	Reverse saturation current of reference
E_g	Energy band gap of silicon (1.1 eV)
T	Temperature of the photovoltaic cell
G	Intensity of solar radiation
M_s	Number of modules in series
M_p	Number of modules in parallel
N_s	Number of cells in series in each module
V_{pv}	Voltage at the output terminals of the PV array
i_{pv}	Current at the output terminals of the PV array
P_{pv}	Power generated by the PV array
V_{pv}^{ref}	Reference for V_{pv} originating from MPPT
ΔV_{pv}^{ref}	Variation applied to reference V_{pv} for MPPT

i_{pv}^{ref}	Reference for i_{pv} originating from MPPT
Δi_{pv}^{ref}	Variation applied to reference i_{pv} for MPPT
d	Duty cycle
Δd	Variation applied to the duty cycle for MPPT
V_g	Grid voltage
i_g	Current entering the grid
P_g	Power delivered to the grid
ω	Grid frequency
V_{dc}	Voltage of the DC link
u_j	Command for the switch s_j
\bar{u}_j	Binary complement of the command u_j

1 GENERAL INTRODUCTION

1.1 Presentation

Switched systems is a designation for an extensive class of control applications (MORSE, 1997). In general terms, this class of applications comprises all the dynamical systems that undergo structural changes over time due to the presence of distinct stages of operation or the presence of restrictions in certain system variables for safety or physical limits of the device. Systems containing devices that act as “logical switches” that are controlled by a switching logic by connecting or disconnecting elements of the system (*e.g.* relays and thyristors) are typical examples of switched systems. Switched systems can be seen as a particular class of hybrid systems (LIBERZON, 2003) or variable structure systems (DECARLO; ZAK; MATTHEWS, 1988). For each position of the switches (on or off) the mode of operation of the system is different, with different properties and structure. The switches are controlled by a switching logic whose role is to define when each switch must be turned on or off, thus defining the mode of operation of the system. The design of this switching ‘rule’ is a crucial step for the correct operation of the controlled system. This task, however, is not trivial and several studies have been conducted focusing on the development of design techniques that provide minimum guarantees of performance and robustness. The following references provide a good overview of the problem: (LIBERZON; MORSE, 1999), (LIBERZON, 2003), (DECARLO et al., 2000), (BOLZERN; SPINELLI, 2004), (LIN; ANTSAKLIS, 2005), (EL-FARRA; MHASKAR; CHRISTOFIDES, 2005), (SUN; GE; LEE, 2002), (SUN, 2006), (COLANERI; GEROMEL; ASTOLFI, 2005), (XU; ZHAI; HE, 2008).

Numerous applications can be classified as switched systems. As examples we can highlight the urban traffic control (PAPAGEORGIOU et al., 2003), chemical processes (MHASKAR; EL-FARRA; CHRISTOFIDES, 2005) and the power electronic circuits containing electronic switches, such as converters and inverters (SHIEH; SHYU, 1999), (SIRA-RAMÍREZ, 2003). The converters are widely used in various applications, including automotive, shipbuilding, aerospace and computer industries, for DC/DC converters, as well as the triggering of induction machines (motors and generators), for DC/AC converters. One area of significant use of converters and inverters is in power generation through renewable sources such as photovoltaic energy, for instance. Obtaining electricity from solar energy has been a major research topic in the last decades, due to its high reliability and decreasing cost, in addition to being an abundant and clean source of energy (BUSQUETS-MONGE et al., 2008), (HUANG

et al., 2006). Among the renewable energy sources, the photovoltaic generation has a great advantage with regard to maintenance. This is due to the fact that this system is purely electrical, not containing moving mechanical parts, unlike wind turbines or solar thermal generation.

Over the past decade, the technology of Photovoltaic (PV) systems has shown potential to become one of the main energy sources for the world (BLAABJERG et al., 2011), with continuous and robust growth, even during times of economic and financial crisis. It is expected that this growth will continue in the coming years as the global awareness about the advantages of the PV systems increases. At the end of the year 2010, the global cumulative installed capacity for photovoltaic generation was near to 40GW and one year later, it was 70GW. In 2012, around 100GW were already installed globally, which could produce 110TWh of electricity per year (EUROPEAN PHOTOVOLTAIC INDUSTRY ASSOCIATION (EPIA), 2013). This amount of energy is enough to cover the annual power demands of more than 30 million households. The exponential growth in installed capacity can be observed¹ in Figure 1 and a forecast for the next years is presented in (EUROPEAN PHOTOVOLTAIC INDUSTRY ASSOCIATION (EPIA), 2013).

Brazil has a great potential for photovoltaic generation, exhibiting a high daily average rate of solar radiation, which ranges between 14 and 20MJ/m² (ANEEL, 2005)², depending on the region. However, the country is not among the leading producers of solar energy, since only recently incentives by the government agencies have grown for implantation and technological development in the area of renewable energies. To get an idea, the installed capacity in the entire American continent in 2013 was around 13.5GW (EUROPEAN PHOTOVOLTAIC INDUSTRY ASSOCIATION (EPIA), 2014a), which is less than 10% of the worldwide total.

Although around 75% of the photovoltaic systems installed on the planet are connected to the electrical distribution grid (YUAN; ZHANG, 2006), solar generation is also an excellent option for stand-alone systems, such as electric vehicles, satellites and space stations, among others. In fact, one can realize that this form of generation has vital importance for space systems, after all, this is the only viable and safe option. There are unmanned satellites that use generation of energy from radioactive materials, but in manned space stations, the containment of these materials and the crew in a small space becomes risky, as in the case of the International Space Station (ISS),

¹ Acronyms used in Figure 1: Rest of the World (ROW); Middle East and Africa (MEA); Asia Pacific (APAC).

² Recall that 3.6MJ/m² are equivalent to 1kWh/m².

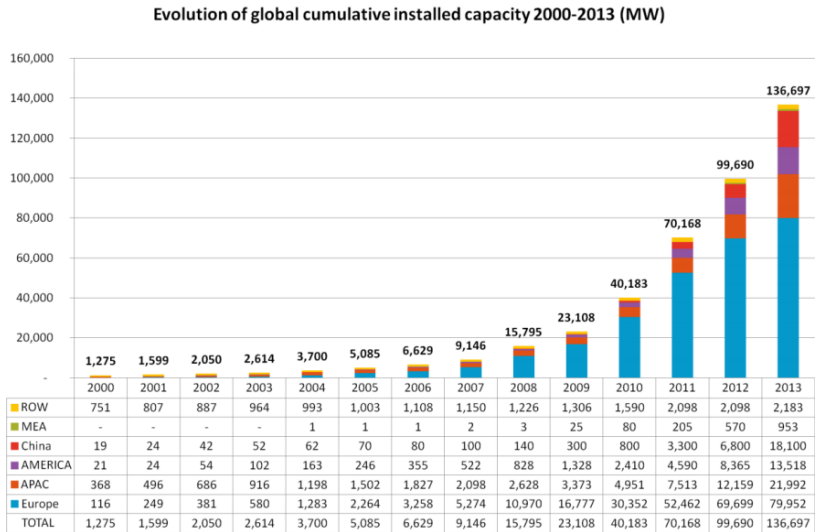


Figure 1: Evolution of global cumulative installed capacity 2000-2013. Source: EPIA (EUROPEAN PHOTOVOLTAIC INDUSTRY ASSOCIATION (EPIA), 2014b).

(LUQUE; HEGEDUS, 2003, p.782). In space systems, it is common that the best use of solar energy received is performed by tracking the position of the sun and then reorienting the solar panels. Examples of control of solar generation for small satellites can be found in (PETER; AGARWAL, 2010), (CHEN; CHEN, 2010).

Due mainly to the large number of PV systems connected to the grid, to determine the Maximum Power Point (MPP) possible to be generated by the PV array is usually an essential goal for this type of system. As such, many methods for Maximum Power Point Tracking (MPPT) have been developed and implemented. These MPPT techniques vary in complexity, required sensors, convergence speed, cost, range of effectiveness, hardware implementation, popularity, and other aspects (ESRAM; CHAPMAN, 2007). Such methods, as well as the overall control of the system, are performed using power electronic converters.

The converters are a key technology for PV systems (BLAABJERG et al., 2011), hence the development of this area relies on research to improve both the structure of the converters and the control techniques applied to them, in-

creasing their efficiency and reducing the system costs. The reference (GOETZBERGER; HOFFMANN, 2005) presents the costs of the system in a general manner and some other reasons for price reductions over time. Usually, the control techniques for switched systems do not act directly in controlling the position of the switches of the converters, the techniques only generate a desired reference waveform (or average value) to an element that performs Pulse Width Modulation (PWM), as in (YAN; UTKIN; XU, 2007) for instance. Another type of control of switched systems is the one that directly determines the position of the switches through a specific switching rule. Some existing switching rule design techniques are based on the Lyapunov stability theory (LIBERZON, 2003), as in (BOLZERN; SPINELLI, 2004) and (TROFINO et al., 2011), for instance.

A difficulty for designing switching rules is the occurrence of sliding modes (UTKIN, 1992), which may destabilize the system if not properly treated, but it is necessary for maintaining the stability of several important applications, as the power converters, for instance. The existence of sliding modes is a challenge even for the stability analysis of Piecewise Affine (PWA) systems, such as the switched affine systems with a given state-dependent switching rule. The problem of stability analysis for hybrid and switched affine systems has received considerable attention over the past two decades. Several approaches to construct Lyapunov functions and provide sufficient conditions for stability are now available in the literature, see for instance the surveys (DECARLO et al., 2000), (LIBERZON, 2003). Considering the case of switched affine systems, the use of Piecewise Quadratic (PWQ) Lyapunov functions is an interesting approach to reduce conservativeness compared to a quadratic Lyapunov function. However, it is a common misunderstanding in the literature to believe that if there is a continuous PWQ function that is positive definite and decreasing with time along each vector field of a PWA system then the system is stable, see (SAMADI; RODRIGUES, 2011) for details. Even Piecewise Linear (PWL) systems composed exclusively by stable subsystems can become unstable in the presence of a sliding mode (SAMADI; RODRIGUES, 2011), (JOHANSSON, 2003).

The methodologies proposed in this thesis consider the control and stability analysis based on Lyapunov functions and the switching rules design are expressed in the form of a Linear Matrix Inequality (LMI). Due to the flexibility in treating problems of mixed nature and the availability of powerful software packages for solving LMI problems, they have been widely used to solve problems of robust control and filtering. In the context of linear uncertain systems, several important results are available in (BOYD et al., 1994).

However, much work remains to be done in order to extend these results to switched and nonlinear systems, in special to renewable energy generation systems.

1.2 Objectives

Within the presented context, the main objective of this work is the development of new control techniques and stability analysis methods for switched systems complying with the following requirements:

- the designed control system must present minimum requirements for robustness with respect to parameter variation (in particular solar energy received and temperature of the solar panel);
- the design technique developed must be flexible for extension to other classes of systems with nonlinear functions of the states and uncertain parameters or with saturation and hysteresis and for the inclusion of minimum guarantees of performance (such as guaranteed cost or attenuation of the input-output gain, H_∞);
- the technique developed must be able to lead to switching strategies with guaranteed tracking of constant or sinusoidal references, either in the situation where all states are available from measurement or in the most critical (and more realistic) situation where only part of the states is available;
- the technique developed must have potential for applications in photovoltaic power generation with the maximization of the generated power;
- the design technique developed should use LMIs as it provides flexibility in the treatment of mixed problems, advantages due to convexity properties and the possibility of having powerful software packages for numerical solution;
- the stability analysis technique should be used to check stability of switched systems even with the occurrence of sliding modes.

In this thesis, the results related to switched systems obtained during the Ph.D. program and some prospects for further research will be presented.

Most of the switched systems to be considered are the ones present in photovoltaic generation systems, such as the power converters, although the techniques are general enough to be applied to any type of switched system. The theoretical results are verified through simulations using models and parameters that reproduce the actual application conditions. General characteristics of the proposed method and connections with other related methods are presented in Section 3.3.

This work is a continuation of earlier research conducted by the author of this thesis, the thesis supervisor and other collaborators, regarding the application of robust control techniques for switched systems. In addition to the presentation of the new results about the control of switched systems, this thesis also contains the application of the results to photovoltaic generation systems. In the sequel, a brief history of some of the previous work of the team is described.

The reference (COUTINHO, 2006) describes preliminary attempts to design a switched control system for induction motors via LMIs, while (DEZUO, 2010) presents a new technique including conditions for stability in the presence of sliding modes for the induction motor. However, in both cases it was not possible to obtain numerical solutions that would enable a conclusion regarding the application of the methods at the time. The reference (ASSMANN, 2008) presents a study on switching strategies for variable structure systems. Results for the control of a step down voltage converter (*Buck*) considering full state feedback of states and also output feedback were obtained. In (SCHARLAU, 2013), conditions that guarantee stability of the system even under sliding mode dynamics are proposed. This reference shows good results achieved by the team regarding the control of induction motors and wind generation systems.

1.3 Description of chapters

This thesis is organized in the following chapters:

- Chapter 2: describes the photovoltaic systems in a general manner, presenting the modeling of a photovoltaic array, usual connection topologies, objectives for the system, techniques for maximizing the power generation, among other information of which prior knowledge is essential for the design of control techniques for this type of system.
- Chapter 3: here a method is proposed to design switching rules that drive the state of switched dynamical systems to a desired equilibrium

point. The method applies to the class of switched systems where each subsystem has an affine vector field. The proposed method considers a switching rule using the ‘max’ composition of auxiliary functions. The results are given in terms of LMIs and ensure global asymptotic stability of the reference tracking error dynamics even if sliding modes occur in any switching surface of the system. The switching rules are based on full and partial state measurement. The motivation for using the proposed method, advantages, limitations and connections with related methods are presented and, at the end, two examples are used to illustrate the approach.

- Chapter 4: proposes an extension of the switching rule design technique from the previous chapter for a class of nonlinear switched systems. The system may contain state-dependent sector-bounded nonlinear functions. These functions may also contain uncertain parameters as long as the function stays inside the given sector bounds for the range of parameter values of interest. Moreover, a method for designing the switching rule that is independent of the equilibrium is also provided and, therefore, the technique becomes robust to changes in the desired operation point. Finally, some considerations about limiting the switching frequency are discussed. Two examples are used to demonstrate the results.
- Chapter 5: contains the application of the techniques described in the previous chapters to two of the most common connexion topologies of a photovoltaic system. Some of the overcome challenges are the presence of variable references and sector-bounded nonlinearities in the same setup. The applicability of the methodology to control the PV system is illustrated through simulation results based on a numerical example using real system parameters. As a result, important requirements are achieved, such as the MPPT and robustness with respect to the uncertain parameters of the PV array. The issues and perspectives for the more complex case (connection to the utility grid) are presented next.
- Chapter 6: offers new sufficient conditions for stability analysis of PWA systems. The conditions are based on a convex combination of PWQ Lyapunov functions and are given in terms of LMIs. The method verifies exponential stability of the state dynamics even in the presence of non-destabilizing sliding modes. The conditions can handle

the important case where the equilibrium point is located at a boundary between affine subsystems. Additionally, sufficient conditions for stability independently of the parameterization of the switching surfaces are derived, that is, the switching surface may be unknown in this case. The new method presented in this chapter leads to a unified methodology for stability analysis of PWA systems and switched affine systems with a previously designed switching surface. Four examples are used to illustrate the approach.

- Chapter 7: presents the main conclusions and some prospectives for continuation of the work.

2 PHOTOVOLTAIC GENERATION SYSTEMS

2.1 Introduction

The photovoltaic cell is a device that converts solar energy into electric energy through the photovoltaic effect. Solar cells are widely used in terrestrial and space applications. In general, it is desired that the cells operate at their maximum power point, which varies according to the panel temperature, level of incoming radiation and other effects caused by aging of the panel (DURGADEVI; ARUSELVI; NATARAJAN, 2011).

The mathematical model of a PV array is based on theoretical equations that describe the operation of photovoltaic cells, which can be obtained by using an equivalent circuit of the cells. The control of a PV system and the treatment of the power generated are achieved through voltage converters arranged in one of several different topologies, isolated or grid-connected, and some of these topologies can be seen in (KJAER; PEDERSEN; BLAAJBERG, 2002).

This chapter is focused on the presentation of a basic theoretical background, exploring mainly the following aspects: mathematical model of the array and its current-voltage characteristic, connection topologies of the converters, MPPT methods and other auxiliary tools necessary for the controller design. Moreover, some preliminary concepts related to switched systems will be presented. The objective is to contextualize the reader regarding the properties, characteristics and tools used in the analysis of switched systems through a brief review of the main studies published on the subject. Initially, the characteristics and properties that distinguish the class of switched systems will be addressed, followed by the different types of switching. Also, the structure of a switching rule based control system will be addressed.

2.2 PV system

The simplest (idealistic) model of a photovoltaic cell consists of a circuit containing a current source in parallel with a diode (BLAABJERG et al., 2011), (KJAER; PEDERSEN; BLAAJBERG, 2005). In a more precise model, non-idealities represented through resistors in series and in parallel are considered, as shown in Figure 2.

Deriving the equation for the circuit of Figure 2, considering the non-

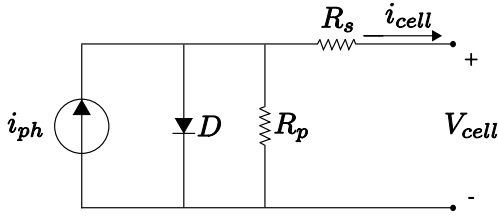


Figure 2: Equivalent circuit of a photovoltaic cell.

ideal diode model, leads to (VILLALVA; GAZOLI; FILHO, 2009)

$$i_{cell} = i_{ph} - i_r \left(\exp \left(\frac{\varepsilon}{\eta \kappa T} (V_{cell} + i_{cell} R_s) \right) - 1 \right), \quad (2.1)$$

where

$$i_{ph} = (i_{sc} + \gamma(T - T_r)) \frac{G}{G_r}, \quad (2.2)$$

$$i_r = i_{rr} \left(\frac{T}{T_r} \right)^3 \exp \left(\frac{\varepsilon E_g}{\eta \kappa} \left(\frac{1}{T_r} - \frac{1}{T} \right) \right), \quad (2.3)$$

$$i_{rr} = \frac{i_{sc} - \frac{V_{oc}}{R_p}}{\exp \left(\frac{\varepsilon V_{oc}}{\eta \kappa T_r} \right) - 1}. \quad (2.4)$$

The symbols on the Equations (2.1)-(2.4) represent the quantities defined below.

Variables:

- V_{cell} - voltage at the output terminals of a cell;
- i_{cell} - current at the output terminals of a cell;
- i_{ph} - photocurrent;
- i_r - reverse saturation current of the cell;

Constants (provided in a datasheet or determinable):

- R_s - series resistance of the cell;
- R_p - parallel resistance of the cell;

- ε - electron charge (1.6×10^{-19} C);
- η - quality factor of the p-n junction;
- κ - Boltzmann constant (1.38×10^{-23} J/K);
- T_r - temperature of reference (298K, *i.e.* 25°C);
- G_r - radiation intensity of reference (1000 W/m²);
- i_{sc} - short circuit current per module;
- V_{oc} - open circuit voltage per module;
- γ - temperature coefficient of i_{sc} ;
- i_{rr} - reverse saturation current of reference;
- E_g - energy band gap of silicon (1.1 eV);

Input parameters:

- T - temperature of the cell, in Kelvin;
- G - intensity of the solar radiation received, in W/m².

Note in Equation (2.1) that the variable i_{cell} cannot be isolated to have its value determined algebraically, but it is possible to apply the Newton's method to determine the value of i_{cell} in only a few iterations for a given voltage V_{cell} and input parameters T and G . Therefore, it is possible to determine the characteristic I - V of the cell by using Equation (2.1). For the simulations presented in this thesis, the algorithm for determining the value of i_{cell} uses the Newton's method in the same way presented in (CASARO, 2009), whose operation is shown to be suitable and fast.

A full PV *array*, or panel, consists of a given configuration of photo-voltaic *modules* in series (M_s - number of modules in series) and in parallel (M_p - number of modules in parallel), where each commercial module consists of a number N_s of *cells* in series.

Consider V_{pv} and i_{pv} as, respectively, the output voltage and the output current of the entire PV array. To compute i_{pv} based on the values of V_{pv} , T and G , similar to the way it was previously done for i_{cell} , simply replace

$$V_{cell} = \frac{V_{pv}}{N_s M_s}, \quad (2.5)$$

in the Equation (2.1) and i_{pv} is then given by

$$i_{pv} = M_p i_{cell}, \quad (2.6)$$

as it can be deduced for the illustrative PV array in Figure 3.

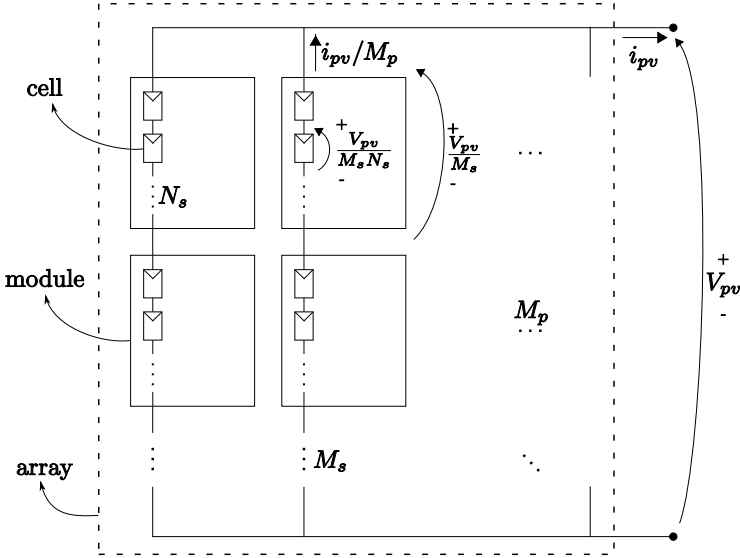


Figure 3: Illustrative diagram of a photovoltaic array.

Using Equations (2.5) and (2.6), it is possible to write a more general version of the Equation (2.1) that applies to an array with any number of modules and cells, which is

$$i_{pv} = M_p i_{ph} - M_p i_r \left(\exp \left(\frac{\varepsilon}{\eta \kappa T} \left(\frac{V_{pv}}{M_s N_s} + \frac{i_{pv} R_s}{M_p} \right) \right) - 1 \right). \quad (2.7)$$

Thus the PV array can be represented by a voltage-controlled current source, as shown in Figure 4.

Note the capacitor C added to the output of the PV array in Figure 4, which is necessary because the current source requires a closed circuit to function properly. The presence of C also serves to prevent the direct connection between the current source (which forces the current to change instantaneously) and the input inductor of some types of converters that can be

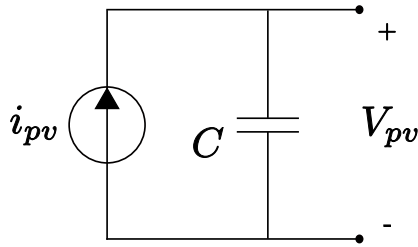


Figure 4: Equivalent circuit of a photovoltaic array.

coupled to the output of the array. Moreover, the voltage on C can be treated as a state variable, which facilitates the control of the voltage of the PV array.

2.2.1 *I-V characteristic*

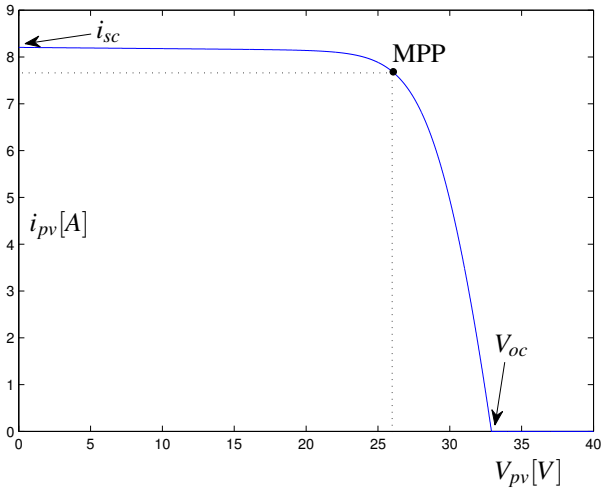
Using the Equation (2.7) it is possible to plot the $I-V$ characteristic curve of the array (or of a module or a cell), whose common waveforms are shown in Figure 5(a) as well as the location of the MPP. With the same data it is possible to trace the curve $P-V$, shown in Figure 5(b), where $P_{pv} = i_{pv}V_{pv}$ is the power provided by the array and the MPP is also indicated.

The polycrystalline module KC200GT from the manufacturer Kyocera, which contains 54 interconnected photovoltaic cells, was used in all the simulations presented in this document. The catalog data for this module in the Standard Test Conditions (STC), *i.e.* $T = 25^\circ\text{C}$ and $G = 1000 \text{ W/m}^2$, are shown in Table 1. Considering only 1 module, the curves of Figure 6 show the influence of the variation of T and G on the $I-V$ curve.

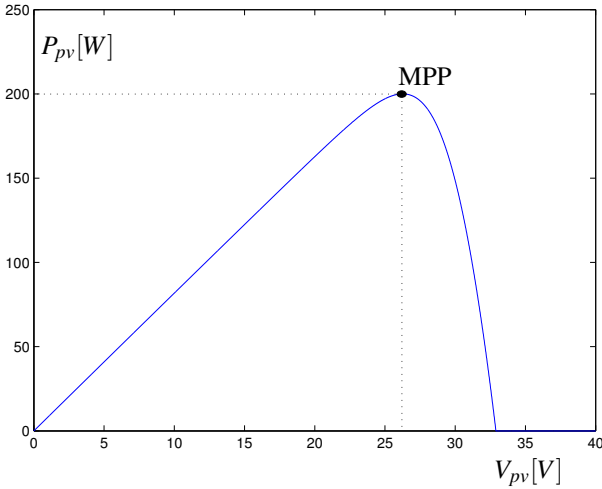
Usually the parameters R_s and R_p are not given in the datasheet of the PV modules, but they can be obtained through the given data according to the method presented in (CASARO, 2009) or estimated as in (ATTIVISSIMO et al., 2012).

2.2.2 *Architectures of photovoltaic systems*

There are several possibilities of converter topologies for applications in the photovoltaic power generation (HUANG et al., 2006), (KJAER; PEDERSEN; BLAAJBERG, 2005), (HAEERLIN, 2001), (SCHIMPF; NORUM, 2008), and the choice of a suitable connection structure is one of the main research topics related to the subject. Some of the factors that may influence the choice of



(a)



(b)

Figure 5: (a) I - V characteristic curve. (b) P - V curve. In both cases, the data of the Table 1 was used with only 1 photovoltaic module.

Parameter	Value
Voltage V_{pv} in MPP	26.3V
Current i_{pv} in MPP	7.61A
Open-circuit voltage (V_{oc})	32.9V
Short-circuit current (i_{sc})	8.21A
Temperature coefficient of i_{sc} (γ)	$3.18 \times 10^{-3} \text{A}/^\circ\text{C}$
η	1.2
R_s	5m Ω
R_p	7 Ω

Table 1: Data of the KC200GT photovoltaic module.

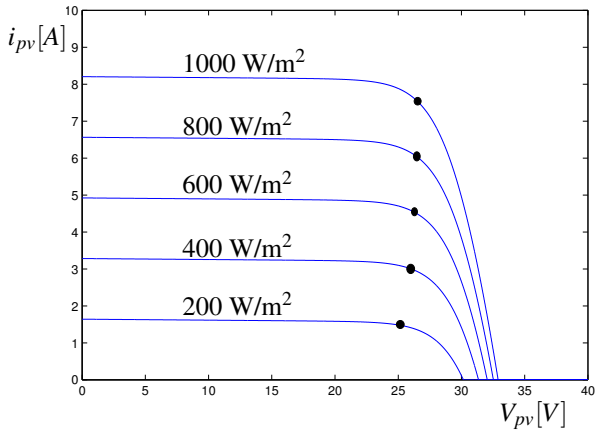
the topology of the converters are the cost, the physical space available and mainly how the PV system is used: stand-alone or connected to utility grid. This section presents some of the topologies in order of structural complexity, citing some of its advantages and disadvantages. For the topologies containing converters between Direct Current (DC) and Alternating Current (AC), only the most usual case where the load or grid is in a *three-phase* AC connection is considered here.

The reference (TEODORESCU; LISERRE; RODRÍGUES, 2011, p.27) lists general control objectives for the structure with connection to the grid. Among them, the main objective considered in this thesis is the achievement of energy efficiency via MPPT. Other possible control objectives include the operation with unitary Power Factor (PF) through synchronization with the grid, the anti-islanding (see Section 2.2.4), the imposition of limits on the Total Harmonic Distortion (THD), stability under variations in the grid voltage, detection of partial shading of the panel, and auxiliary functions for the grid as harmonic compensation and reactive power compensation.

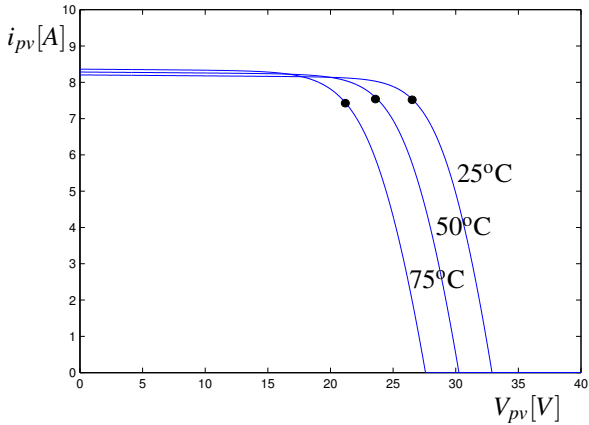
In this thesis, the following will be treated: the design of a control technique for some of these topologies, aiming to explore the possibilities of partial state measurement; robustness to variations in the input parameters and in the desired operation point; and the achievement of the control objectives previously mentioned.

2.2.2.1 Local topology without converters

Topologies without converters, such as shown in Figure 7 applied to charging a battery (without grid connection) or feeding a load, although pos-



(a)



(b)

Figure 6: (a) I - V curves for several levels of solar radiation G ($T = T_r = 25^\circ\text{C}$). (b) I - V curves for different temperatures T ($G = G_r = 1000 \text{ W/m}^2$). The MPP of each curve is indicated by the symbol \bullet .

sible, are almost not used due to their disadvantages. Their only benefit is the low cost. As disadvantages, note that the voltage at the terminals of PV array is fixed to be equal to the voltage of the battery (if it is the case); it is a

system that only operates in open loop. Thus, it is not possible to attain the required voltage for the MPP unless the voltage of the battery coincides with it, but there is still no robustness with respect to T and G . In addition, in case the battery is replaced with a load, it is not possible to adjust the voltage on it. The operating point would be determined by the intersection between the characteristic curve I - V and the load line (COELHO; CONCER; MARTINS, 2009), as shown in Figure 8, whose slope is the inverse value of the load resistance.

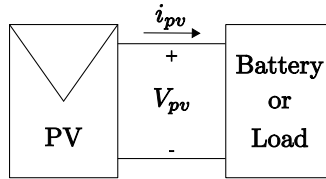


Figure 7: Local topology without converters.

2.2.2.2 Local topology with a DC/DC converter

The topology shown in Figure 9 is the most appropriate to treat local DC loads or battery charging. With this structure, it is possible to maintain the output voltage V_o at a constant value, which is usually desirable in the case of having a local load. Even if there is a battery in the output, which keeps V_o fixed, it is still possible to use the DC/DC converter to regulate V_{pv} , thus performing MPPT to raise the energy efficiency of the system.

It should be noted that the choice of a proper DC/DC converter is of great importance for making the MPPT possible. In general, the step-down (Buck) converters or the step-up (Boost) converters are chosen for being simpler and less expensive. However, when the goal is to perform MPPT these converters may not be suitable in some cases. Consider that in steady state V_o will have a fixed desired value. When using the Buck converter, we have that $V_{pv} \geq V_o$; when using the Boost converter, we have $V_{pv} \leq V_o$. It is easy to realize that if the voltage V_{pv} needed to reach the MPP in steady state is not within the ranges specified above for the respective converters, it is not possible to perform the MPPT and thus the system operates with reduced efficiency (HU; MA; LIN, 2008).

Because of the previously exposed reasons, the best type of converters to ensure the realization of MPPT are the converters that can do both step-down and step-up operations, such as the Buck-Boost, Ćuk, Sepic and Zeta

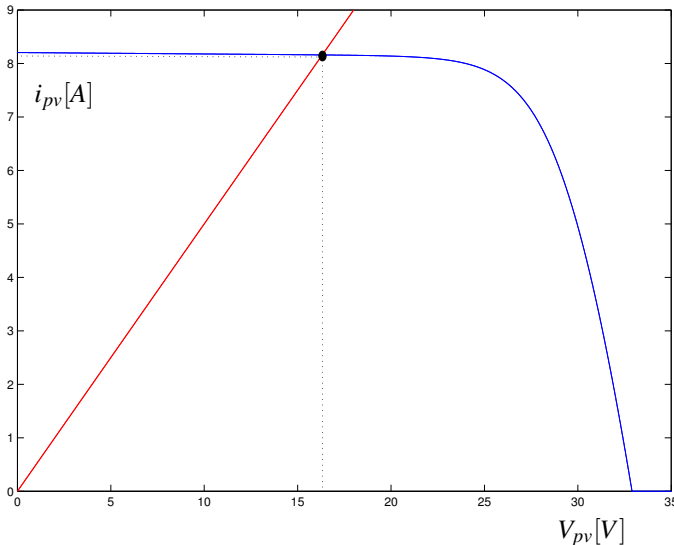


Figure 8: I - V characteristic curve (blue) and load line (red). The data of the Table 1 was used with only 1 photovoltaic module and the load considered was $R = 2\Omega$. The operating point is denoted by the symbol \bullet .

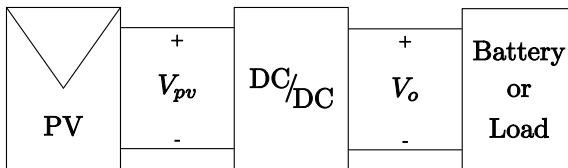


Figure 9: Local topology with a DC/DC converter.

(COELHO; CONGER; MARTINS, 2009).

The topology presented in Figure 9 has several practical applications in autonomous systems, such as power generation for the electronics of satellites or space stations, for instance. These components typically operate with small values of voltage, allowing the use of the converter Buck as in (PETER; AGARWAL, 2010). Another application using this topology can be found in

(CHIU; OUYANG, 2011).

2.2.2.3 Grid-connected topology without a DC/DC converter

The topology presented in Figure 10 is connected to the load or grid in three-phase AC and thus the use of DC/AC converters, as the Voltage Source Inverter (VSI), is required. This layout has the advantage of economy of hardware in relation to the structure that will be presented in the next section, for not having an additional DC/DC converter. As a disadvantage we can cite the greater complexity introduced in the design of the control techniques, which must perform both the MPPT and the synchronization with the grid on the same converter.

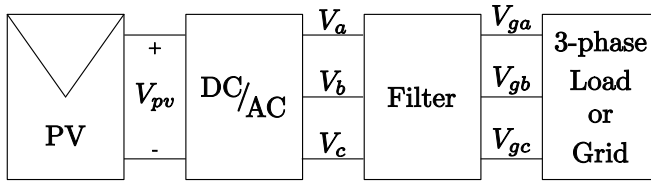


Figure 10: Grid-connected topology with a DC/AC converter only.

The Figure 10 also shows the need for a low-pass filter¹ between the grid and the output of the inverter in order to reduce the harmonic components present in the output waveform of the converter (basically formed by steps) and adapt it to the sinusoidal wave of the grid. The filter also has the interesting feature of allowing the control of the currents flowing into the grid by making these as state variables of the system (currents in the inductors of the filter). This single stage topology with connection to the three-phase grid can be seen in (BLAABJERG et al., 2011), (YAZDANI; DASH, 2009). An example with connection to a single-phase sinusoidal grid can be seen in (CIOBOTARU; TEODORESCU; BLAABJERG, 2005). Among the most common filters, the *LCL* (inductor-capacitor-inductor) filter is employed to achieve decreased switching ripple with only a small increase in filter hardware as compared to the ripple of the *L* or *LC* filter (MARANDI; SOWMYA; BABU, 2012), (SANDEEP; MURTHY; KULKAMI, 2014).

A detailed description of various types of DC/AC converters can be found in (MARTINS; BARBI, 2008) and their components and applications in (BOSE, 2002), (BOSE, 1996).

¹The inductive component used in this type of filter is commonly known as “choke coil”.

2.2.2.4 Grid-connected topology with a DC/DC converter

The Figure 11 presents the most common topology in the literature, which is due to its main advantages: (i) control of MPPT held in the DC/DC converter and synchronization with the grid performed in the DC/AC converter, separately; (ii) the possibility of MPPT for any V_o , as long as the proper choice of the DC converter is made, as commented in Section 2.2.2.2. This topology also presents the filter between the inverter and the grid for the same reasons as in Section 2.2.2.3. This system configuration can be seen in (TEODORESCU; LISERRE; RODRÍGUES, 2011, p.27), for instance.

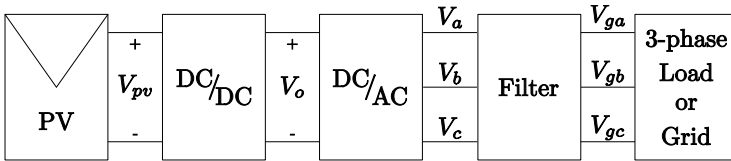


Figure 11: Grid-connected topology with both DC/DC and DC/AC converters.

In practice, most topologies require an energy storage element between the DC/DC and the DC/AC converters, which also decouples the output of the DC/DC converter from the input of the DC/AC converter (MOHAN; UNDELAND; ROBBINS, 2003).

2.2.3 MPPT techniques

The goal of performing MPPT is present in most of the available references on control of photovoltaic systems, which demonstrates the importance and necessity of research in this direction and the reason why there are several techniques for MPPT available nowadays, with 19 of them presented in (ESRAM; CHAPMAN, 2007). In general, these techniques consist of simple implementations which serve to generate a reference to V_{pv} at each instant of time, until this reference becomes the one that occurs at the MPP.

The MPPT techniques are necessary because when the radiation intensity G or the temperature T vary, the curves $I-V$ or $P-V$ also change which causes the MPP to change its $I-V$ coordinates, as shown in Figure 6.

Note that, by replacing i_{pv} from (2.7) in $P_{pv} = i_{pv}V_{pv}$, we get

$$P_{pv} = M_p i_{ph} V_{pv} - M_p i_r \left(\exp \left(\frac{\varepsilon}{\eta \kappa T} \left(\frac{V_{pv}}{M_s N_s} + \frac{i_{pv} R_s}{M_p} \right) \right) - 1 \right) V_{pv} \quad (2.8)$$

and recalling that the MPP occurs in the only peak of the characteristic curve P - V presented in Figure 5(b), we have that the MPP occurs when

$$\frac{\partial P_{pv}}{\partial V_{pv}} = i_{pv} + V_{pv} \frac{\partial i_{pv}}{\partial V_{pv}} = 0. \quad (2.9)$$

However, (2.9) is clearly not a simple equation to be treated, as T and G are unknown and the equation must be solved for V_{pv} , which cannot be isolated. The MPPT techniques are developed in order to circumvent this difficulty.

One of the simplest MPPT techniques is known as Constant Voltage (CV) and is based in Figure 6(a). Note in that figure that the voltage V_{pv} at MPP remains almost constant (around 70% to 80% of the open circuit voltage V_{oc}) for a wide range of radiation values, and thus it is reasonable to adopt V_{pv}^{ref} to be equal to 75% of V_{oc} , that is, a constant reference. Nevertheless, this technique fails when there is temperature variation, as can be seen in Figure 6(b).

Another straightforward technique, but one that solves the preceding problem, is known as Perturb & Observe (P&O). This technique is used in conjunction with the control method proposed in this thesis and thus it will be explored in more detail. A miscellaneous of other MPPT techniques, comparisons between them and efficiency tests can be found in (DE BRITO et al., 2010). In the same reference, the technique that obtained the highest efficiency index is the one known as β method from (JAIN; AGARWAL, 2004), which consists of treating the Equation (2.9) via an intermediate variable β through changes of variables.

In Section 2.2.3.1 a P&O algorithm (available in the literature) that generates references for the voltage variable is presented, while in Section 2.2.3.2 a P&O algorithm is proposed with the purpose of generating references for the current variable. This second algorithm was developed especially for the needs of this work, but it is general enough for the joint application with other control techniques that operate based on the error of the current variable of the PV system.

2.2.3.1 Voltage P&O algorithm

In the Voltage P&O MPPT algorithm, a small perturbation is introduced at each iteration to change the reference for the voltage V_{pv} in order to force the operating point to move closer to the MPP. This algorithm compares the power measured in the current iteration with the power of the previous iteration to determine the direction of the next disturbance (ARMSTRONG; HUR-

LEY, 2004), (JAMRI; WEI, 2010). Based on the P - V characteristic presented in Figure 5(b), if the power increases due to the disturbance then the next disturbance will remain in the same direction. If the operating point exceeds the peak power, the power shall decrease and then the direction of the disturbance is reversed.

When the MPP is reached, the operating point oscillates around the peak power (ARMSTRONG; HURLEY, 2004) because the algorithm disturbs the reference continually reversing direction at each iteration. To keep a small variation in the power, the size of the perturbation is kept small, although it causes slower system responses during transients. Therefore, there is a compromise between the precision and the speed of convergence of the algorithm.

The algorithm of this MPPT technique can be seen in the flowchart of Figure 12, where the output of the algorithm is V_{pv}^{ref} .

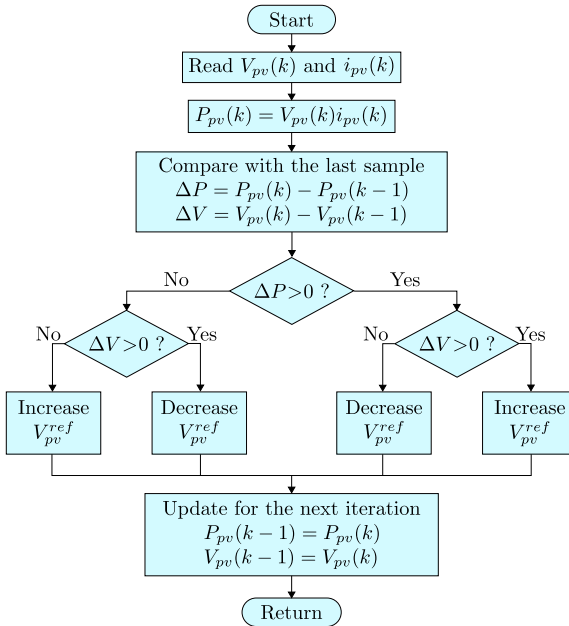


Figure 12: Flowchart of the P&O algorithm for voltage control.

In summary, the algorithm of Figure 12 implies in subtracting a small amount ΔV_{pv}^{ref} from V_{pv}^{ref} if it is observed that variations in power and voltage

have opposite signs or in adding ΔV_{pv}^{ref} to V_{pv}^{ref} if it is observed that the variations have the same sign, with respect to the previous disturbance in V_{pv}^{ref} . The value of ΔV_{pv}^{ref} is chosen *a priori*, typically around 1% of the maximum variation that can occur in V_{pv} (which assumes values between 0 and V_{oc}).

Another popular version of the P&O algorithm has as its output the duty cycle d to be imposed on the system through PWM. In this version, the algorithm increases Δd in d , if the variations of voltage and power have opposite signs or decreases Δd in d otherwise (JAMRI; WEI, 2010). The value of the variation Δd of the duty cycle is also typically chosen as 1% of the maximum possible variation in d (which ranges between 0 and 1). For this thesis, we opted for the version with V_{pv}^{ref} as output for compatibility with the method proposed here, that does not use PWM.

2.2.3.2 Current P&O algorithm

This algorithm is based on the P - I characteristic of the arrangement, which has a similar shape to the curve P - V of Figure 5(b). Likewise, observing the signs of the variations in P_{pv} and i_{pv} when a small perturbation is applied to i_{pv} , we can infer on which side of the MPP curve the operation point is and what action should be taken to bring it closer to the MPP. Thus the algorithm to make changes in the reference for the current (i_{pv}^{ref}) is exactly the same as shown in Figure 12, simply by replacing V by i , as shown in Figure 13.

MPPT algorithms that generate references for the current of the PV array are less common in the literature, and they are present only in cases of current feedback control. An example is the MPPT algorithm proposed in (TAN; GREEN; HERNANDEZ-ARAMBURO, 2005) that, in addition to generating the current reference, uses perturbations Δi_{pv}^{ref} with variable amplitudes, aiming at a faster convergence of the algorithm to the MPP and less oscillation in the power after the MPP is achieved.

2.2.4 Grid model

The grid-connected systems presented in this thesis consider the utility grid voltage as a pure sinusoidal wave and constant amplitude, *i.e.* $V_g = A \sin(\omega t)$. In the case of a balanced three-phase grid, the voltages in each phase (V_{ga} , V_{gb} , V_{gc}) have the same amplitude and a phase shift of 120° between them. This model represents an approximation of the actual grid, because the grid voltage may not behave as a pure sinusoidal wave, some-

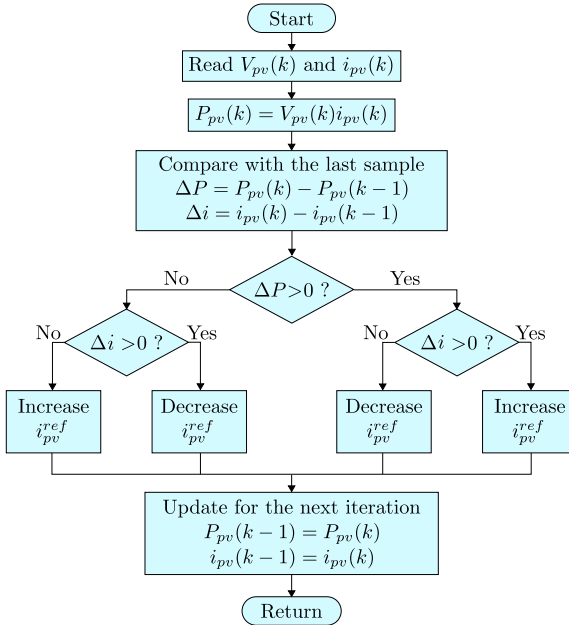


Figure 13: Flowchart of the P&O algorithm for current control.

times containing harmonic components that could not be ignored (BENAVIDES, 2007).

Furthermore, in the real grid, undesirable phenomena such as “islanding” may occur. Islanding is a condition that can occur in grid-connected PV systems in which a portion of the grid that contains both load and generation is isolated from the rest of the network. All generation sources over which the electrical system has no direct control, such as grid-connected PV systems, should have an anti-islanding system, that is, an inverter that is able to detect the islanding condition and to stop energizing the lines while subject to the islanding. This phenomenon is undesirable because it can damage consumer equipment, interfere with the restoration of normal power distribution from the electrical system, and create risks to workers of transmission lines maintenance for causing the phases to remain energized when it is assumed they are disconnected from all energy sources (IEEE STANDARDS, 2000). A survey about islanding detection methods can be found in (BALAGUER et al., 2008).

2.2.5 Coordinate transformations and reference frames

The dynamic equations of the inverter-grid system can be written directly in a three-phase coordinate basis, however, the representation is usually done in two-phase coordinates to simplify the model. When the control technique is based on a biphasic system of coordinates, the coordinate transformation that perform the conversion between three-phase and two-phase are necessary in order to adapt the variables of the three-phase system to the control block.

Another transformation of interest is the one that causes the biphasic coordinates to be at a certain rotating reference frame. One of the major advantages of this is being able to choose a specific reference frame that makes the representation of the state variables to be constant in steady state. Moreover, with two-phase coordinates in a synchronous reference frame the implementation of a synchronization method between the variables of the inverter and the grid is simplified.

2.2.5.1 Coordinate transformation from three-phase to two-phase

The Clarke's transformation, or $\alpha\beta 0$, given in Equation (2.10) can be used to transform three-phase variables into two-phase variables, with the characteristic of preserving the amplitude and the frequency of the three-phase variables. In this work, it will be considered the $\alpha\beta$ transformation, ignoring the 0 component because of the assumption that the system is balanced and therefore this component is always zero.

$$\begin{bmatrix} f_\alpha \\ f_\beta \end{bmatrix} = \frac{2}{3} \underbrace{\begin{bmatrix} 1 & -\frac{1}{2} & -\frac{1}{2} \\ 0 & \frac{\sqrt{3}}{2} & -\frac{\sqrt{3}}{2} \end{bmatrix}}_{K_{\alpha\beta}} \begin{bmatrix} f_a \\ f_b \\ f_c \end{bmatrix} \quad (2.10)$$

In Equation (2.10), f_α, f_β and f_a, f_b, f_c are components of a generic vector variable f represented in the two-phase $\alpha\beta$ and the three-phase abc coordinates, respectively. The zero coordinate is null in balanced three-phase systems and thus the quantities will be represented only as $f_{\alpha\beta}$, *i.e.* without the 0 component in the notation for convenience. Finally, the pseudo-inverse of

(2.10) is

$$\begin{bmatrix} f_a \\ f_b \\ f_c \end{bmatrix} = \underbrace{\begin{bmatrix} 1 & 0 \\ -\frac{1}{2} & \frac{\sqrt{3}}{2} \\ -\frac{1}{2} & -\frac{\sqrt{3}}{2} \end{bmatrix}}_{K_{\alpha\beta}^{\#}} \begin{bmatrix} f_{\alpha} \\ f_{\beta} \end{bmatrix}. \quad (2.11)$$

The deduction of the Equations (2.10), (2.11) as well as the orientation of the coordinate systems used can be found in Appendix B.

2.2.5.2 Reference frame transformation from stationary to synchronous

In the case of the photovoltaic systems studied in this thesis, the state variables that are sinusoidal in steady state are the grid voltage and the current delivered to the grid by the DC/AC converter. As shown in Section 2.2.4, the grid voltage has a constant frequency (ω) and the switching in the inverter must be such that, in steady state, the current delivered must have the same frequency ω and be in phase with the grid voltage, in order to obtain unitary power factor. The conversion between the reference frames is accomplished through the Park's transformation (BARBI, 1985) shown in Equation (2.12), for which the deduction and orientation of the Cartesian axes are shown in Appendix C.

$$\begin{bmatrix} f_d \\ f_q \end{bmatrix} = \underbrace{\begin{bmatrix} \cos(\phi) & \sin(\phi) \\ -\sin(\phi) & \cos(\phi) \end{bmatrix}}_{K_{dq}} \begin{bmatrix} f_{\alpha} \\ f_{\beta} \end{bmatrix} \quad (2.12)$$

In Equation (2.12), f_d, f_q and f_{α}, f_{β} are components of a generic variable f respectively represented in the synchronous dq and stationary $\alpha\beta$ reference frames. In the same equation, ϕ is the angular position of the rotating synchronous reference frame with respect to the stationary frame.

The inverse of (2.12) is given by

$$\begin{bmatrix} f_{\alpha} \\ f_{\beta} \end{bmatrix} = \underbrace{\begin{bmatrix} \cos(\phi) & -\sin(\phi) \\ \sin(\phi) & \cos(\phi) \end{bmatrix}}_{K_{dq}^{-1}} \begin{bmatrix} f_d \\ f_q \end{bmatrix}. \quad (2.13)$$

The deduction of Equation (2.13) can also be found in Appendix C.

It is intended to synchronize the reference frame to the grid and, therefore, it must rotate with a constant angular velocity ω , that is, $\phi = \omega t$ and ϕ must be equal to the angular position of sinusoidal waveform of the voltage of the grid. Note that while ω is known, it is still necessary to measure the grid voltage to determine its angular position ϕ at each instant of time. The next section is devoted to present a method that provides this synchronization.

2.2.6 Grid synchronization

The control of the DC/AC converters (inverters and rectifiers) connected to the grid requires a synchronization block that provides the angular position of the grid at any instant of time. This synchronizer must also be suitable for the conditions of the power grid, in order to be immune to several possible interferences, such as harmonics, voltage amplitude variations between phases, frequency variations, measurement noise, among others. If the operation of the synchronizer is not appropriate, then there may be degradation of the converter operation and even instability (DA SILVA, 2004). This section describes a vector synchronization method based on the voltage vector of the grid.

As in vector control algorithms in general, the case of the control technique for DC/AC inverters presented in this document requires knowledge of the angular position of the grid voltage at each instant of time. This information is used in the synchronization of the waveforms of the output current of the converter to the grid voltage, in order to obtain unitary power factor and thus deliver only active power to the grid. It may also be desirable to supply some reactive power to the grid in some cases, although the knowledge of the angular position is still required.

Due of the need to know the angular position at each calculation cycle of the control algorithm, the synchronizer must be fast, avoiding the direct calculation of trigonometric functions, which would require a much higher processing time than the method that will be presented in the sequence.

According to (SVENSSON, 2001), it is possible to build a synchronizer that provides the angular position simply by acquiring the values of the three-phase voltage. These values are used to calculate the voltages in $\alpha\beta$ coordinates, as shown in Equation (2.10). After the coordinate transformation, a low-pass filter is usually applied to each voltage component to eliminate the possible existence of noise. The filter introduces a phase delay that can be easily compensated with the method presented in (DA SILVA, 2004). In principle, in this thesis, the grid voltage will be considered ideal and therefore the

filter is discarded.

Finally, it is possible to calculate the sine and cosine of the angle of the grid voltage vector, by dividing the α and β components by the norm of the vector. Thus, we obtain the information necessary for transforming the components of the voltage and the current from the static reference frame $\alpha\beta$ to the synchronous reference frame dq of Equation (2.12). The method of vector synchronization is summarized in Figure 14, where the Low-Pass Filter (LPF) is illustrated and the trigonometric relations presented can be easily obtained from the right triangle formed by the vector module and its components.

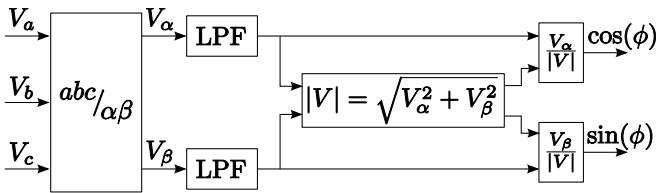


Figure 14: Vector synchronizer based on the utility grid voltage.

2.3 Switched systems

As mentioned in Section 2.2.2, the control of PV systems is performed through power electronic converters, which are systems containing one or more controllable switching devices. For this reason, the control problem of a PV system can be viewed as a problem of designing a switching rule for the converters. In this case, the PV system and the converters can be represented as a switched system for which a switching rule must be designed in order to achieve some performance requirements for the closed loop system. This will be the focus of the next chapters. We end this chapter by presenting some important aspects of switched systems that are particular cases of hybrid systems.

Hybrid systems is a designation for systems where two types of dynamics coexist and interact: a continuous-time dynamic (typically modeled by differential equations) and other composed of discrete events (typically modeled by automata with finite or infinite states) (LIBERZON, 2003). As examples of events that produce a hybrid behavior, it is possible to mention the opening and closing of a valve or an electronic switch, such as the ones

present in the power electronic devices used to control the PV systems. The fact that there are many practical examples with hybrid systems features is a strong motivation for research in this area.

The research involving hybrid systems has very interdisciplinary characteristics. This is because the studies have been made by different scientific communities, each treating the issue within their own approaches. For example, researchers from computer science focus their work in the discrete behavior of the hybrid system, treating the dynamics in continuous time in a simplified form. On the other hand, researchers at the system control area emphasize the work in the dynamic properties of continuous time of hybrid systems (LIBERZON, 2005). In this thesis we give emphasis to the second approach, treating the hybrid systems as dynamic systems with continuous-time and representing the switched discrete events as isolated events. Thus, it is possible to distinguish a particular class of hybrid systems, called switched systems.

A switched system can be defined as a dynamic system composed of a family of subsystems with dynamic continuous-time and a law that organizes the switching between them (LIBERZON; MORSE, 1999). Each subsystem corresponds to an operation mode of the switched system. It is possible to obtain a switched system from a hybrid system disregarding the details about the behavior of the discrete events, and instead of that, considering all possible switching signals for a given class. Therefore, switched systems can be seen as an abstraction that corresponds to a particular case of a higher level hybrid systems. Typically, this abstraction generates a system with simpler description, but with more solutions than the original system (LIBERZON, 2005). More information about the relationship between hybrid systems and switched systems can be seen in (HESPANHA, 2004).

A switched system can be mathematically represented by a differential equation of the form

$$\dot{x}(t) = f_{\sigma}(x(t)) \quad (2.14)$$

where $\{f_i : i \in \mathbb{I}_m\}$ is a family of sufficiently regular functions (at least locally Lipschitz²) from \mathbb{R}^n to \mathbb{R}^n , \mathbb{I}_m is an index set and $\sigma : [0, \infty) \rightarrow \mathbb{I}_m$ is a piecewise constant set valued function referred to as switching signal. In this context, a piecewise constant set valued function is a signal that has the following characteristics: it presents a finite amount of discontinuities in any

²A function $f(x)$ is said to be locally Lipschitz in the domain $D \subset \mathbb{R}^n$ if all points in D have a neighborhood D_0 such that f satisfies the Lipschitz condition ($\|f(t, x) - f(t, y)\| \leq L\|x - y\|$) for all points in D_0 with a Lipschitz constant $L > 0$. The symbol $\|x\|$ corresponds to the Euclidian norm of $x \in \mathbb{R}^n$.

finite time interval and it is constant between two consecutive discontinuities.

When a switched system has only linear subsystems, it is called a linear switched system

$$\dot{x}(t) = A_{\sigma}x(t) \quad (2.15)$$

with a finite index set $\mathbb{I}_m = \{1, 2, \dots, m\}$, where m is the number of subsystems (or operation modes) of the switched system. In other hand, when a switched system is composed by affine subsystems, it is denominated an affine switched system

$$\dot{x}(t) = A_{\sigma}x(t) + b_{\sigma}. \quad (2.16)$$

2.3.1 Classification according to the type of commutation

Regarding the commutation, the switched systems may be classified as: commutation dependent of the states *versus* commutation dependent of the time; or autonomous commutation *versus* controlled commutation (LIBERZON, 2003). The main aspects of each type of commutation is presented in the sequence:

- State-dependent commutation: systems where the switching signal will change as a function of the system states. In this case, the state space is partitioned into regions, each region corresponding to the activation of one of the subsystems that comprise the switched system. The boundaries of these regions are called switching surfaces;
- Time-dependent commutation: systems where there is a change in the switching signal after a certain time interval. For this type of commutation, the switching signal is described as $\sigma(t)$ in order to emphasize the temporal dependence;
- Autonomous commutation: systems where there is no direct control over switching signal. In this group are included systems with state-dependent switching in which the location of switching surfaces is pre-determined, or systems with time-dependent switching where the rule that defines the switching signal is unknown or neglected in system modeling stage;
- Controlled commutation: systems where the switching signal is imposed to achieve a desired behavior. The switching mechanism is directly controlled, and it can be either state-dependent or time-dependent.

The content of this thesis is divided in two branches: **(i)** the design of stabilizing *state-dependent controlled* switching rules; **(ii)** the stability analysis of switched systems with *state-dependent autonomous* commutation.

It is noteworthy that combinations of different types of switching can exist in a switched system. Furthermore, it is not simple to determine an accurate distinction between autonomous and controlled commutation, as well as state-dependent and time-dependent switching (LIBERZON, 2003).

2.3.2 Sliding modes

Sliding mode is a special type of switched system behavior that may occur in the presence of fast enough switching frequency. For the definition of sliding modes, a switched system with a state-dependent commutation between two operation modes will be considered as an example. The switching surface, represented by \mathcal{S} , divides the state space in two regions, and in each region one of the two subsystems $\dot{x} = f_i(x)$, $i = 1, 2$, is active. In this case, it is assumed that there are no discontinuities in the values of the states at the switching instant. If the vector fields $f_1(x)$ and $f_2(x)$ are pointing to the same direction with respect to \mathcal{S} , the continuous state trajectory reaches the surface \mathcal{S} and crosses to the other side. This situation is depicted in Figure 15(a). On the other hand, it is possible that the vector fields $f_1(x)$ and $f_2(x)$ are both pointing towards the surface, as shown in Figure 15(b). In this case, when the trajectory reaches the surface \mathcal{S} , it cannot leave this surface and the trajectory moves over the surface, that is, the vector field defining the system dynamics in this case is tangent to the surface. This phenomenon is known as sliding mode (LIBERZON, 2003).

The system behavior in sliding mode can be described using the concepts introduced by Filippov (1988). According to these concepts, the vector field that defines the dynamics in sliding mode must be tangent to the switching surface and there are several ways to define this tangent vector field. The simplest and most common form in the literature is to define the tangent vector field through the convex combination of the vector fields of the subsystems at each point of the trajectory over the surface. For example, in Figure 15(b) the tangent vector field is given by

$$f_{\theta}(x) := \theta(x)f_1(x) + (1 - \theta(x))f_2(x), \quad \theta(x) \in [0, 1] \quad (2.17)$$

where $\theta(x)$ is the convex combination element that can be obtained through orthogonal projection rules (FILIPPOV, 1988, p.52). Note that this way of defining the vector field also allows the definition of the system dynamics

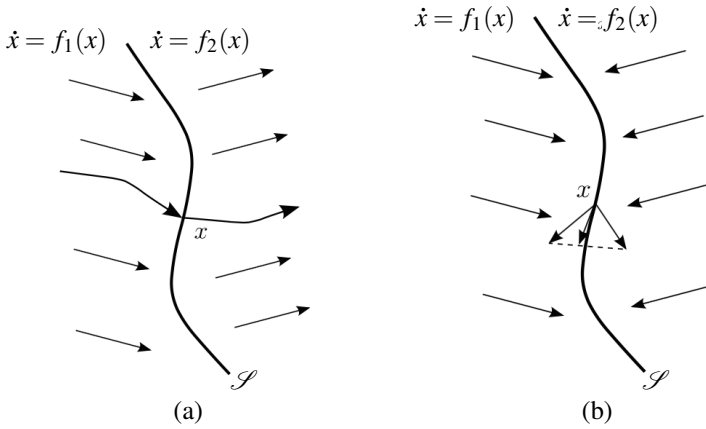


Figure 15: Example of trajectories of a bimodal switched system: (a) crossing the switching surface; (b) resulting in sliding mode. Source: (SCHARLAU, 2013).

for a singleton, that is, for $\dot{x} = f_1(x)$, $\theta(x) = 1$ and for $\dot{x} = f_2(x)$, $\theta(x) = 0$. Thus, the dynamics of a switched system with or without sliding modes can be viewed as a differential inclusion

$$\dot{x} = f_\theta(x). \quad (2.18)$$

For a more formal and general presentation of sliding modes, see (FILIPPOV, 1988, p.50). Also, on page 54 of this book, an alternative characterization of tangent vector field, different of the convex combination, can be found.

2.3.3 Control structure

The classes of switched systems considered in this thesis have a special control structure. This is illustrated in Figure 16, which presents the control scheme for a switched system with m different subsystems and a state-based switching rule $\sigma(x)$ that forces the system to operate in a particular mode. In this figure, the innermost dashed area represents the ideal switching devices receiving the value σ which determines the position of the switches (on or off). Each combination of the positions of the set of switches defines

one subsystem that is connected in the closed circuit (the active mode). The switching signal σ can somehow be viewed as a control input for the switched system, although we must keep in mind that it is just a logical variable that determines the operation mode at a given instant.

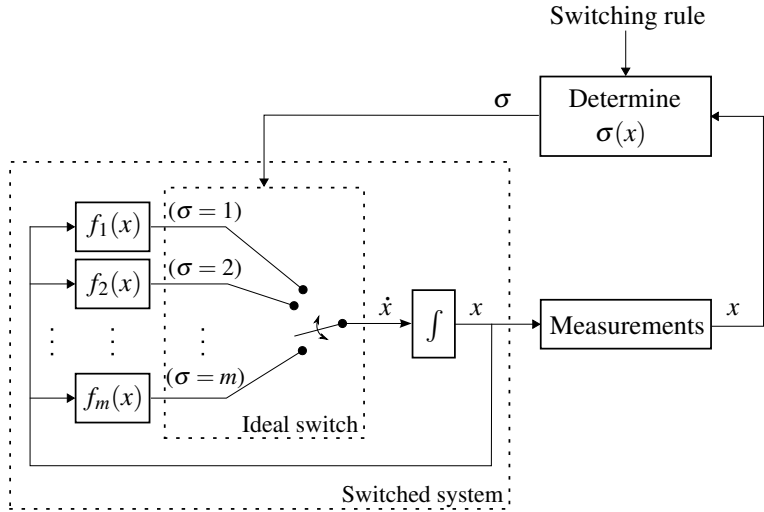


Figure 16: Basic control scheme for switched system with a state-dependent switching rule.

Note that the structure presented in Figure 16 represents ideal switches where the positions of the switches can be changed arbitrarily fast. In practice, real switches are performed by PWM devices having a small PWM switching period (the period of the PWM carrier signal) and, in general, a moving averaging filter is necessary to take into account the limited bandwidth of the actuators whose models are included in the vector fields $f_i(x)$. The control structure in this case is presented in Figure 17, where an averaging block computes the duty cycle d from the switching signal and PWM devices determine the switches positions p . The calculation of the duty cycle based on the switching signal will be discussed in more detail in Section 4.4.

In the case of Figure 17, there is a mixture between state-dependent switching and time-dependent switching, as the switching rule is based on state feedback and the averaging technique and the PWM convert the switching signal into a time-based signal. This structure is used by (SENGER; TROFINO, 2014) in a real application and some performance advantages

against the usual PWM are commented.

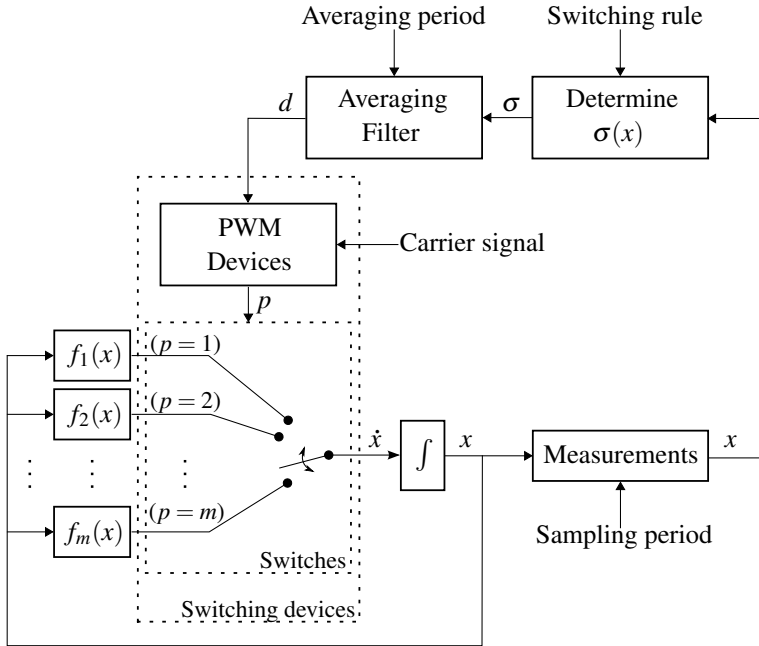


Figure 17: Control scheme for a state-dependent switching rule with an interface to PWM controlled devices.

The particular structure adopted in this work for the definition of σ , as well as the design procedure, will be presented in Chapter 3.

2.4 Additional mathematical background

This section presents some useful mathematical definitions to be explored in several of the next chapters. More specifically, the Kronecker product, a version of the Finsler's Lemma, the definitions of annihilators and of class \mathcal{K} functions. Other definitions to be used locally will appear where they are necessary.

Definition 2.1 (Kronecker product (LAUB, 2005)) *Let $A \in \mathbb{R}^{m \times n}$, $B \in \mathbb{R}^{p \times q}$. Then the Kronecker product (or tensor product) of A and B is defined as the*

matrix

$$A \otimes B = \begin{bmatrix} a_{11}B & \dots & a_{1n}B \\ \vdots & \ddots & \vdots \\ a_{m1}B & \dots & a_{mn}B \end{bmatrix} \in \mathbb{R}^{mp \times nq}. \quad (2.19)$$

□

Obviously, the same definition holds if A and B are complex-valued matrices. However, in this thesis, our attention is restricted to real-valued matrices and the Kronecker product will be used only to simplify some complicated notation. For more details and properties of the Kronecker product, see (LAUB, 2005, p.139).

Lemma 2.1 (Finsler's Lemma) *Let $\mathcal{W} \subseteq \mathbb{R}^s$ be a given polytopic set, $M(\cdot) : \mathcal{W} \mapsto \mathbb{R}^{q \times q}$, $G(\cdot) : \mathcal{W} \mapsto \mathbb{R}^{r \times q}$ be given matrix functions, with $M(\cdot)$ symmetric. Let $Q(w)$ be a matrix whose columns are base vectors for the null space of $G(w)$. Then the following statements are equivalent:*

- (i) $\forall w \in \mathcal{W}$ the condition $z' M(w) z > 0$ is satisfied $\forall z \in \mathbb{R}^q$ such that $G(w)z = 0$.
- (ii) $\forall w \in \mathcal{W}$ there exists a matrix function $L(\cdot) : \mathcal{W} \mapsto \mathbb{R}^{q \times r}$ such that $M(w) + L(w)G(w) + G(w)'L(w)' > 0$.
- (iii) $\forall w \in \mathcal{W}$ the condition $Q(w)'M(w)Q(w) > 0$ is satisfied. □

Two cases are of particular interest to this work. The first is when $M(\cdot), G(\cdot)$ are affine functions and L is constrained to be constant. In this situation (i), (ii) are no longer equivalent, but (ii) is clearly a sufficient polytopic LMI condition for (i). The second case is when $M(\cdot)$ is an affine function and $G(\cdot)$ is constrained to be constant, leading Q to be constant as well. In this case (i), (iii) are yet equivalent and (iii) is a polytopic LMI with a smaller number of decision variables when compared to (ii). The interest of these two polytopic LMI problems is that they are numerically efficient alternatives for condition (i), which is difficult to be tested for being an infinite dimensional problem. Finally, Lemma 2.1 is still valid when the inequalities are replaced by equality conditions. See for instance (DE OLIVEIRA; SKELTON, 2001), (TROFINO; DEZUO, 2013) for more details on the Finsler's Lemma.

Definition 2.2 (Annihilator) *Given a positive integer r and a vector function $f(\cdot) : \mathbb{R}^q \mapsto \mathbb{R}^s$, a matrix function $\mathfrak{K}_f(\cdot) : \mathbb{R}^q \mapsto \mathbb{R}^{r \times s}$ will be called an annihilator of $f(\cdot)$ if $\mathfrak{K}_f(z)f(z) = 0$, $\forall z \in \mathbb{R}^q$. Moreover, if $\mathfrak{K}_f(\cdot)$ is a linear function, it will be referred to as a linear annihilator. □*

Observe that the matrix representation of a linear annihilator is not unique. In this work, we are interested in a general formula for a linear annihilator for the case of $f(z) = z = [z_1 \dots z_q]^t \in \mathbb{R}^q$. Taking into account all possible pairs z_i, z_j for $i \neq j$ without repetition, *i.e.* for $\forall i, j \in \{1 \dots q\}$ with $j > i$, we obtain a linear annihilator given by the formula

$$\mathfrak{N}_z(z) = \begin{bmatrix} \phi_1(z) & Y_1(z) \\ \vdots & \vdots \\ \phi_{(q-1)}(z) & Y_{(q-1)}(z) \end{bmatrix} \in \mathbb{R}^{r \times q}, \quad r = \sum_{j=1}^{q-1} j \quad (2.20)$$

$$\phi_1(z) = [z_2 \quad \dots \quad z_q]^t$$

$$\phi_i(z) = \begin{bmatrix} & z_{(i+1)} \\ 0_{(q-i) \times (i-1)} & \vdots \\ & z_q \end{bmatrix}, \quad i \geq 2$$

$$Y_i(z) = -z_i I_{(q-i)}, \quad i \geq 1$$

Throughout the thesis, annihilators are used jointly with the Finsler's Lemma to reduce the conservativeness of parameter dependent LMIs. See, for instance (TROFINO; DEZUO, 2013) where linear annihilators are also used to reduce the conservativeness of state dependent LMIs.

Finally, consider the following definition.

Definition 2.3 (Class \mathcal{K} function (KHALIL, 2002)) *A continuous function $\beta : [0, a) \rightarrow [0, \infty)$ is said to belong to class \mathcal{K} if it is strictly increasing and $\beta(0) = 0$. It is said to belong to class \mathcal{K}_∞ if $a = \infty$ and $\beta(r) \rightarrow \infty$ as $r \rightarrow \infty$. \square*

2.5 Concluding remarks

This chapter addressed the presentation of photovoltaic generation systems to serve as reference for the next chapters. The presentation started with a brief discussion on the model of a photovoltaic array, followed by the main connection topologies for this type of system. In the sequel, some of the most common methods for performing MPPT were presented, in particular the algorithm P&O was described in more detail, because it is used in Chapter 5 together with the switching technique proposed in this document. Some coordinate transformations and a method for synchronizing the PV system to the grid were also presented. Finally, an additional mathematical background was introduced.

One possibility for further work, not exploited here, is the development of an alternative method for performing the MPPT. The main advantage in creating a new MPPT method is the possibility to achieve higher system performances than the current approaches, that is, a better use of the energy that can be generated. It would also be desirable for the proposed method to be general enough to be applied to the search of extreme points in other kinds of systems, not only PV, as in the case of the technique of (ARIYUR; KRSTIC, 2000).

The author of this thesis is also interested in the control of battery charging using the power generated by the PV system. To this end, more detailed research on the behavior of the batteries under charging conditions, not presented in this document, should be taken into account. Additional variable structure elements may be present in the model of the battery charger: the charge controllers. Such controllers (the simplest) are basically composed of a switch that disconnects the battery from the PV array when it is fully charged and another switch that disconnects the battery from the load in case it is discharged. Some work that can be cited as references for battery charging control are: (ZHENG; WANG, 2011), (WANG; LIN, 2007), (CHEN; CHEN, 2010), (RADWAN et al., 2011), (EGIZIANO et al., 2007), (TASDIGHI et al., 2012). A comparison between different types of batteries can be found in (PATEL, 1999).

3 CONTROL OF AFFINE SWITCHED SYSTEMS

3.1 Introduction

A switched system can be defined as a dynamical system composed of a set of subsystems with continuous time dynamics and a rule that organizes the switching between them (LIBERZON; MORSE, 1999). Each of these subsystems corresponds to a particular operation mode of the switched system. The problem of designing switching rules for switched systems has been largely studied and several results are available in the literature. See the surveys presented in (DECARLO et al., 2000), (LIN; ANTSAKLIS, 2009), for a large list of references, and Section 3.3 for a small comparative study between some of these techniques and the one used in this thesis.

The results presented in this chapter enable the design of a stabilizing switching rule that allows the occurrence of sliding modes among any number of subsystems with affine vector fields. The content of this chapter is an updated version of (TROFINO et al., 2011) and of (SCHARLAU, 2013, chap. 4), which generalizes and extends the results of (TROFINO et al., 2009a), (TROFINO; SCHARLAU; COUTINHO, 2012). Furthermore, the results provide the necessary basis for the methods developed in the next chapters. The main feature of the method is that the results are based on a Lyapunov function of the type $\max_i \{v_i(x)\}$ where x is the system state and $\{v_i(x)\}$ is a set of auxiliary functions to be determined. This particular type of Lyapunov function was also considered in (TROFINO et al., 2009a), (PETTERSSON, 2003), (HU; MA; LIN, 2008). In (TROFINO et al., 2009a), (PETTERSSON, 2003) each subsystem is associated with an auxiliary function $v_i(x)$, while in (HU; MA; LIN, 2008) each subsystem is associated with the entire set of functions $\{v_i(x)\}$. In the latter, the number of auxiliary functions can be greater than the number of subsystems. The composition $\max_i \{v_i(x)\}$ has interesting properties, but some technical difficulties arise when dealing with sliding modes. See, for instance, (HU; MA; LIN, 2006), (HU; MA; LIN, 2008), (PETTERSSON, 2003) for details.

3.2 Preliminaries

Consider the following affine switched system composed of m affine subsystems.

$$\dot{x}(t) = f_i(x) = A_i x(t) + b_i \quad , \quad i \in \mathbb{I}_m := \{1, \dots, m\} \quad , \quad (3.1)$$

where $x \in \mathbb{R}^n$ is the system state, which is assumed to be available from measurement at this point. The case of partial state measurement will be addressed later. The matrices A_i and the vectors b_i are real and have compatible dimensions. The class of systems described in (3.1) can represent the dynamics of various control applications. See (MORSE, 1997), (LIBERZON, 2003), (SHTESSEL; ZINOBER; SHKOLNIKOV, 2002), (DIAKAKI; PAPAGEORGIOU; ABOUDOLAS, 2002), for instance.

The goal is to design a switching rule that asymptotically drives the state of the system to a given constant equilibrium \bar{x} . This is done by forcing \bar{x} to be a globally asymptotically stable equilibrium point in closed-loop.

Given the desired (constant) equilibrium point \bar{x} , it is possible to represent the dynamics of the tracking error by the following switched system.

$$\dot{e}(t) = A_i e(t) + k_i \quad , \quad k_i = b_i + A_i \bar{x} \quad , \quad e(t) := x(t) - \bar{x} \quad , \quad (3.2)$$

where $i \in \mathbb{I}_m := \{1, \dots, m\}$. Using the error system described in (3.2), the idea is to make the error states $e(t)$ converge to the origin. With that in mind, consider the switching rule given by

$$\sigma(e(t)) := \arg \max_{i \in \mathbb{I}_m} \{v_i(e(t))\} \quad , \quad v_i(e(t)) = e(t)' P_i e(t) + 2e(t)' S_i \quad , \quad (3.3)$$

where $P_i = P_i' \in \mathbb{R}^{n \times n}$ and $S_i \in \mathbb{R}^n$ are matrices to be determined. At each instant of time, $\sigma(e(t)) \in \mathcal{P}(\mathbb{I}_m) \setminus \{\emptyset\}$ is a set of indexes corresponding to the set of subsystems with “maximum energy”, represented by

$$V(e(t)) = \max_{i \in \mathbb{I}_m} \{v_i(e(t))\}. \quad (3.4)$$

For instance, $\sigma(e(t_0)) = \{i, j, k\}$ means that at the instant $t = t_0$ the trajectory of the error is at the switching surface defined by the subsystems $\{i, j, k\}$, because $v_i(e(t_0)) = v_j(e(t_0)) = v_k(e(t_0)) = \max_{i \in \mathbb{I}_m} \{v_i(e(t_0))\}$.

Now consider the following definition.

Definition 3.1 (Filippov solution (FILIPPOV, 1988)) *An absolutely continuous function $x(t)$ is regarded to be a Filippov solution of $\dot{x} = f_i(x)$ if it satisfies the differential inclusion*

$$\dot{x} \in \mathcal{F}(x) := \mathbf{Co}\{f_i(x)\} \quad (3.5)$$

for almost all $t \geq 0$. Observe that any element of the convex hull can be

represented as a convex sum of $\{f_i(x)\}$. In this sense we use the notation

$$\dot{x} := \sum_{i \in \sigma(x)} \theta_i(x) f_i(x) \quad (3.6)$$

where $\theta(x) = [\theta_1(x) \quad \dots \quad \theta_m(x)]'$ satisfies $\theta \in \Theta$ with Θ defined as the simplex

$$\Theta := \left\{ \theta : \theta_i \geq 0, \sum_{i=1}^m \theta_i = 1 \right\}. \quad (3.7)$$

If $\sigma(x)$ is singleton, then $\mathcal{F}(x) = f_i(x)$. □

See the Chapter 2 of (FILIPPOV, 1988) for the proof of existence of solution for the differential equations with discontinuous right-hand side considered in this thesis and more details on the differential inclusion presented in Definition 3.1.

Assuming that the sliding mode dynamics of the system can be represented as convex combinations of the subsystems as in Definition 3.1, the global switched system, including the subsystems and the sliding mode dynamics that may occur on any switching surface, is represented by

$$\dot{e}(t) = \sum_{i=1}^m \theta_i(e(t)) (A_i e(t) + k_i) \quad , \quad \theta(e(t)) \in \Theta, \quad (3.8)$$

where $\theta(e(t))$ is the vector with components $\theta_i(e(t))$, Θ is the unitary simplex (3.7) and $\theta_i(e(t)) = 0$ if $i \notin \sigma(e(t))$ with $\{\theta_i(e(t)), \forall i \in \sigma(e(t))\}$ defined according to Filippov (FILIPPOV, 1988, p.50). Recall that sliding mode dynamics may occur at a point $e(t)$ only if it is possible to find a convex combination of the vector fields of the subsystems such that $\dot{e}(t)$ is a vector in the hyperplane tangent to the switching surface at the point $e(t)$. It is assumed that $\theta(e(t))$ and $\sigma(e(t))$ are respectively piecewise continuous and piecewise constant. Under these regularity assumptions, the vector field of (3.8) has a finite number of discontinuous points on any system trajectory.

In order to have $e(t) = 0$ as the equilibrium point of (3.8), it is necessary that $\sum_{i=1}^m \theta_i(0)k_i = 0$, where $\{\theta_i(0), i \in \mathbb{I}_m\}$ are piecewise continuous functions of time and characterize the equilibrium condition. With this observation in mind, let us define constant scalars $\bar{\theta}_i$ satisfying the following lemma.

Lemma 3.1 *The origin is an equilibrium point of (3.8) iff there exists $\bar{\theta} \in \Theta$ such that*

$$\sum_{i=1}^m \bar{\theta}_i k_i = 0. \quad (3.9)$$

□

Proof: Set $\dot{e}(t) = 0$ and $e(t) = 0$ in (3.8). □

While $\theta(0)$ is associated with the equilibrium condition, and in general is unknown and possibly not constant, the parameter $\bar{\theta}$ is an auxiliary constant representing one particular value that $\theta(0)$ may take.

See the Remark 3.4.1 for comments on the matrix $\sum_{i=1}^m \bar{\theta}_i A_i$.

3.3 Related methods

As previously mentioned, several other types of switching rules and Lyapunov functions, different of (3.3), (3.4) do exist in the literature. In the sequel we highlight some aspects of these techniques.

Methods using a quadratic Lyapunov function of the type $V(x) = x'Px$ and switching rules based on its time derivative can be found, for instance, in (DEAECTO et al., 2010), (BOLZERN; SPINELLI, 2004) and references therein. Another class of methods are those based on Lyapunov functions of the type

$$V(x) = \min_{i \in \mathbb{I}_m} \{v_i(x)\} \quad , \quad v_i(x) > 0 \quad (3.10)$$

and switching rules based on

$$\sigma(x) := \arg \min_{i \in \mathbb{I}_m} \{v_i(x)\} \quad (3.11)$$

In this direction we could cite, for instance, (HU; MA; LIN, 2008), (CARDIM et al., 2009) and their references. Methods based on Polyhedral Lyapunov functions are proposed in (LIN; ANTISAKLIS, 2004), (LIN; ANTISAKLIS, 2009). For a general overview of the methods for the class of linear and affine systems, we recommend the surveys (DECARLO et al., 2000), (LIBERZON, 2003), (LIN; ANTISAKLIS, 2009).

All these methods have advantages and limitations and, except for some specific cases, the results are based on sufficient conditions, leading a conclusive comparative study difficult to be established.

The motivation for using (3.3), (3.4) in this work is that (3.4) represents a Lyapunov function with interesting degrees of freedom, if compared

with the quadratic form $x'Px$, or the ‘min’ type function (3.11) or even the polyhedral functions. Observe that the functions v_i in (3.4) have linear and quadratic terms while polyhedral functions have only linear terms. The min type have only quadratic terms and in addition these terms must be positive definite. Observe this positiveness constraints are not present in (3.4). In order to reduce the conservatism of the results, it is important to correctly exploit the degrees of freedom available in the function (3.4) and this is the main challenge of the method.

To illustrate this fact, observe that some results found in the literature, as for instance (DEAECTO et al., 2010), (BOLZERN; SPINELLI, 2004), are based on the existence of a convex combination $\bar{\theta}$ such that $\sum_{i=1}^m \bar{\theta}_i A_i$ is Hurwitz stable and $\sum_{i=1}^m \bar{\theta}_i k_i = 0$. When this condition is met, a stabilizing switching rule can be determined. A potential difficulty of this type of method is that to find such $\bar{\theta}$ parameter is a Non-deterministic Polynomial-time hard (NP-hard) problem (SKAFIDAS et al., 1999). On the other hand, results based on (3.3), (3.4), which are presented in this work, do not depend explicitly on the existence of such $\bar{\theta}$ parameter to be applied, but the current version of the results depend on the existence of this $\bar{\theta}$ parameter to be feasible. This point is emphasized in (SCHARLAU et al., 2014), where it is shown that we can successfully check the design conditions for systems without a Hurwitz stable convex combination, however, we still do not know an LMI formulation to solve the problem automatically. This fact, discussed in detail in the Remark 3.4.1, reveals a potencial conservatism of the current version of the results proposed in this thesis, but important perspectives of improvement of the method, based on a better usage of the degrees of freedom in (3.4), remain open in order to overcome the conservative aspects above. It is important to emphasize that the existence of a convex combination $\bar{\theta}$ such that $\sum_{i=1}^m \bar{\theta}_i A_i$ is Hurwitz stable is only sufficient for the existence of a stabilizing switching rule. Several systems that do not satisfy this condition are known to have a stabilizing switching rule.

3.4 Switching rule design

Before presenting the main results, some auxiliary notation is introduced. Consider the vectors $\theta, \bar{\theta} \in \mathbb{R}^m$ with components $\theta_i, \bar{\theta}_i$ defined in (3.8), (3.9), respectively. Let \aleph_θ be the linear annihilator of θ as in Defini-

tion 2.2, and consider the following set of auxiliary matrices.

$$A = [A_1 \quad \dots \quad A_m] \quad , \quad K = [k_1 \quad \dots \quad k_m] \quad (3.12)$$

$$P = [P_1 \quad \dots \quad P_m] \quad , \quad S = [S_1 \quad \dots \quad S_m] \quad (3.13)$$

$$\alpha = [\alpha_1 I_n \quad \dots \quad \alpha_m I_n] \quad , \quad \mathbf{1}_m = [1 \quad \dots \quad 1] \in \mathbb{R}^{1 \times m} \quad (3.14)$$

$$C_a = [0_{(1 \times mn)} \quad \mathbf{1}_m] \quad , \quad C_b(\theta) = [\mathfrak{K}_\theta \otimes I_n \quad 0_{(rn \times m)}] \quad (3.15)$$

$$I_o = \mathbf{1}_m \otimes I_n \quad , \quad \mathfrak{K}_\theta \in \mathbb{R}^{r \times m} \quad (3.16)$$

$$P_{\bar{\theta}} = \sum_{i=1}^m \bar{\theta}_i P_i \quad , \quad S_{\bar{\theta}} = \sum_{i=1}^m \bar{\theta}_i S_i \quad (3.17)$$

$$\Psi = \begin{bmatrix} (A + \alpha)'P + P'(A + \alpha) - \alpha' P_{\bar{\theta}} I_o - I_o' P_{\bar{\theta}} \alpha & \star \\ K'P + S'A + 2S'\alpha & K'S + S'K \end{bmatrix} \quad (3.18)$$

Theorem 3.1 *Let \bar{x} be a given constant vector, representing the desired equilibrium point of the switched system (3.1), and suppose the state $x(t)$ is available from measurements. Consider the error system (3.8) under the Lemma 3.1. With the auxiliary notation (3.12)-(3.18), let Q_a be a basis for the null space of C_a and L be a matrix to be determined with the dimensions of $C_b(\theta)'$. Suppose $\exists P, S, L$ solving the following LMI problem.*

$$P_{\bar{\theta}} > 0 \quad , \quad S_{\bar{\theta}} = 0 \quad (3.19)$$

$$Q_a'(\Psi + LC_b(\theta) + C_b(\theta)'L')Q_a < 0 \quad , \quad \forall \theta \in \vartheta(\Theta) \quad (3.20)$$

Then the system (3.8) is globally asymptotically stable with the switching rule (3.3) and

$$V(e(t)) := \max_{i \in \mathbb{I}_m} \{v_i(e(t))\} \quad , \quad v_i(e(t)) = e(t)'P_i e(t) + 2e(t)'S_i \quad , \quad (3.21)$$

is a Lyapunov function for the switched system. \square

Proof: Firstly, observe that $v_i(e(t))$ in (3.3) are continuously differentiable functions, and thus $V(e(t))$ in (3.4) is a locally Lipschitz continuous function. As $\theta_i(e(t)) = 0$ for $i \notin \sigma(e(t))$ and $V(e(t)) = v_i(e(t))$, $\forall i \in \sigma(e(t))$, we get the identities

$$\sum_{i=1}^m \theta_i(e(t)) = \sum_{i \in \sigma(e(t))} \theta_i(e(t)) = 1 \quad (3.22)$$

and

$$\sum_{i=1}^m \theta_i(e(t)) v_i(e(t)) = \sum_{i \in \sigma(e(t))} \theta_i(e(t)) v_i(e(t)) = \left(\sum_{i \in \sigma(e(t))} \theta_i(e(t)) \right) V(e(t)) = V(e(t)). \quad (3.23)$$

Thus, the following holds.

$$V(e(t)) := \max_{i \in \mathbb{I}_m} \{v_i(e(t))\} = \sum_{i=1}^m \theta_i(e(t)) v_i(e(t)) \quad (3.24)$$

From (3.19) it follows that, for any element $\bar{\theta}$ of the unity simplex satisfying the condition (3.9), we have

$$\sum_{i=1}^m \bar{\theta}_i v_i(e(t)) = e(t)' \left(\sum_{i=1}^m \bar{\theta}_i P_i \right) e(t) + 2e(t)' \left(\sum_{i=1}^m \bar{\theta}_i S_i \right) = e(t)' P_{\bar{\theta}} e(t) > 0, \quad \forall e(t) \neq 0. \quad (3.25)$$

Keeping in mind that the maximum element of a finite set of real numbers is always greater than or equal to any convex combination of the elements of the set, it can be concluded from (3.24), (3.25) that $\forall e(t) \neq 0$ we have

$$V(e(t)) \geq e(t)' \left(\sum_{i=1}^m \bar{\theta}_i P_i \right) e(t) = e(t)' P_{\bar{\theta}} e(t) > 0. \quad (3.26)$$

Thus $V(e(t))$ is positive definite and radially unbounded as the right hand side of (3.26) is a positive definite quadratic form. Moreover, $v_i(e(t)) \leq \beta_i(\|e(t)\|)$ where $\beta_i(\|e(t)\|) := \|P_i\| \|e(t)\|^2 + 2\|S_i\| \|e(t)\|$. This shows that

$$\lambda_{\min}(P_{\bar{\theta}}) \|e(t)\|^2 \leq V(e(t)) \leq \max_{i \in \mathbb{I}_m} \{\beta_i(\|e(t)\|)\} \quad (3.27)$$

where the lower and upper bounds are class \mathcal{K}_∞ functions, as in Definition 2.3. Next, it is shown that $V(e(t))$ is strictly decreasing. With this purpose, note that for any point $e(t)$ and direction h , the directional derivative of $V(e(t))$

exists and is given by (LASDON, 1970, p.420)

$$\mathcal{D}_h V(e(t)) = \max_{i \in \sigma(e(t))} \nabla v_i(e(t)) h \quad (3.28)$$

where $\nabla v_i(e(t)) = 2(e(t)'P_i + S_i')$ denotes the gradient of $v_i(e(t))$.

With (3.8), consider the notation

$$f(e(t)) := \sum_{i=1}^m \theta_i(e(t)) (A_i e(t) + k_i) \quad (3.29)$$

and take the directional derivative in the direction $h = f(e(t))$. In the sequel we construct the expression (3.28) for the system (3.8). The first situation to be considered is when $\sigma(e(t))$ is singleton. In this case, as $\theta_i(e(t)) = 1$ for $i \in \sigma(e(t))$ and thus $\theta_i(e(t)) = 0$ for $i \notin \sigma(e(t))$, we can rewrite (3.28) as

$$\mathcal{D}_{f(e(t))} V(e(t)) = \sum_{i=1}^m \theta_i(e(t)) \nabla v_i(e(t)) f(e(t)). \quad (3.30)$$

Another situation of interest is when $\sigma(e(t))$ is not a singleton on a point “ $e(t)$ ” of a switching surface and the trajectory does not leave the switching surface at that point, *i.e.* $\sigma(e(t))$ remains constant during a certain time interval. In this case a sliding mode is occurring, and for all points of the trajectory $e(t)$ during this time interval we have

$$\begin{cases} v_i(e(t)) = v_j(e(t)) = V(e(t)) \\ \nabla v_i(e(t)) f(e(t)) = \nabla v_j(e(t)) f(e(t)) \end{cases}, \quad \forall i, j \in \sigma(e(t)). \quad (3.31)$$

In particular, as $\nabla v_i(e(t)) f(e(t)) = \nabla v_j(e(t)) f(e(t))$ and as $\theta_i(e(t)) = 0$ for $i \notin \sigma(e(t))$, we can also rewrite (3.28) as in (3.30).

The last situation to be analyzed is when $\sigma(e(t))$ is not a singleton on a point “ $e(t)$ ” of a switching surface and the trajectory leaves the switching surface at that point. In this situation, $\sigma(e(t))$ will change and, as $\sigma(e(t))$ is piecewise constant, the trajectory will move to a new region or switching surface under one of the two cases previously discussed. Thus, these points where σ is discontinuous correspond to isolated points of a system trajectory. Keeping in mind that $V(e(t))$ from (3.4) is locally Lipschitz continuous, we conclude that $V(e(t))$ is decreasing along any system trajectory $e(t)$ if it is decreasing in the two previous cases where (3.30) is valid. Observe that σ is piecewise constant and thus the behavior of V along a system trajectory in

the neighborhoods of the points where σ is discontinuous is characterized by (3.30).

From the above discussion, it is clear that the condition $\mathcal{D}_{f(e(t))}V(e(t)) < 0$, obtained from (3.30), guarantees the decreasing of $V(e(t))$ along any trajectory of the system (3.8) under the switching rule (3.3). Observe that as $V(e(t))$ is locally Lipschitz, it follows that the directional derivative and time derivative coincide almost everywhere, and $\mathcal{D}_{f(e(t))}V(e(t)) < 0$ guarantees the decreasing of $V(e(t))$ even for system trajectories moving along lines or surfaces where the gradient of $V(e(t))$ does not exist and thus the usual expressions for the time derivative cannot be used. See (FILIPPOV, 1988, p.155) for more details on this point.

For global stability it is required $\mathcal{D}_{f(e(t))}V(e(t)) < 0$, $\forall e(t) \neq 0$, $\forall \theta(e(t)) \in \Theta$. As $V(e(t))$ is positive definite from (3.27) and non increasing from $\mathcal{D}_{f(e(t))}V(e(t)) < 0$, we conclude that the origin is an equilibrium point of the system whenever these conditions are satisfied. The global asymptotic stability follows from the same arguments in (FILIPPOV, 1988, p.155).

Now, applying the S -Procedure to the condition $\mathcal{D}_{f(e(t))}V(e(t)) < 0$ and taking into account the constraint (3.26) that represents the relation $V(e(t)) - e(t)'P_{\theta}e(t) \geq 0$, we get

$$\mathcal{D}_{f(e(t))}V(e(t)) + 2\alpha_{\theta} (V(e(t)) - e(t)'P_{\theta}e(t)) < 0, \quad (3.32)$$

$\forall e(t) \neq 0$, $\forall \theta(e(t)) \in \Theta$, and $\alpha_{\theta} := \sum_{i=1}^m \alpha_i \theta_i(e(t)) > 0$ is a scaling factor with positive constants α_i chosen according to the Remark 3.4.1, introduced after the proof.

As, in general, $\theta(e(t))$ is multivalued and of difficult characterization, *i.e.* it is difficult to take into account the dependence of $\theta(e(t))$ with respect to $e(t)$, we will use a more conservative condition where $\theta(e(t))$ is replaced by an arbitrary time-varying parameter, namely θ , free to take any value in the unitary simplex Θ independently of $e(t)$. Now with the notation

$$P_{\theta} := \sum_{i=1}^m \theta_i P_i \quad , \quad A_{\theta} := \sum_{i=1}^m \theta_i A_i \quad , \quad K_{\theta} := \sum_{i=1}^m \theta_i k_i \quad , \quad S_{\theta} := \sum_{i=1}^m \theta_i S_i \quad , \quad (3.33)$$

$\mathcal{D}_{f(e(t))}V(e(t))$ from (3.30) and $V(e(t))$ from (3.24), it is possible to rewrite (3.32) as

$$\begin{bmatrix} e(t) \\ 1 \end{bmatrix}' \begin{bmatrix} A'_\theta P_\theta + P_\theta A_\theta + 2\alpha_\theta(P_\theta - P_{\bar{\theta}}) & \star \\ K'_\theta P_\theta + S'_\theta A_\theta + 2S'_\theta \alpha_\theta & 2K'_\theta S_\theta \end{bmatrix} \begin{bmatrix} e(t) \\ 1 \end{bmatrix} < 0. \quad (3.34)$$

Now define the following vector according to Definition 2.1,

$$e_\theta := \theta \otimes e = \begin{bmatrix} \theta_1 e(t) \\ \vdots \\ \theta_m e(t) \end{bmatrix} \in \mathbb{R}^{mn} \quad (3.35)$$

and note that $e(t) = I_o e_\theta$. Thus, we can rewrite (3.34) with the notation (3.12)-(3.18) as

$$\begin{bmatrix} e_\theta \\ \theta \end{bmatrix}' \Psi \begin{bmatrix} e_\theta \\ \theta \end{bmatrix} < 0. \quad (3.36)$$

Observe from (3.9) that $K\bar{\theta} = 0$ and from (3.19) that $S\bar{\theta} = 0$. With Ψ given in (3.18), it follows that the left side of the inequality (3.36) is null for $e(t) = 0$, that is

$$\begin{bmatrix} 0_{mn \times 1} \\ \bar{\theta} \end{bmatrix}' \Psi \begin{bmatrix} 0_{mn \times 1} \\ \bar{\theta} \end{bmatrix} = 0. \quad (3.37)$$

Therefore, it is possible to rewrite the left side of the inequality (3.36) by subtracting the null identity (3.37) from it as

$$\begin{bmatrix} e_\theta \\ \theta \end{bmatrix}' \Psi \begin{bmatrix} e_\theta \\ \theta \end{bmatrix} = \begin{bmatrix} e_\theta \\ \theta - \bar{\theta} \end{bmatrix}' \Psi \begin{bmatrix} e_\theta \\ \theta - \bar{\theta} \end{bmatrix} < 0. \quad (3.38)$$

With $C_a, C_b(\theta)$ from (3.15), it follows that

$$C_a \begin{bmatrix} e_\theta \\ \theta - \bar{\theta} \end{bmatrix} = 0 \quad , \quad C_b(\theta) \begin{bmatrix} e_\theta \\ \theta - \bar{\theta} \end{bmatrix} = 0. \quad (3.39)$$

Therefore, for any matrix L with suitable dimensions we can rewrite (3.38) as

$$\begin{bmatrix} e_\theta \\ \theta - \bar{\theta} \end{bmatrix}' (\Psi + LC_b(\theta) + C_b(\theta)'L') \begin{bmatrix} e_\theta \\ \theta - \bar{\theta} \end{bmatrix} < 0. \quad (3.40)$$

Taking into account the null space of C_a through the Finsler's Lemma, we get the LMI in (3.20) as a sufficient condition for $\mathcal{D}_{f(e(t))}V(e(t))$ in (3.30)

to satisfy $\mathcal{D}_{f(e(t))}V(e(t)) < 0$, $\forall e(t) \neq 0 \in \mathbb{R}^n$ and $\forall \theta \in \Theta$ (consequently $\forall \theta(e(t)) \in \Theta$), where $e(t) = 0$ is the desired equilibrium.

In summary, the inequality (3.27) shows that $V(e(t))$ is positive definite and radially unbounded. The expression (3.32) implies $V(e(t))$ is globally decreasing, even if sliding motions occur, and the global asymptotic stability follows from the same arguments in (FILIPPOV, 1988). \square

Remark 3.4.1 *Note that for the global stability problem considered in this chapter, a necessary condition for (3.34) to be satisfied is $A'_\theta P_\theta + P_\theta A_\theta + 2\alpha_\theta(P_\theta - P_{\bar{\theta}}) < 0$. As $\theta(e(t)) \in \Theta$, this condition implies, for $\theta(e(t)) = \bar{\theta}$, that $A'_\theta(\bar{\theta})P_\theta(\bar{\theta}) + P_\theta(\bar{\theta})A_\theta(\bar{\theta}) < 0$, which in turn implies that $A_\theta(\bar{\theta})$ must be Hurwitz stable, because $P_\theta(\bar{\theta}) = P_{\bar{\theta}} > 0$ from (3.19). The requirement of $A_\theta(\bar{\theta})$ being Hurwitz stable is removed if $\theta(e(t))$ is not allowed to take values in the whole simplex Θ , so that $\theta(e(t)) = \bar{\theta}$ cannot occur, which would characterize a situation where the equilibrium can be maintained without the intermittent switching of a sliding mode. However, note that it is hard to remove this requirement, specially because $\theta(e(t)) = \bar{\theta}$ may also occur for $e(t) \neq 0$.*

If there exists a suitable region of the simplex Θ that contains the equilibrium $\bar{\theta}$ and that is known to be free of sliding motions, then it is possible to consider problems in which $A_\theta(\bar{\theta})$ is not Hurwitz stable after minor changes in the Theorem 3.1. This point will be addressed in future research. Observe that the existence of $\bar{\theta}$ such that $A_{\bar{\theta}}$ is Hurwitz stable is a sufficient condition for the existence of a stabilizing switching rule (FERON, 1996). This fact suggests the conditions of the Theorem 3.1 may be conservative because $A_{\bar{\theta}}$ Hurwitz is only necessary for this theorem. A study of the conservativeness of the conditions of the Theorem 3.1 is another point to be investigated, as discussed in Section 3.3.

Observe in addition that we can rewrite the inequality above as $(A_\theta + \alpha_\theta I_n)'P_\theta + P_\theta(A_\theta + \alpha_\theta I_n) - 2\alpha_\theta P_{\bar{\theta}} < 0$. As $\alpha_\theta P_{\bar{\theta}} > 0$, this condition suggests the constants α_i can be chosen as in (TROFINO et al., 2009a) in the interval $0 < \alpha_i < |\underline{\lambda}_i|$ where $\underline{\lambda}_i$ denotes the real part of the stable (negative) eigenvalue of A_i nearest to the imaginary axis and $|\underline{\lambda}_i|$ is its absolute value. The idea is to get exponential decreasing of $V(e(t))$ in the directions where the negative term $-2\alpha_\theta e(t)'P_{\bar{\theta}}e(t)$ in (3.32) can be neglected. In this case, (3.32) becomes the exponential performance requirement of (TROFINO et al., 2009a).

Notice that the choice of the parameters α_i and the exponential decay analysis previously presented are not valid for the case where the matrices P_i are the same for all operation modes, let us say $P_i = P_u, \forall i \in \mathbb{I}_m$. See that in

this case we would have $P_\theta = P_{\bar{\theta}} = P_u$ and then the terms in which α_θ appears in the previous inequality disappear and the stability condition to be satisfied becomes $A'_\theta P_u + P_u A_\theta < 0$, which requires A_θ to be Hurwitz stable $\forall \theta \in \Theta$. Therefore, for this case the constants α_i can be chosen freely, just aiming to get a feasible solution for the LMIs. \square

Remark 3.4.2 By observing the differences between Equations (3.36) and (3.38), it is possible to check that the part of the vector K_θ that is the same for all modes is cancelled and consequently does not appear in the LMIs of the Theorem 3.1. To show this, recall from Lemma 3.1, that in equilibrium we have $K_{\bar{\theta}} = 0$, and note that it is possible to replace K_θ from Equation (3.36) by $K_\theta - K_{\bar{\theta}}$, which appears in Equation (3.38). Now suppose the notation $k_i = h_0 + h_i$, $i \in \mathbb{I}_m$, where h_0 is the part of k_i that is common to all the modes and h_i the part that is dependent of each mode. Thus, $K_\theta = h_0 + h_\theta$ and $K_{\bar{\theta}} = h_0 + h_{\bar{\theta}}$ and hence $K_\theta - K_{\bar{\theta}} = h_0 + h_\theta - h_0 - h_{\bar{\theta}} = h_\theta - h_{\bar{\theta}}$.

The fact that the common part of the vectors k_i do not need to be considered in the LMIs may be of great interest for some systems, specially those containing uncertain variables or variables that are difficult to express in terms of LMIs in case they affect all operation modes equally and only through the vector k_i . Finally, as the LMIs become independent of these variables, the switching rule design is robust in relation to these variables. This observation will be explored in more detail in the next chapters. \square

3.4.1 Partial state measurement

The results of the Theorem 3.1 are essentially state feedback: the complete state of the system is necessary to determine the active mode according to the switching rule (3.3). In practice, however, the whole state is often not available. In the sequel, we introduce a switching rule based on output feedback, *i.e.* partial state measurements. Consider the system (3.1) with a measurement vector $y(t) = C_i x(t) \in \mathbb{R}^{g_i}$, where $C_i \in \mathbb{R}^{g_i \times n}$, $\forall i \in \mathbb{I}_m$, are given matrices. Define the output tracking error

$$\varepsilon(t) = y(t) - C_i \bar{x} = C_i e(t). \quad (3.41)$$

Assume that the auxiliary functions $v_i(e(t))$, $i \in \mathbb{I}_m$, have the structure

$$P_i := P_0 + C_i' Q_i C_i \quad , \quad S_i := S_0 + C_i' R_i \quad , \quad \forall i \in \mathbb{I}_m \quad , \quad (3.42)$$

where $P_0 = P'_0 \in \mathbb{R}^{n \times n}$, $S_0 \in \mathbb{R}^n$, $R_i \in \mathbb{R}^{g_i}$, $Q_i = Q'_i \in \mathbb{R}^{g_i \times g_i}$. In this case, the auxiliary functions $v_i(e(t))$ can be rewritten as

$$v_i(e(t)) = e(t)'(P_0 + C'_i Q_i C_i)e(t) + 2e(t)'(S_0 + C'_i R_i) \quad (3.43)$$

$$= e(t)'P_0 e(t) + 2e(t)'S_0 + \mu_i(\varepsilon(t)), \quad (3.44)$$

where

$$\mu_i(\varepsilon(t)) := \varepsilon(t)'Q_i \varepsilon(t) + 2\varepsilon(t)'R_i. \quad (3.45)$$

Consequently,

$$\max_{i \in \mathbb{I}_m} \{v_i(e(t))\} = e(t)'P_0 e(t) + 2e(t)'S_0 + \max_{i \in \mathbb{I}_m} \{\mu_i(\varepsilon(t))\} \quad (3.46)$$

and from (3.3) the switching rule becomes a function of the output tracking error as

$$\arg \max_{i \in \mathbb{I}_m} \{v_i(e(t))\} = \arg \max_{i \in \mathbb{I}_m} \{\mu_i(\varepsilon(t))\} = \sigma(\varepsilon(t)). \quad (3.47)$$

This shows that the Theorem 3.1 can be directly applied to cope with the case of partial state information by introducing the constraints (3.42) on the structure of the matrices P_i, S_i .

3.5 Numerical examples

In the following examples, we have used the software Matlab, with the computational package SeDuMi (STURM, 2001), through the parser YALMIP (LÖFBERG, 2004), to solve the LMIs and Simulink to obtain the trajectories of the switched systems.

Example 3.1 (Buck-Boost) Consider the Buck-Boost converter presented in the Figure 18 with a linear load (resistor R). The constant parameters of the system are given in the Table 2 and D is considered as an ideal diode.

Assuming as the system states the current flowing through the inductor L (x_1) and the voltage over the output capacitor C (x_2), we have the state space representation (3.1) with two subsystems, $\mathbb{I}_m = \{1, 2\}$, depending on

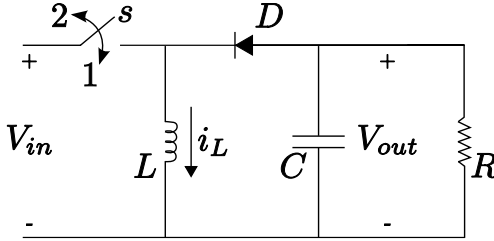


Figure 18: Buck-Boost converter used in the Example 3.1.

Parameter	Value
V_{in}	15V
L	10^{-3}H
C	10^{-6}F
R	30Ω

Table 2: Data of the Buck-Boost converter used in the Example 3.1.

the position of the switch s , where

$$A_1 = \begin{bmatrix} 0 & 0 \\ 0 & -1/RC \end{bmatrix}, A_2 = \begin{bmatrix} 0 & 1/L \\ -1/C & -1/RC \end{bmatrix}, b_1 = \begin{bmatrix} V_{in} \\ L \\ 0 \end{bmatrix}, b_2 = \begin{bmatrix} 0 \\ 0 \\ 0 \end{bmatrix}. \quad (3.48)$$

The eigenvalues of A_1 and A_2 are, respectively, $\{-33333.34, 0\}$ and $\{-16666.7 \pm j26874.1\}$. According to the Remark 3.4.1, the design parameters were chosen as $\alpha_1 = 333$ and $\alpha_2 = 166$.

The desired equilibrium point \bar{x} and the constants k_i from (3.2) are

$$\bar{x} = \begin{bmatrix} \frac{V_{out}^2 - V_{out}V_{in}}{V_{in}R} \\ V_{out} \end{bmatrix}, \quad k_1 = \begin{bmatrix} \frac{V_{in}}{L} \\ -\frac{V_{out}}{RC} \end{bmatrix}, \quad k_2 = \begin{bmatrix} \frac{V_{out}}{L} \\ -\frac{V_{out}^2}{V_{in}RC} \end{bmatrix}, \quad (3.49)$$

where V_{out} is the desired value of the regulated output voltage. Based on the Lemma 3.1, the following relations can be established, where we can see that

the output voltage has opposite polarity when compared to the input:

$$\frac{V_{out}}{V_{in}} = -\frac{\bar{\theta}_1}{\bar{\theta}_2} = -\frac{\bar{\theta}_1}{1 - \bar{\theta}_1} \quad (3.50)$$

The Equation (3.50) also shows that the converter operates as a Buck if $\bar{\theta}_1 < 0.5$, and as a Boost if $\bar{\theta}_1 > 0.5$. Therefore, there exists a convex combination $\bar{\theta}$ for any desired output voltage, differently of what would happen for a Buck converter or for a Boost converter, for the reasons shown in Section 2.2.2.2. Note that the subsystem 1 is not Hurwitz stable, however any convex combination of the two subsystems is stable (except the one with $\bar{\theta}_1 = 1$).

Assume now that $V_{out} = -9V$, which means that the converter operates as a Buck. Solving the LMIs of the Theorem 3.1, we get the matrices P_1, S_1, P_2, S_2 , from which the switching rule (3.3) can be computed.

The switched system response to the zero initial state is shown in Figure 19. Observe that the output voltage is correctly regulated. The phase plane of the tracking error is also shown in Figure 19. Note that, when the trajectory touches the switching surface for the second time, a sliding motion occurs driving the error towards the origin.

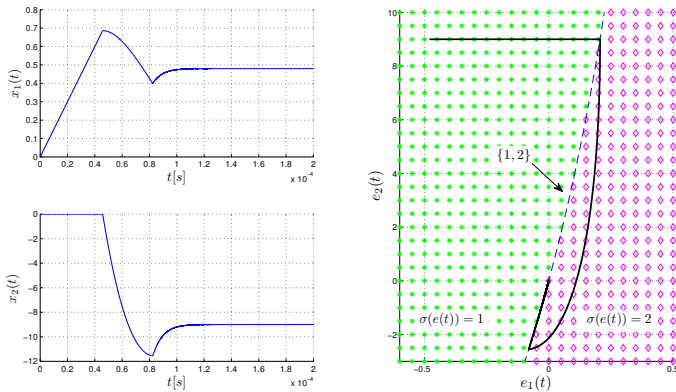


Figure 19: Buck-Boost converter operating as a Buck with $V_{out} = -9V$.

The case where $V_{out} = -21V$, which means the converter operates as a Boost, was also considered. The system response and the phase plane are shown in the Figure 20, where one can observe that the output voltage is also

correctly regulated in this case. There are several switchings in finite time before the sliding motion starts driving the error to the origin.

The oscillations of the regulated output could be attenuated by including a performance requirement to the problem. The Theorem 3.1 deals only with the regulation problem. However, according to Remark 3.4.1, it is possible to improve the transient response with a suitable choice of the parameters α_i . It is important to emphasize that feasibility of the conditions in Theorem 3.1 typically occurs for a wide range of these parameters. For this converter, in particular, the range is approximately $\alpha_i \in \{20|\lambda_i|, |\lambda_i|/1000\}$, where λ_i denotes the real part of the stable eigenvalue of A_i nearest to the imaginary axis. Typically, the response is fast, often oscillatory, for small values of α_i , and slow, often damped, for large values of α_i . The Figure 21 shows the system response in both Buck and Boost operations for a switching rule designed with $\alpha_1 = 24.975 \times 10^3$ and $\alpha_2 = 12.450 \times 10^3$, which corresponds to $\alpha_i = 0.75 |\lambda_i|$. \square

For several examples of switching rule design based on the ‘min’ function (3.11) with application to DC/DC converters, we recommend the reference (MAINARDI JÚNIOR et al., 2012). Numerical comparisons are not performed in this thesis for the reasons exposed in Section 3.3.

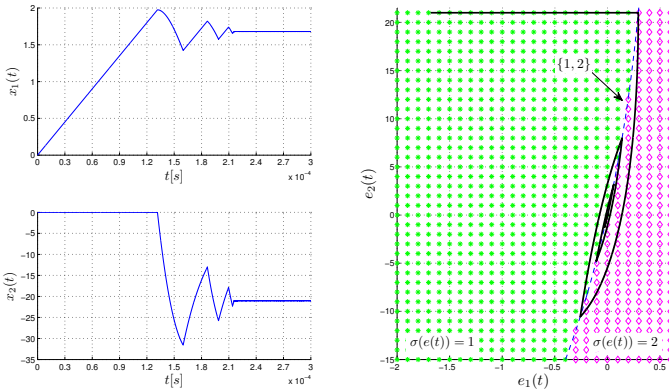


Figure 20: Buck-Boost converter operating as a Boost with $V_{out} = -21V$.

Example 3.2 (Three subsystems) In this example, we consider a system in the state space representation (3.2) with three subsystems, $\mathbb{I}_m = \{1, 2, 3\}$,

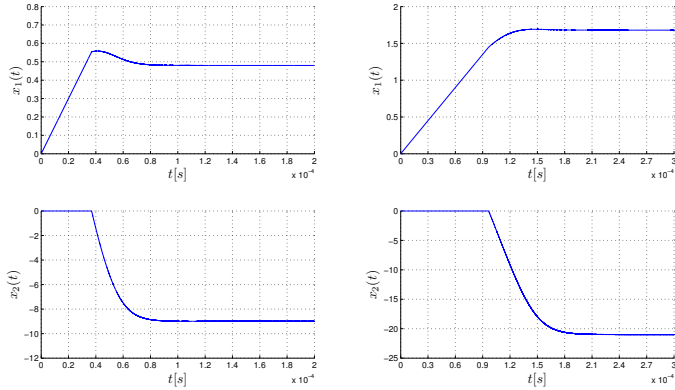


Figure 21: Buck-Boost converter operating as a Buck (left side curves) and as a Boost (right side curves) with a switching rule designed with an adequate choice of the parameters α_i .

where $A_1, A_2, A_3, k_1, k_2, k_3$ are respectively:

$$\begin{bmatrix} 0 & 1 \\ -1 & -\beta \end{bmatrix}, \begin{bmatrix} 0 & 1 \\ -2\beta & -2 \end{bmatrix}, \begin{bmatrix} 0 & 1 \\ -3 & -3 \end{bmatrix}, \begin{bmatrix} 1 \\ 0 \end{bmatrix}, \begin{bmatrix} 1 \\ 1 \end{bmatrix}, \begin{bmatrix} -2 \\ -1 \end{bmatrix}. \quad (3.51)$$

For this system the desired equilibrium is the origin and $\bar{\theta}_1 = \bar{\theta}_2 = \bar{\theta}_3 = 1/3$ satisfies the Lemma 3.1. As $\bar{\theta}$ has an interpretation similar to the duty cycle, we must have a sliding mode among the three subsystems at the equilibrium point.

Let us start with the case where $\beta = 1$, where all subsystems are Hurwitz stable, but the desired equilibrium point (the origin) is not an equilibrium of any subsystem. The eigenvalues of A_1, A_2 and A_3 are, respectively, $\{-0.5 \pm j0.866\}$, $\{-1 \pm j\}$, and $\{-1.5 \pm j0.866\}$. According to Remark 3.4.1, observe that the matrix $A_{\bar{\theta}}(\bar{\theta}) = \sum_{i=1}^3 A_i \bar{\theta}_i$ is Hurwitz stable and the design parameters α_i were chosen as $\alpha_1 = 0.25$, $\alpha_2 = 0.50$, and $\alpha_3 = 0.75$. The Theorem 3.1 was applied to get the matrices P_i, S_i , $i \in \mathbb{I}_m$, from which the switching rule (3.3) is computed. Simulation results for different initial conditions are shown in the phase plane of the Figure 22. It can be seen that in all cases the error system states converge to the origin. When the trajectory reaches the origin, a sliding mode involving the three subsystems occurs,

as expected. Sliding motions outside the origin also occur in the switching surfaces of the subsystems $\{1,2\}$, $\{2,3\}$ and $\{3,1\}$, although for the cases presented in the Figure 22 only sliding motions on $\{2,3\}$ and $\{3,1\}$ were observed.

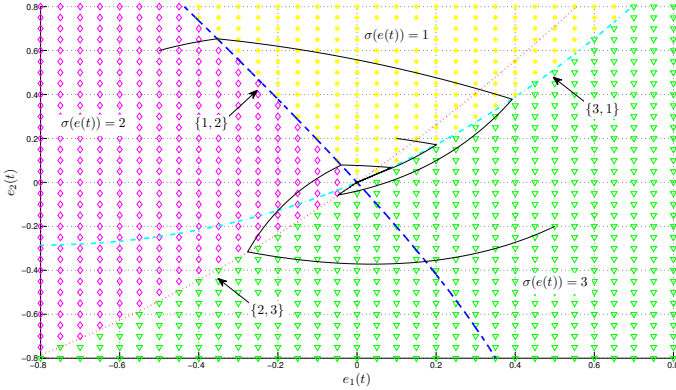


Figure 22: Stable subsystems ($\beta = 1$). Solid (black) curves are the error trajectories; dashed curves (in assorted colors) are switching surfaces.

Next consider the case where $\beta = -1$. In this situation, the system has two unstable subsystems, A_1 and A_2 with eigenvalues $\{0.5 \pm j0.866\}$ and $\{0.73, -2.73\}$ respectively, and one Hurwitz stable subsystem, A_3 with eigenvalues $\{-1.5 \pm j0.866\}$. The design parameters α_i , $i \in \mathbb{I}_m$, and $\bar{\theta}$ have the same values used in the previous case and $A_{\bar{\theta}}$ is also Hurwitz stable in this instance. The Figure 23 presents the simulation results in a phase plane for one specific initial condition. As in the previous occasion, a sliding motion among the three subsystems is observed at the origin; outside the origin two sliding motions occur for this trajectory in the switching surfaces of the subsystems $\{1,2\}$ and $\{3,1\}$. \square

3.6 Concluding remarks

In this chapter, the theoretical basis and formulation required for the design of the proposed switching rules were presented. The results were illustrated through two examples of switched systems control: a Buck-Boost converter and a system with three operation modes. It is shown in the ex-

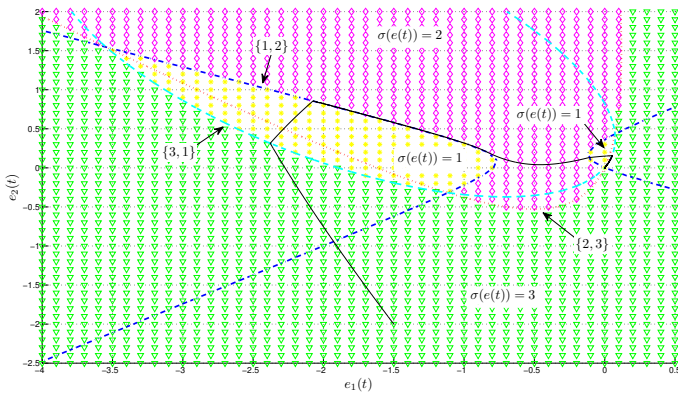


Figure 23: Unstable subsystems ($\beta = -1$). Solid (black) curve is a error trajectory; dashed curves (in assorted colors) are switching surfaces.

amples that the technique can be applied to systems with unstable operation modes, provided that the system has a stable convex combination at the equilibrium point, otherwise it is not possible to find a solution for the proposed LMIs. The case of systems without a stable convex combination at the equilibrium is a topic for future research.

The switching rule proposed in this chapter can be extended in several directions. For instance, it is possible to include the optimization criterion H_∞ and guaranteed cost performance. The case of affine subsystems is easily recovered from (TROFINO et al., 2009b) if the equilibrium point ($\bar{\theta}$) is not uncertain. Expansions to some classes of nonlinear switched systems will be presented in the next chapters.

Finally, the switching rules developed in this work are allowed to produce ideal sliding modes, which in theory may have infinite switching frequency. The extension to the case where dwell time constraints are applied to limit the switching frequency are currently being investigated and will be presented in future work.

4 CONTROL OF SWITCHED SYSTEMS WITH SECTOR-BOUNDED NONLINEARITIES

4.1 Introduction

Among the switching rule design techniques, some of them are based on Lyapunov functions and LMI techniques, as for instance in (BOLZERN; SPINELLI, 2004) and (TROFINO et al., 2011). The interest of recasting the problem as LMIs is that it is easy to incorporate new constraints to the problem, provided that these constraints can be also expressed as LMIs, and the availability of powerful computational packages to solve the LMI problems. However, extending the results obtained for the class of linear switched systems to the class of nonlinear switched systems is a difficult task, and the design conditions for general nonlinear systems usually result in conservative LMIs. A possible way to reduce the conservatism is to take advantage of the structure of a specific class of nonlinear functions, such as the sector-bounded functions of the state (see (KHALIL, 2002)).

Renewable energy generation systems, as the PV systems, can be viewed as nonlinear switched systems due to the combination of power electronic devices and the nonlinear model of the generation apparatus. For PV systems in particular, one of the biggest challenges for control is the fact that the system presents a highly nonlinear model. This nonlinear behavior is due to the I - V characteristic of the PV array described in Section 2.2.1. The I - V characteristic curves of devices in general are usually sector-bounded nonlinear functions of the state, not only for the PV array but for any element that presents a nonlinear resistance characteristic such as tunnel diodes (DEMASSA, 1970), (NG, 2002), (WALKER; COAKLEY; SPLETT, 2004), for instance.

This chapter presents an extension of the results from Chapter 3 (TROFINO et al., 2011) to the class of nonlinear switched systems containing state-dependent sector-bounded nonlinear functions. A multiple Lyapunov function approach is used to design switching rules based on the ‘max’ composition that guarantee global asymptotic stability of the switched system with convergence to a desired equilibrium point even if sliding motions occur on any switching surface of the system. An extension to the switching rule design based on partial state measurement is presented. It is also shown that, depending on the system structure, it is not necessary to know all the state vector at the desired equilibrium point *a priori* for the design of the switching rule.

4.2 Preliminaries

Consider a nonlinear switched system composed of m affine subsystems as indicated below.

$$\dot{x}(t) = A_i x(t) + b_i + B \psi_x(q_x(x(t))), \quad i \in \mathbb{I}_m := \{1, \dots, m\}, \quad (4.1)$$

where $x \in \mathbb{R}^n$ is the system state, $\psi_x : \mathbb{R} \mapsto \mathbb{R}$ is a nonlinear function of the state-dependent scalar

$$q_x(x(t)) := C_q x(t), \quad (4.2)$$

with a given vector $C_q \in \mathbb{R}^{1 \times n}$, and $A_i \in \mathbb{R}^{n \times n}$, $b_i \in \mathbb{R}^n$, $B \in \mathbb{R}^n$ are given matrices of structure.

The problem of concern is to design a switching rule that asymptotically drives the system state to a constant reference \bar{x} . In other words, the desired equilibrium point \bar{x} of the (closed-loop) switched system must be asymptotically stable. In the sequel, we will consider the case of full state information. The case of partial state information will be treated in Section 4.3.1.

Given \bar{x} , we can represent the tracking error dynamics as a switched system with the following subsystems

$$\dot{e}(t) = A_i e(t) + A_i \bar{x} + b_i + B \psi(q(e(t))), \quad i \in \mathbb{I}_m, \quad (4.3)$$

where

$$\psi(q(e(t))) := \psi_x(q(e(t)) + C_q \bar{x}) = \psi_x(q_x(x(t))), \quad (4.4)$$

$$e(t) := x(t) - \bar{x}, \quad q(e(t)) := C_q e(t). \quad (4.5)$$

Note that $\psi(q(e(t)))$ is just $\psi_x(q_x(x(t)))$ rewritten as a function of $e(t)$. Now consider the following decomposition of A_i, b_i .

$$A_i = \bar{A}_o + \bar{A}_i, \quad b_i = \bar{b}_o + \bar{b}_i, \quad (4.6)$$

where \bar{A}_o, \bar{b}_o denote the component of A_i, b_i , respectively, that is common for all $i \in \mathbb{I}_m$ and \bar{A}_i, \bar{b}_i contain the terms that vary according to i . Now defining

$$h_o = \bar{A}_o \bar{x} + \bar{b}_o, \quad h_i = \bar{A}_i \bar{x} + \bar{b}_i, \quad (4.7)$$

we can rewrite $A_i \bar{x} + b_i$ as $h_o + h_i$.

Assume the sliding mode dynamics of the system can be represented

as convex combinations of the subsystems as in Definition 3.1 (FILIPPOV, 1988). Therefore, the global switched system, that includes the subsystem dynamics and the sliding mode dynamics that may eventually occur on any switching surface, is represented by

$$\dot{e}(t) = \sum_{i=1}^m \theta_i(e(t))(A_i e(t) + h_o + h_i + B\psi(q(e(t))))), \quad \theta(e(t)) \in \Theta, \quad (4.8)$$

where $\theta(e(t))$ is the vector with entries $\theta_i(e(t))$ and Θ is the unitary simplex defined in (3.7).

Recall that a sliding motion may be occurring at a point $e(t)$ if it is possible to find a convex combination of the subsystem vector fields such that $\dot{e}(t)$ is a vector that belongs to the tangent hyperplane of the switching surface at the point $e(t)$.

In order to achieve the tracking objective, the origin must be an asymptotically stable equilibrium point of (4.8), thus it is necessary that $\sum_{i=1}^m \theta_i(0)k_i = 0$, where $\{\theta_i(0), i \in \mathbb{I}_m\}$ are piecewise continuous functions of time and characterize the equilibrium condition. Then, let us define $\bar{\psi} := \psi(0)$ and constant scalars $\bar{\theta}_i$ satisfying the following lemma.

Lemma 4.1 *The origin is an equilibrium point of (4.8) iff there exists $\bar{\theta} \in \Theta$ such that*

$$\sum_{i=1}^m \bar{\theta}_i (h_o + h_i + B\bar{\psi}) = 0. \quad (4.9)$$

□

Proof: Set $\dot{e}(t) = 0$ and $e(t) = 0$ in (4.8). □

While $\theta(0)$ is associated with the equilibrium condition, and in general is unknown and possible not constant, the parameter $\bar{\theta}$ is an auxiliary constant representing one particular value that $\theta(0)$ may take.

As (4.9) is a zero identity, we can subtract the left-hand side of (4.9) from (4.8) and rewrite the error dynamics in the following more convenient form.

$$\dot{e} = A_\theta e + k_\theta, \quad \theta(e) \in \Theta, \quad (4.10)$$

where $A_\theta = \sum_{i=1}^m \theta_i(e)A_i$ and $k_\theta = \sum_{i=1}^m \theta_i(e)k_i$ with

$$k_i = h_i - h_{\bar{\theta}} + B\Delta\psi, \quad (4.11)$$

where $h_{\bar{\theta}} = \sum_{i=1}^m \bar{\theta}_i h_i$ and $\Delta\psi = \psi - \bar{\psi}$. Note that the operation that eliminates the term h_o , commented in the Remark 3.4.2, was incorporated into the

system definition in this chapter.

4.2.1 Switching rule using a max composition

Thanks to the error system (4.10), the problem of concern can be restated as to design a switching rule that asymptotically drives the error state to the origin. For this purpose, consider the switching rule given by

$$\sigma(e) := \arg \max_{i \in \mathbb{I}_m} \{v_i(e)\} \quad , \quad v_i(e) = e' P_i e + 2e' (S_i - S_{\bar{\theta}}) \quad , \quad (4.12)$$

where $S_{\bar{\theta}} := \sum_{i=1}^m \bar{\theta}_i S_i$ and $P_i \in \mathbb{R}^{n \times n}$ and $S_i \in \mathbb{R}^{n \times 1}$ are matrices to be determined. The set valued signal $\sigma(e) : \mathbb{R}^n \mapsto \mathcal{P}(\mathbb{I}_m)$ is a map specifying the set of subsystems having ‘maximum energy’. For instance, $\sigma(e(t_0)) = \{j, k, l\}$ means that at instant $t = t_0$ the error trajectory is at the switching surface defined from the subsystems $\{j, k, l\}$ because $v_j(e(t_0)) = v_k(e(t_0)) = v_l(e(t_0)) = \max_{i \in \mathbb{I}_m} \{v_i(e(t_0))\}$. Whenever the set $\sigma(e)$ has more than one element, a sliding mode may be occurring at that instant and the elements of convex combination, the entries of the vector $\theta(e)$, are such that $\theta_i(e) = 0$ if $i \notin \sigma(e)$. We refer the reader to (FILIPPOV, 1988, p.50) for details on this point. It is assumed that $\theta(e(t))$ and $\sigma(e(t))$ are respectively piecewise continuous and piecewise constant. Under these regularity assumptions, the vector fields of (4.10) have a finite number of discontinuous points on any system trajectory.

4.2.2 Sector-bounded nonlinearity

Consider the following definition.

Definition 4.1 (Sector-bounded function) *A function $\varphi(q) : \mathbb{R} \mapsto \mathbb{R}$, with $\varphi(0) = 0$, is said to be in sector $[l, u]$ if for all $q \in \mathbb{R}$, $p = \varphi(q)$ lies between $p = lq$ and $p = uq$. Then, the inequality*

$$(p - uq)(p - lq) \leq 0 \quad (4.13)$$

holds for all q , $p = \varphi(q)$. □

For example, a visual representation of a particular¹ sector-bounded function and its sector bounds can be seen in Figure 24.

¹The plot in Figure 24 was generated with the nonlinear function $\varphi(q) = \sin(3\pi q)/5 + q$ and sector bounds $[l, u] = [2 + 3\pi/5, 0.5]$.

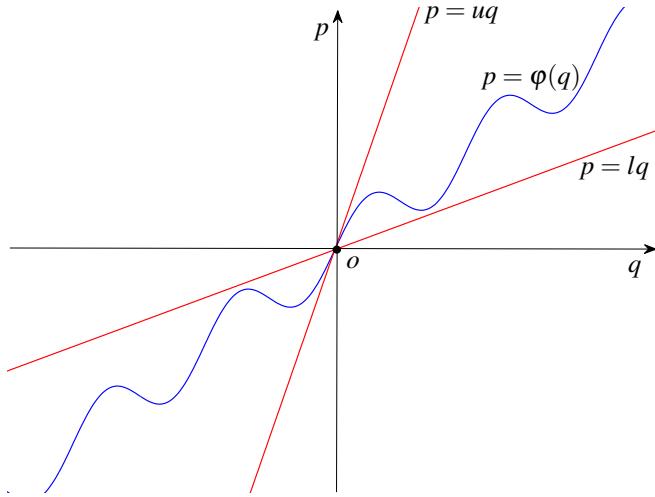


Figure 24: Example of sector bounds (red lines) for a particular nonlinear function (blue curve).

Consider the Definition 4.1 with the nonlinear function $p = \Delta\psi(q)$, $q = C_q e$, and note that $\Delta\psi = 0$ for $C_q e = 0$. Therefore, it is possible to rewrite (4.13) as

$$-(\Delta\psi - uC_q e)(\Delta\psi - lC_q e) \geq 0. \quad (4.14)$$

Remark 4.2.1 *There always exists a sector $[l, u]$ large enough to contain a continuous nonlinear function $\varphi(q)$. For instance, the sector $[-\infty, \infty]$ contains all points $(p, q) \in \mathbb{R}^2$. See (KHALIL, 2002, p.232) for more details on sector-bounded nonlinear functions. \square*

4.3 Switching rule design

Before presenting the theorem for the switching rule design, let us introduce some auxiliary notation. Let $\mathfrak{K}_\theta : \mathbb{R}^m \mapsto \mathbb{R}^{r \times m}$ be a linear annihilator of θ as in Definition 2.2, *i.e.* \mathfrak{K}_θ is a linear function of θ with $\mathfrak{K}_\theta \theta = 0$, $\forall \theta \in \Theta$, let $\alpha_i, i \in \mathbb{I}_m$, be given positive scalars chosen according to Remark

3.4.1 and consider the following set of auxiliary matrices.

$$A = [A_1 \quad \dots \quad A_m], \quad H = [h_1 \quad \dots \quad h_m] \quad (4.15)$$

$$\alpha = [\alpha_1 I_n \quad \dots \quad \alpha_m I_n], \quad P = [P_1 \quad \dots \quad P_m], \quad S = [S_1 \quad \dots \quad S_m] \quad (4.16)$$

$$\mathbf{1}_m = [1 \quad \dots \quad 1] \in \mathbb{R}^{1 \times m}, \quad I_o = \mathbf{1}_m \otimes I_n \quad (4.17)$$

$$C_a = [0_{(1 \times mn)} \quad \mathbf{1}_m \quad 0], \quad C_b(\theta) = [\mathfrak{K}_\theta \otimes I_n \quad 0_{(m \times m+1)}] \quad (4.18)$$

$$L_a(\theta) = \sum_{i=1}^m \theta_i L_i, \quad P_{\bar{\theta}} = \sum_{i=1}^m \bar{\theta}_i P_i \quad (4.19)$$

$$\Gamma = \begin{bmatrix} -l'_o C'_q(u) C_q I_o & \star & \star \\ 0_{m \times mn} & 0_m & \star \\ C_q I_o (u+l)/2 & 0_{1 \times m} & -1 \end{bmatrix} \quad (4.20)$$

$$\Psi = \begin{bmatrix} A'P + P'A + (P - P_{\bar{\theta}} I_o)' \alpha + \alpha' (P - P_{\bar{\theta}} I_o) & \star & \star \\ H'P + S'A + 2S' \alpha & H'S + S'H & \star \\ B'P & B'S & 0 \end{bmatrix} \quad (4.21)$$

In this chapter, annihilators are used jointly with the Finsler's Lemma to reduce the conservativeness of parameter dependent LMIs as in (TROFINO; DEZUO, 2013).

Theorem 4.1 *Let \bar{x} be a given constant vector representing the desired equilibrium point of the system (4.1), and suppose that $x(t)$ is available online. Consider the error system (4.10) and let $\bar{\theta} \in \Theta$ be a given constant vector according to Lemma 4.1. With the auxiliary notation (4.15)-(4.21), let $L_b, L_i, i \in \mathbb{I}_m$, be matrices to be determined with the dimensions of $C_b(\theta)', C'_a$, respectively.*

Suppose that $\exists P, S, \tau, L_b, L_i, i \in \mathbb{I}_m$, solving the following LMI problem.

$$P_{\bar{\theta}} > 0 \quad (4.22)$$

$$\Psi + \tau \Gamma + L_b C_b(\theta) + C_b(\theta)' L'_b + L_a(\theta) C_a + C'_a L_a(\theta)' < 0, \quad \forall \theta \in \vartheta(\Theta) \quad (4.23)$$

Then the nonlinear switched system (4.10) is globally asymptotically stable

with the switching rule (4.12) and

$$V(e) := \max_{i \in \mathbb{I}_m} \{v_i(e)\} \quad , \quad v_i(e) = e' P_i e + 2e' (S_i - S_{\bar{\theta}}) \quad , \quad (4.24)$$

is a Lyapunov function for the system. \square

Proof: The proof consists of showing that if the LMIs (4.22) and (4.23) are satisfied, then the continuous function $V(e)$ defined in (4.24) satisfies the conditions

$$\phi_1(e) \leq V(e) \leq \phi_2(e) \quad , \quad (4.25)$$

$$\mathcal{D}_h V(e) \leq -\phi_3(e) \quad , \quad (4.26)$$

where $\phi_1(e)$, $\phi_2(e)$, and $\phi_3(e)$, are continuous positive definite functions and $\mathcal{D}_h V(e)$ is the Dini's directional derivative of $V(e)$ in the direction h , and is given by (LASDON, 1970, p.420)

$$\mathcal{D}_h V(e) = \max_{i \in \sigma(e)} \nabla v_i(e) h \quad , \quad (4.27)$$

where $\nabla v_i(e) = 2(e' P_i + S'_i - S'_{\bar{\theta}})$ denotes the gradient of $v_i(e)$. The local asymptotic stability follows from (4.25), (4.26) using the same arguments in (FILIPPOV, 1988, p.155).

First, it will be demonstrated that the condition (4.25) is satisfied. As $\theta_i(e) = 0$ for $i \notin \sigma(e)$ and $V(e) = v_i(e)$, $\forall i \in \sigma(e)$, we get the identities below.

$$\sum_{i=1}^m \theta_i(e) = \sum_{i \in \sigma(e)} \theta_i(e) = 1 \quad (4.28)$$

$$\sum_{i=1}^m \theta_i(e) v_i(e) = \sum_{i \in \sigma(e)} \theta_i(e) v_i(e) = \sum_{i \in \sigma(e)} \theta_i(e) V(e) = V(e) \quad (4.29)$$

Therefore, the following is true.

$$V(e) = \max_{i \in \mathbb{I}_m} \{v_i(e)\} = \sum_{i=1}^m \theta_i(e) v_i(e) \quad (4.30)$$

Keeping in mind that $\sum_{i=1}^m \bar{\theta}_i S_i = S_{\bar{\theta}}$, we get that

$$\sum_{i=1}^m \bar{\theta}_i (S_i - S_{\bar{\theta}}) = S_{\bar{\theta}} - S_{\bar{\theta}} = 0 \quad (4.31)$$

and from (4.12), (4.19), (4.31) it follows that

$$\sum_{i=1}^m \bar{\theta}_i v_i(e) = e' \left(\sum_{i=1}^m \bar{\theta}_i P_i \right) e + 2e' \sum_{i=1}^m \bar{\theta}_i (S_i - S_{\bar{\theta}}) = e' P_{\bar{\theta}} e. \quad (4.32)$$

Note that the maximum element of a finite set of real numbers is always greater than or equal to any convex combination of the elements of the set. Therefore, we can conclude from (4.22), (4.30), (4.32) that $\forall e \neq 0$ we have

$$V(e) \geq \sum_{i=1}^m \bar{\theta}_i v_i(e) = e' P_{\bar{\theta}} e > 0. \quad (4.33)$$

Thus, $V(e)$ is positive definite and radially unbounded, because $e' P_{\bar{\theta}} e$ is a positive quadratic form in view of (4.22). Besides, $v_i(e) \leq \beta_i(\|e\|)$ where $\beta_i(\|e\|) := \|P_i\| \|e\|^2 + 2\|S_i - S_{\bar{\theta}}\| \|e\|$. Hence, (4.25) is satisfied with

$$\phi_1(e) = \lambda_{\min}(P_{\bar{\theta}}) \|e\|^2, \quad \phi_2(e) = \max_{i \in \mathbb{I}_m} \{\beta_i(\|e\|)\}, \quad (4.34)$$

where the lower and upper limits are class \mathcal{K}_∞ functions.

Next, it is shown that $V(e(t))$ is strictly decreasing along any system trajectory for any $\Delta\psi$ belonging to a given sector $[l, u]$. With this purpose, note that for any point $e(t)$ and direction h , the directional derivative of $V(e(t))$ exists and is given by (4.27).

With (4.10), consider the notation

$$f(e(t)) := \sum_{i=1}^m \theta_i(e(t)) (A_i e(t) + k_i) \quad (4.35)$$

and take the directional derivative in the direction $h = f(e(t))$. In the sequel we construct the expression (4.27) for the system (4.10). The first situation to be considered is when $\sigma(e(t))$ is singleton. In this case, as $\theta_i(e(t)) = 1$ for

$i \in \sigma(e(t))$ and thus $\theta_i(e(t)) = 0$ for $i \notin \sigma(e(t))$, we can rewrite (4.27) as

$$\mathcal{D}_{f(e(t))}V(e(t)) = \sum_{i=1}^m \theta_i(e(t)) \nabla v_i(e(t)) f(e(t)) =: \Omega(\theta(e)). \quad (4.36)$$

Another situation of interest is when $\sigma(e(t))$ is not a singleton on a point “ $e(t)$ ” of a switching surface and the trajectory does not leave the switching surface at that point, *i.e.* $\sigma(e(t))$ remains constant during a certain time interval. In this case a sliding mode is occurring, and for all points of the trajectory $e(t)$ during this time interval we have

$$\begin{cases} v_i(e(t)) = v_j(e(t)) = V(e(t)) \\ \nabla v_i(e(t)) f(e(t)) = \nabla v_j(e(t)) f(e(t)) \end{cases}, \quad \forall i, j \in \sigma(e(t)). \quad (4.37)$$

In particular, as $\nabla v_i(e(t)) f(e(t)) = \nabla v_j(e(t)) f(e(t))$ and as $\theta_i(e(t)) = 0$ for $i \notin \sigma(e(t))$, we can also rewrite (4.27) as in (4.36).

The last situation to be analyzed is when $\sigma(e(t))$ is not a singleton on a point “ $e(t)$ ” of a switching surface and the trajectory leaves the switching surface at that point. In this situation, $\sigma(e(t))$ will change and, as $\sigma(e(t))$ is piecewise constant, the trajectory will move to a new region or switching surface under one of the two cases previously discussed. Thus, these points where σ is discontinuous correspond to isolated points of a system trajectory. Keeping in mind that $V(e(t))$ from (4.24) is locally Lipschitz continuous, we conclude that $V(e(t))$ is decreasing along any system trajectory $e(t)$ if it is decreasing in the two previous cases where (4.36) is valid. Observe that σ is piecewise constant and thus the behavior of V along a system trajectory in the neighborhoods of the points where σ is discontinuous is characterized by (4.36).

From the above discussion, it is clear that the condition $\mathcal{D}_{f(e(t))}V(e(t)) < 0$, obtained from (4.36), guarantees the decreasing of $V(e(t))$ along any trajectory of the system (4.10) under the switching rule (4.12). Observe that as $V(e(t))$ is locally Lipschitz, it follows that the directional derivative and time derivative coincide almost everywhere, and $\mathcal{D}_{f(e(t))}V(e(t)) < 0$ guarantees the decreasing of $V(e(t))$ even for system trajectories moving along lines or surfaces where the gradient of $V(e(t))$ does not exist and thus the usual expressions for the time derivative cannot be used. See (FILIPPOV, 1988, p.155) for more details on this point.

For global stability it is required $\mathcal{D}_{f(e(t))}V(e(t)) < 0$, $\forall e(t) \neq 0$, $\forall \theta(e(t)) \in \Theta$. As $V(e(t))$ is positive definite from (4.25), (4.34) and

non increasing from $\mathcal{D}_{f(e(t))}V(e(t)) < 0$, we conclude that the origin is an equilibrium point of the system whenever these conditions are satisfied. The global asymptotic stability follows from the same arguments in (FILIPPOV, 1988, p.155).

Recall that $\theta(e)$, present in the condition (4.36), is of difficult characterization. One idea to overcome this issue is to use a more conservative condition where $\theta(e)$ is replaced with an arbitrary time varying parameter θ in the unity simplex Θ . To reduce the conservativeness associated with this relaxation of the problem, we can apply the S -Procedure to the condition (4.26) and take into account the constraint (4.33) that represents the ‘max’ composition. Therefore, we replace (4.26) with the following condition.

$$\Omega(\theta) + 2\alpha_\theta (V(e) - e'P_{\bar{\theta}}e) < -\phi_3(e), \quad \forall \theta \in \Theta, \quad (4.38)$$

where $\Omega(\theta)$ is the function indicated in (4.36) with $\theta(e)$ replaced by an arbitrary time-varying parameter θ , $V(e)$ is indicated in (4.30) and $\alpha_\theta := \sum_{i=1}^m \alpha_i \theta_i > 0$ is a scaling factor with given positive constants α_i . Observe that (4.38) implies from (4.36) that $\Omega(\theta(e)) = \mathcal{D}_e V(e) < -\phi_3(e)$ because $2\alpha_\theta (V(e) - e'P_{\bar{\theta}}e)$ is non-negative from (4.33) and $\theta \in \Theta$.

Next we show that (4.23) implies (4.38) for a suitable positive definite function $\phi_3(e)$ to be specified later. Consider the notation $P_\theta := \sum_{i=1}^m \theta_i P_i$ and $S_\theta := \sum_{i=1}^m \theta_i S_i$. Let us rewrite the left-hand side of (4.38) as

$$\begin{bmatrix} e \\ 1 \end{bmatrix}' \begin{bmatrix} A'_\theta P_\theta + P_\theta A_\theta + 2\alpha_\theta (P_\theta - P_{\bar{\theta}}) & * \\ k'_\theta P_\theta + (S_\theta - S_{\bar{\theta}})' A_\theta + 2(S_\theta - S_{\bar{\theta}})' \alpha_\theta & k'_\theta (S_\theta - S_{\bar{\theta}}) + (S_\theta - S_{\bar{\theta}})' k_\theta \end{bmatrix} \begin{bmatrix} e \\ 1 \end{bmatrix} < 0. \quad (4.39)$$

Note that $S_\theta - S_{\bar{\theta}} = S(\theta - \bar{\theta})$ and $k_\theta = h_\theta - h_{\bar{\theta}} + B\Delta\psi = H(\theta - \bar{\theta}) + B\Delta\psi$. Therefore, it is possible to rewrite (4.39) using the auxiliary notation (4.15)-(4.21) as

$$\Omega(\theta) + 2\alpha_\theta (V(e) - e'P_{\bar{\theta}}e) = \xi' \Psi \xi < 0, \quad (4.40)$$

$$\xi = \begin{bmatrix} e_\theta \\ \theta - \bar{\theta} \\ \Delta\psi \end{bmatrix}, \quad e_\theta = \begin{bmatrix} \theta_1 e \\ \vdots \\ \theta_m e \end{bmatrix} \in \mathbb{R}^{mn}. \quad (4.41)$$

Now it is possible to incorporate to the condition (4.40) the fact that $\Delta\psi$ is a sector-bounded function of the error. Using the notation (4.20), we

can rewrite (4.14) as

$$\xi' \Gamma \xi \geq 0. \quad (4.42)$$

The inequality (4.40) must be satisfied whenever (4.42) is satisfied. By using the (lossless) S -Procedure, this occurs if there exists a scalar $\tau \geq 0$ such that

$$M := \xi' (\Psi + \tau \Gamma) \xi < 0. \quad (4.43)$$

With C_a and $C_b(\theta)$ from (4.18), it follows that $C_a \xi = 0$ and $C_b(\theta) \xi = 0$. From the Finsler's Lemma, (4.43) is satisfied if there exist scaling matrices $L_b \in \mathbb{R}^{nm+m+1 \times m}$, $L_i \in \mathbb{R}^{nm+m+1 \times 1}$, $\forall i \in \mathbb{I}_m$, and $L_a(\theta)$ defined in (4.19) such that

$$U(\theta) < 0, \quad \forall \theta \in \Theta, \quad (4.44)$$

where

$$U(\theta) := \Psi + \tau \Gamma + L_b C_b(\theta) + C_b(\theta)' L_b' + L_a(\theta) C_a + C_a' L_a(\theta)'. \quad (4.45)$$

The expression (4.44) shows that if (4.23) is satisfied then $M < 0$ which in turn implies (4.40). Note that the element in the last row and last column of (4.23) is $-\tau$, thus feasibility of (4.23) already implies $\tau > 0$, avoiding the need for this additional LMI condition.

Define the positive constants

$$\varepsilon_0 = \min_{\theta \in \Theta} (\theta' \theta) \quad , \quad \varepsilon_3 = \min_{\theta \in \Theta} \lambda_{\min}(-U(\theta)). \quad (4.46)$$

Now multiplying the inequality (4.23) by ξ to the right and by its transpose to the left and keeping in mind that $C_a \xi = 0$ and $C_b(\theta) \xi = 0$, we get

$$\xi' (\Psi + \tau \Gamma) \xi \leq -\varepsilon_3 \|\xi\|^2 < 0. \quad (4.47)$$

As $\|\xi\|^2 = \|e_\theta\|^2 + \|\theta - \bar{\theta}\|^2 + \|\Delta \Psi\|^2$ and $\|e_\theta\|^2 = \|\theta\|^2 \|e\|^2$, we conclude that $\|\xi\|^2 \geq \|e_\theta\|^2 \geq \varepsilon_0 \|e\|^2$, which in turn implies

$$\xi' (\Psi + \tau \Gamma) \xi \leq -\varepsilon_3 \varepsilon_0 \|e\|^2. \quad (4.48)$$

Using $\phi_3(e) = \varepsilon_3 \varepsilon_0 \|e\|^2$ we have shown that the LMI (4.23) is a sufficient condition for (4.43), thus for (4.38) whenever $\Delta \Psi \in [l, u]$, and finally for (4.26). Thus, global asymptotic stability follows using the same arguments in (FILIP-

POV, 1988, p.155). \square

Remark 4.3.1 *The Theorem 4.1 requires the nonlinear function ψ_x to equally influence all the modes of the switched system (4.1) by considering the same vector B for all subsystems. The difficulty of considering a different vector B for each subsystem lies in the construction of the LMIs, as shown in the sequel. Suppose that instead of B , we had B_i , $i \in \mathbb{I}_m$, in (4.1). Note in the text after Equation (4.39) that in this case $k_\theta = H(\theta - \bar{\theta}) + B_\theta \psi - B_{\bar{\theta}} \bar{\psi}$, where $B_\theta = \sum_{i \in \mathbb{I}_m} \theta_i B_i$ and $B_{\bar{\theta}} = \sum_{i \in \mathbb{I}_m} \bar{\theta}_i B_i$. Therefore, it would not be possible to isolate neither $\theta - \bar{\theta}$ nor $\Delta \psi = \psi - \bar{\psi}$, variables that compose the vector ξ given in (4.40), which is the basis for constructing the current LMI. Recall that $\Delta \psi$ is the variable that is sector-bounded and thus it is of interest to maintain it in the vector ξ to include the sector-bounded restriction (4.42) in order to relax the LMI conditions. \square*

4.3.1 Partial state measurement

The results of the Theorem 4.1 are state feedback, however, the design of a switching rule that uses output feedback can be performed in the same manner as in Section 3.4.1. In order to show that, define the output tracking error as in (3.41) and assume the auxiliary functions $v_i(e(t))$, $i \in \mathbb{I}_m$, from (4.12) have the matrices P_i, S_i with the structure given in (3.42). In this case, the auxiliary functions $v_i(e(t))$ can be rewritten as

$$v_i(e(t)) = e(t)'(P_0 + C_i' Q_i C_i) e(t) + 2e(t)'(S_0 + C_i' R_i - S_0 - \sum_{i \in \mathbb{I}_m} \bar{\theta}_i C_i R_i) \quad (4.49)$$

$$= e(t)' P_0 e(t) - 2e(t)' \sum_{i \in \mathbb{I}_m} \bar{\theta}_i C_i R_i + \mu_i(\varepsilon(t)), \quad (4.50)$$

where $\mu_i(\varepsilon(t))$ is defined as in (3.45). Note that $\sum_{i \in \mathbb{I}_m} \bar{\theta}_i C_i R_i$ is a constant convex combination and thus this term does not change according to the operation mode. Consequently,

$$\max_{i \in \mathbb{I}_m} \{v_i(e(t))\} = e(t)' P_0 e(t) - 2e(t)' \sum_{i \in \mathbb{I}_m} \bar{\theta}_i C_i R_i + \max_{i \in \mathbb{I}_m} \{\mu_i(\varepsilon(t))\} \quad (4.51)$$

and from (4.12) the switching rule becomes a function of the output tracking error as

$$\arg \max_{i \in \mathbb{I}_m} \{v_i(e(t))\} = \arg \max_{i \in \mathbb{I}_m} \{\mu_i(\bar{\varepsilon}(t))\} = \sigma(\varepsilon(t)). \quad (4.52)$$

This shows that the Theorem 4.1 can be directly applied to cope with the case of partial state information by introducing the constraints (3.42) on the structure of the matrices P_i, S_i .

4.3.2 LMIs independent of the equilibrium point

In this section we show that it is possible to have the LMIs in Theorem 4.1 independent of the equilibrium variables $\bar{x}, \bar{\theta}$ if the matrices A_i (from the system) and P_i (from the Lyapunov function) have particular structures. To be more specific, the application of the result presented in the sequel is possible when both of these matrices are the same for all subsystems, that is

$$A_i = \bar{A}_o, \quad P_i = P_0, \quad i \in \mathbb{I}_m, \quad (4.53)$$

where \bar{A}_o is given by the decomposition (4.6) with $\bar{A}_i = 0$, $i \in \mathbb{I}_m$, and $P_0 \in \mathbb{R}^{n \times n}$ is a matrix to be determined. Also, consider the following auxiliary notation used in the next corollary.

$$\Phi = \begin{bmatrix} A'P + P'A & \star & \star \\ H'P + S'A + 2S'\alpha & H'S + S'H & \star \\ B'P & B'S & 0 \end{bmatrix} \quad (4.54)$$

Corollary 4.1 *Let \bar{x} be a constant vector, not necessarily known a priori, representing the desired equilibrium point of the system (4.1), and suppose that $x(t)$ is available online. Consider the error system (4.10) and let $\bar{\theta} \in \Theta$ be a given constant vector according to Lemma 4.1. With the auxiliary notation (4.15)-(4.20) and (4.54), let L_b, L_i , $i \in \mathbb{I}_m$, be matrices to be determined with the dimensions of $C_b(\theta)'$, C'_a , respectively.*

Suppose that $\exists P, S, \tau, L_b, L_i$, $i \in \mathbb{I}_m$, solving the following LMI problem.

$$P_0 > 0 \quad (4.55)$$

$$\Phi + \tau\Gamma + L_b C_b(\theta) + C_b(\theta)' L'_b + L_a(\theta) C_a + C'_a L_a(\theta)' < 0, \quad \forall \theta \in \mathfrak{D}(\Theta) \quad (4.56)$$

Then the nonlinear switched system (4.10) is globally asymptotically stable with the switching rule (4.12) and

$$V(e) := \max_{i \in \mathbb{I}_m} \{v_i(e)\}, \quad v_i(e) = e' P_0 e + 2e'(S_i - S_{\bar{\theta}}) \quad (4.57)$$

is a Lyapunov function for the system. \square

Proof: First, note from (4.7), (4.15) that if the matrices \bar{A}_i , from the decomposition (4.6), are equal to zero $\forall i \in \mathbb{I}_m$ (i.e. A_i is the same for all $i \in \mathbb{I}_m$), then the LMIs in Theorem 4.1 are independent of equilibrium point \bar{x} . That is because \bar{x} only appears in the LMI (4.23) multiplied by \bar{A}_i (implicitly inside the definition of the vectors h_i).

Now consider $v_i(e)$ with the structure (4.12), (3.42) and recall that the full state feedback case is recovered with $C_i = I_n, \forall i \in \mathbb{I}_m$. It is possible to get the LMIs in Theorem 4.1 also independent of $\bar{\theta}$ by forcing $Q_i = 0, \forall i \in \mathbb{I}_m$. In this case, we have $P_{\bar{\theta}} = \sum_{i=1}^m \theta_i P_i = P_0$ and $P_{\bar{\theta}} = \sum_{i=1}^m \bar{\theta}_i P_i = P_0$. Therefore, the LMI (4.22) can be replaced by (4.55) and the term $(P - P_{\bar{\theta}} I_o)' \alpha + \alpha' (P - P_{\bar{\theta}} I_o)$ is eliminated from (4.23), resulting in the LMI (4.56). \square

The Corollary 4.1 allows the results of the Theorem 4.1 to be applied even if some entries of the desired operation point \bar{x} , and consequently $\bar{\theta}$, are not known *a priori*. In this case, changes in the equilibrium point with time are also possible to take into account, provided that the changes in \bar{x} can be represented by piecewise constant vectors varying slowly enough when compared to the system dynamics, as shown in Remark (4.3.2) in the sequence.

Remark 4.3.2 (Piecewise constant equilibrium) *When the reference variable \bar{x} varies continuously, it can still be approximated by a piecewise constant function, as illustrated in Figure 25, which can be obtained by passing the real continuous reference signal to be approximated through a Zero-Order Holder (ZOH), sampling every T_s seconds. The value of T_s must be greater than the time necessary for the accommodation (within a given precision) of the step response of the state variables of the switched system. Thus, the hypothesis that $\dot{\bar{x}} = 0$ is realistic. It should be emphasized that T_s does not enter in the design of the switching rule, being selected a posteriori to accommodate the response of the system in each step.* \square

4.4 Limited switching frequency

At this point, all switching rule design procedures proposed in this thesis were presented, and all of them are based on the assumption that ideal

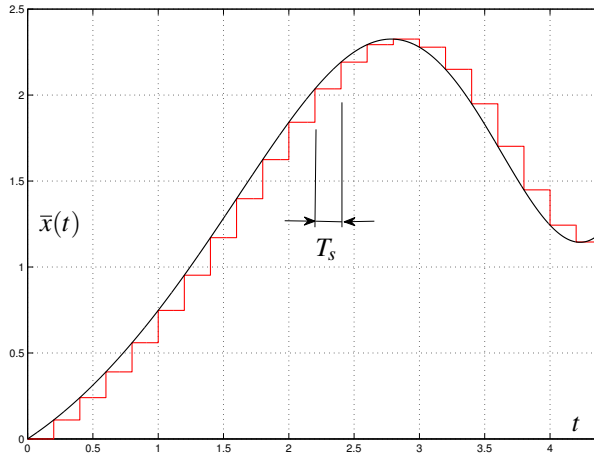


Figure 25: Illustration of the piecewise-constant approximation \bar{x} for a variable reference $\bar{x}(t)$. The ideal $\bar{x}(t)$ is represented in black color and the approximate \bar{x} in red.

sliding modes can occur. However, real switched systems often require a certain minimum time τ_s^{min} between two switchings, which results in a limited switching frequency². This minimum time before updating the switching signal is due to two main reasons: **(i)** slow microprocessors generating the control signal (inherent problem of any control system); **(ii)** slow switching devices, which is often the most restrictive reason for power electronics converters.

Various types of switches can be used for the converter circuits, among which the most commonly employed are the Metal Oxide Semiconductor Field Effect Transistor (MOSFET), the Insulated Gate Bipolar Transistor (IGBT) and the Gate Turn-Off (GTO). A comparison between the power capacities and switching speed of these types of switches can be seen in Table 3, extracted from (MOHAN; UNDELAND; ROBBINS, 2003). For these types of switches (not mechanical, but electrical), the switching speed is mainly related to the dynamics of the voltages and currents in the switch³ during the

²The term ‘limited switching frequency’ may be misleading, as the problem is in fact the time between switches, specially for asynchronous switching rules, as presented in this thesis.

³With the switch in the closed state, the voltage over the switch is zero and the current has a

switching, which are usually neglected in the modeling of the system for being much faster than the dynamics of the rest of the system. Although, they do not have instantaneous variation, typically taking a time in the order of microseconds to open or close (BARBI, 2006).

Switching device	Power capacity	Switching speed
MOSFET	175kW (low)	1MHz (fast)
IGBT	1MW (medium)	100kHz (medium)
GTO	6MW (high)	1kHz (slow)

Table 3: Power properties and switching speed of the controlled switches: MOSFET, IGBT e GTO.

The typical waveforms of the dynamics of the voltage over a switch and the current flowing through it during a switching transient are presented in Figure 26, where t_r is defined as the rise time (time for the current to go from 10% to 90% of its value in the closed state) and t_f is defined as the fall time (time for the current to go from 90% to 10% of its value in the closed state). During the time intervals t_r and t_f , the switch state is undefined and it is not possible to assert that the switching have already occurred. For this reason, the switching signal should not be updated during this intervals and, therefore, $\tau_s^{min} \geq \max\{t_r, t_f\}$.

Another problem arises due to the switching transient time in systems with certain circuit topologies. This is the case of DC/AC converters, for instance, where a pair of switches connected in series in each leg of the converter have a parallel connexion to a DC voltage source, as illustrated in Figure 27. In the ideal situation, the states of the two switches are considered complementary, *i.e.* one switch is closed when the other is open. However, the opening switch needs a time t_f to be considered open and, thus, there must exist a minimum delay τ_d^{min} before closing the other switch. Otherwise, both switches could be momentarily closed and the voltage source would be short-circuited. This delay is referred to as *dead time*⁴ and it must be defined as $\tau_d^{min} \geq t_f$. Figure 27 also shows the waveforms of the current flowing through both switches and the introduction of the dead time.

The reference (TORRES; LOPES, 2013) shows the introduction of dead time for controlling a real system. Also, there are some techniques to com-

certain value, with the switch in the open state, the voltage over the switch has a certain value and the current is zero.

⁴Also known as *blanking time*.

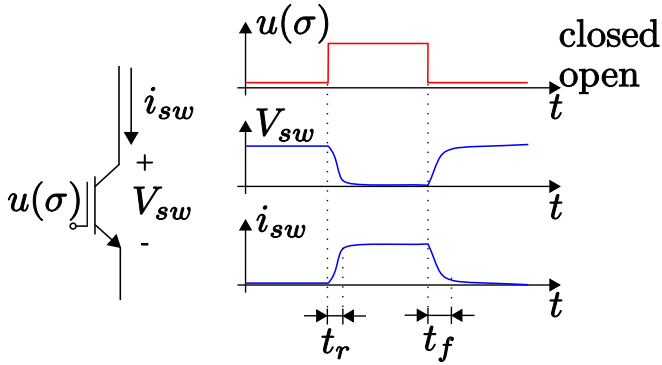


Figure 26: Voltage and current dynamics on a switch during switching transient.

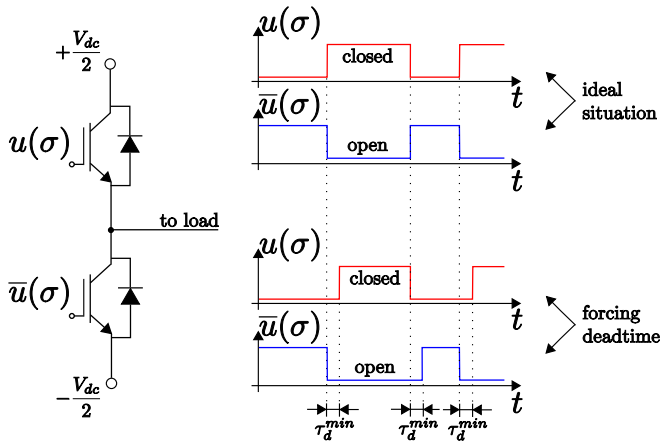


Figure 27: A generic DC/AC converter leg with dead time introduced in the switching rule.

pensate (BEN-BRAHIM, 2004), (HWANG; KIM, 2010) or eliminate (CHEN; PENG, 2007) the effects of dead time. Although not all DC/AC converters require the introduction of dead time, as the Opposed Current Converter (OCC) from (SCHELLEKENS et al., 2011), which does not have switches connected in series at the cost of more structural complexity.

The introduction of τ_s^{min} and τ_d^{min} may cause some undesired effects on

the system response. For instance, the greater the dwell time τ_s^{min} , the larger is the ripple effect. Moreover, the average value of the states may undergo a deviation from the desired value. This deviation may be positive or negative, depending on the side of the switching surface that is closer to points where the switchings are occurring, as shown in Figure 28. In relation to introducing the delay τ_d^{min} in DC/AC converters, the sinusoidal system response may present an amplitude deviation and also a phase shift.

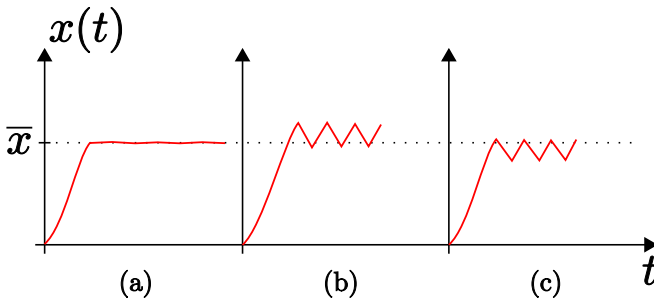


Figure 28: Deviation in the desired average value for a switching surface $x(t) = \bar{x}$. (a) Ideal sliding mode (no deviation); (b) dwell time with positive deviation; (c) dwell time with negative deviation.

Remark 4.4.1 *One can realize that exact sliding modes do not occur if the switching frequency is bounded. As in practice this is always the case, we present in the sequel a procedure to get an approximation of the Filippov's convex parameter $\theta(e(t))$ used in the switched system (4.10). The idea is usual in PWM based models (YOUNG, 1993) and consists of replacing the ideal sliding mode dynamics associated with unbounded switching frequency, with a bounded but sufficiently high switching frequency. For this purpose, it is required that the switching frequency must be higher than the spectrum of subsystems, i.e. the switching frequency is associated with a time scale where the subsystems vector field can be considered almost constant. In this case, the Filippov's convex parameter $\theta(e(t))$ can be approximated by the average value of a logical variable. To illustrate the ideas, suppose that $f_i(e(t), z(t))$ are Lipschitz continuous functions representing the vector fields of the subsystems and $f(e(t)) = \sum_{i=1}^m \theta_i(e(t)) f_i(e(t))$ is the vector field of the switched system, where $\theta_i(e(t))$ is the convex combination parameter according to Fil-*

ippov's results. Consider the approximation

$$f(e(t)) = \sum_{i=1}^m \theta_i(e(t)) f_i(e(t)) \approx \frac{1}{\Delta t} \int_{t-\Delta t}^t \sum_{i=1}^m \gamma_i(t) f_i(e(t)) dt, \quad (4.58)$$

where $\Delta t > 0$ is a sufficiently small time interval, $\gamma_i(t)$ are logical variables defined as

$$\begin{cases} \gamma_i(t) = 1 & \text{for some } i \in \sigma(e(t)) \\ \gamma_j(t) = 0 & \text{for } j \neq i \end{cases} \quad (4.59)$$

and $\sigma(e(t))$ is defined as in (4.12). As the functions $f_i(e(t))$ are Lipschitz, the more Δt is reduced, the more $f_i(e(t))$ approaches a fixed value in the interval, in the sense that $f_i(e(t))$ is practically constant in the interval $[t - \Delta t, t]$. Thus, for sufficiently small $\Delta t > 0$, the right-hand side of (4.58) can be approximated as

$$\frac{1}{\Delta t} \int_{t-\Delta t}^t \sum_{i=1}^m \gamma_i(t) f_i(e(t)) dt \approx \sum_{i=1}^m \left(\frac{1}{\Delta t} \int_{t-\Delta t}^t \gamma_i(t) dt \right) f_i(e) \quad (4.60)$$

that in turn yields the approximation

$$\theta_i(e(t)) \approx \frac{1}{\Delta t} \int_{t-\Delta t}^t \gamma_i(t) dt \quad (4.61)$$

that is valid for a sufficiently small $\Delta t > 0$. Observe that (4.61) express an approximation based on the average value of the logical variables $\gamma_i(t)$. \square

According to Remark 4.4.1, the introduction of the minimum dwell time $\tau_s^{min} > 0$ and the dead time $\tau_d^{min} > 0$ are not an issue for stability, provided that they are small enough. The same approximation presented in Remark 4.4.1 was considered for the characterization of state and parameter estimation using switched observers in (PINTO; TROFINO, 2014). Moreover, the approximation (4.61) can be used to get a duty cycle, in case the input of the switching devices passes through a PWM as in Figure 17.

4.5 Numerical examples

In the following examples, we have used the software Matlab, with the computational package SeDuMi (STURM, 2001), through the parser YALMIP (LÖFBERG, 2004), to solve the LMIs and Simulink to obtain the trajectories of the nonlinear switched systems.

Example 4.1 (Saturation) Consider a nonlinear switched system represented in the form (4.1) with the matrices

$$\begin{aligned}
 A_1 &= \begin{bmatrix} 0 & 1 \\ -1 & -1 \end{bmatrix}, \quad A_2 = \begin{bmatrix} 0 & 1 \\ -2 & -2 \end{bmatrix}, \\
 b_1 &= \begin{bmatrix} -2 \\ -1 \end{bmatrix}, \quad b_2 = \begin{bmatrix} 0 \\ 2 \end{bmatrix}, \quad B = \begin{bmatrix} 0 \\ 1 \end{bmatrix}.
 \end{aligned}
 \tag{4.62}$$

and the following nonlinear function.

$$\psi_x(q_x(x(t))) = \text{sat}(x_2) := \begin{cases} 2 & \text{if } x_2 \geq 2 \\ x_2 & \text{if } -2 < x_2 < 2 \\ -2 & \text{if } x_2 \leq -2 \end{cases}
 \tag{4.63}$$

As $q_x(x(t)) := C_q x = x_2$, we have that $C_q = [0 \ 1]$.

Note that the Corollary 4.1 cannot be applied to this case because the matrices A_i are not equal for the two subsystems and, therefore, a switching rule must be designed for every desired equilibrium point. Assume the desired equilibrium in this case is

$$\bar{x} = \begin{bmatrix} 0 \\ 1 \end{bmatrix}.
 \tag{4.64}$$

Using the decomposition (4.6), we have

$$\begin{aligned}
 \bar{A}_0 &= \begin{bmatrix} 0 & 1 \\ 0 & 0 \end{bmatrix}, \quad \bar{A}_1 = \begin{bmatrix} 0 & 0 \\ -1 & -1 \end{bmatrix}, \quad \bar{A}_2 = \begin{bmatrix} 0 & 0 \\ -2 & -2 \end{bmatrix}, \\
 \bar{b}_0 &= \begin{bmatrix} 0 \\ 0 \end{bmatrix}, \quad \bar{b}_1 = \begin{bmatrix} -2 \\ -1 \end{bmatrix}, \quad \bar{b}_2 = \begin{bmatrix} 0 \\ 2 \end{bmatrix}
 \end{aligned}
 \tag{4.65}$$

and now we can determine the vectors in (4.7) as

$$h_0 = \begin{bmatrix} 1 \\ 0 \end{bmatrix}, \quad h_1 = \begin{bmatrix} -2 \\ -2 \end{bmatrix}, \quad h_2 = \begin{bmatrix} 0 \\ 0 \end{bmatrix}.
 \tag{4.66}$$

Also knowing that

$$\bar{\psi} = \psi(0) = \psi_x(\bar{x}_2) = 1,
 \tag{4.67}$$

we can solve the equilibrium condition (4.9) for $\bar{\theta} \in \Theta$, which results in the

unique solution

$$\bar{\theta}_1 = \bar{\theta}_2 = \frac{1}{2}. \quad (4.68)$$

The sector $[l, u]$ can be determined by analyzing the function $\psi(q(e(t)))$ given by Equation (4.4) and represented in Figure 29. It is easy to notice that the sector $[l, u] = [0, 1.1]$ (also represented in Figure 29) contains the nonlinear function $\psi(q(e(t))), \forall q(e(t)) \in \mathbb{R}$.

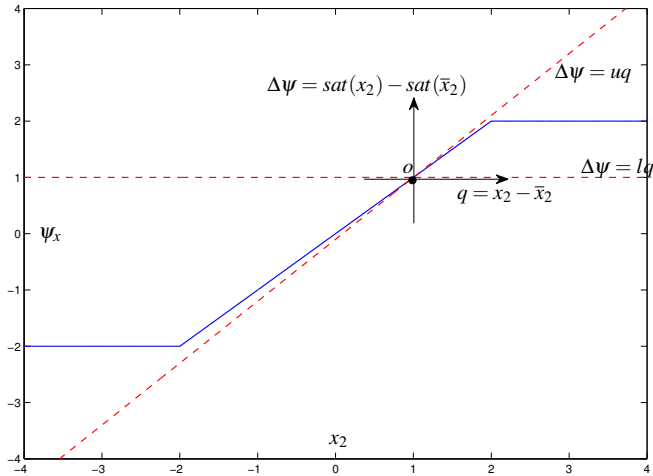


Figure 29: Sector bounds (red dashed lines) for the nonlinear saturation function (4.63) (blue lines).

Setting $\alpha_1 = \alpha_2 = 0.25$ according to Remark 3.4.1 and solving the LMIs in Theorem 4.1, a feasible solution is found and we get the following matrices used to construct the switching rule (4.12).

$$P_1 = \begin{bmatrix} 0.3913 & -0.0263 \\ -0.0263 & 0.3420 \end{bmatrix}, \quad P_2 = \begin{bmatrix} 0.8232 & 0.1796 \\ 0.1796 & 0.5248 \end{bmatrix}, \quad (4.69)$$

$$S_1 = \begin{bmatrix} 0.4633 \\ -0.2158 \end{bmatrix}, \quad S_2 = \begin{bmatrix} -0.4633 \\ 0.2158 \end{bmatrix}$$

Simulation results showing the state trajectories for a given initial condition $x(0) = [0 \quad -3]'$ are presented in Figure 30. Note that the

state is correctly regulated to the equilibrium point. Also, Figure 31(a) displays the auxiliary functions $v_i(e(t))$, $i \in \mathbb{I}_m$, and Figure 31(b) shows $\sigma(e(t))$, in which we can see a sliding mode starting at $t = 2.5295s$ (area in black color representing the fast switching). Note that the max composition $V(e(t)) = \max_{i \in \mathbb{I}_m} \{v_i(e(t))\}$ is positive and decreasing even though the individual auxiliary functions are not, which would not be possible by using a ‘min’ composition.

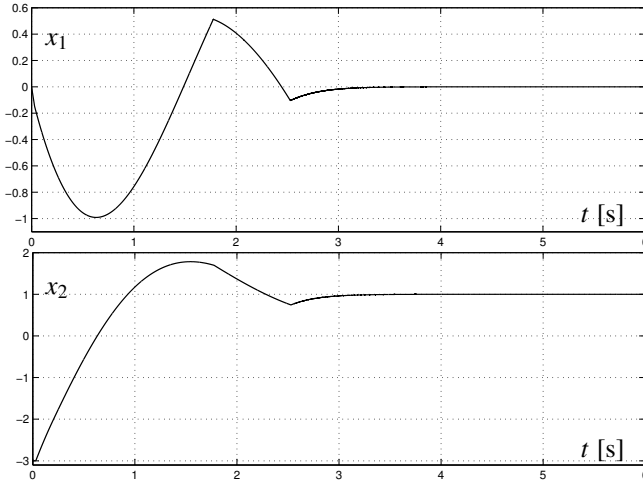


Figure 30: State trajectories for the given initial condition $x(0)$.

Finally, Figure 32 shows the effects of limiting the switching frequency for the system under study. A minimum time $\tau_s^{\min} = 0.1s$ was introduced between two consecutive switchings. Note in Figure 32 that the trajectories converged to a region around the desired equilibrium point, although a small negative deviation can be perceived after the equilibrium is achieved, as expected according to Section 4.4. \square

Example 4.2 (Variable equilibrium) Consider a nonlinear switched system represented in the form (4.1) with the matrices

$$A_1 = A_2 = \begin{bmatrix} 0 & 1 \\ -2 & -2 \end{bmatrix}, \quad b_1 = \begin{bmatrix} -2 \\ -1 \end{bmatrix}, \quad b_2 = \begin{bmatrix} 0 \\ 2 \end{bmatrix}, \quad B = \begin{bmatrix} 0 \\ 1 \end{bmatrix}, \quad (4.70)$$

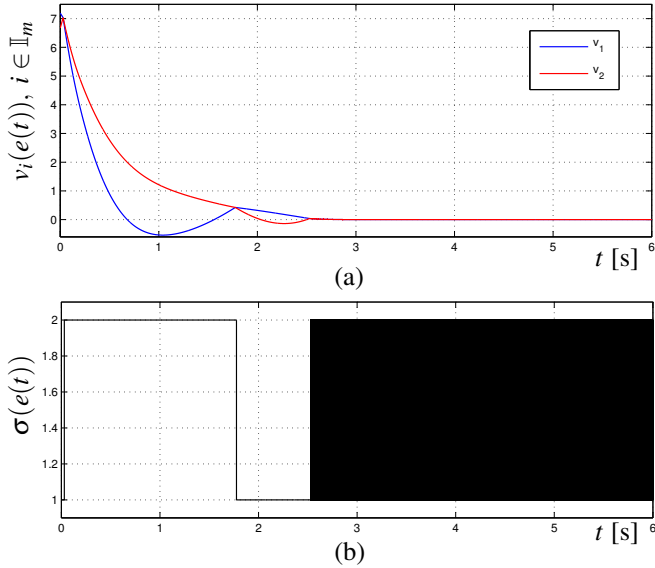


Figure 31: (a) Auxiliary functions $v_i(e(t))$, $i \in \mathbb{I}_m$. (b) Active mode $\sigma(e(t))$.

and the nonlinear function (4.63). As the nonlinear function is the same as in Example 4.1, $C_q = \begin{bmatrix} 0 & 1 \end{bmatrix}$ and the same sector $[l, u] = [0, 1.1]$ will be considered.

Note that the Corollary 4.1 can be applied to this case because the matrices A_i are equal for the two subsystems. For this reason, it is not necessary to know the equilibrium point a priori and it is allowed to change in accordance to Section 4.3.2. Using the decomposition (4.6), we get

$$\bar{A}_0 = \begin{bmatrix} 0 & 1 \\ -2 & -2 \end{bmatrix}, \quad \bar{A}_1 = \bar{A}_2 = 0_2, \quad (4.71)$$

$$\bar{b}_0 = \begin{bmatrix} 0 \\ 0 \end{bmatrix}, \quad \bar{b}_1 = \begin{bmatrix} -2 \\ -1 \end{bmatrix}, \quad \bar{b}_2 = \begin{bmatrix} 0 \\ 2 \end{bmatrix},$$

and, as the matrices \bar{A}_i are zero $\forall i \in \mathbb{I}_m$, we can determine the vectors h_i in

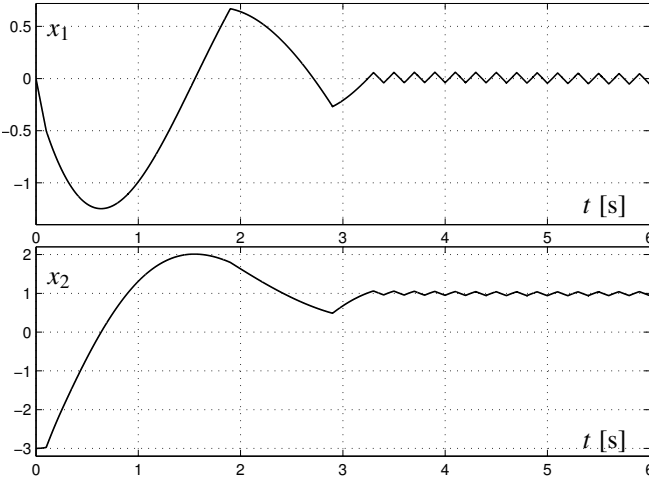


Figure 32: State trajectories for the given initial condition $x(0)$ with dwell time $\tau_s^{\min} = 0.1\text{s}$.

(4.7) independently of \bar{x} as

$$h_1 = \bar{b}_1 = \begin{bmatrix} -2 \\ -1 \end{bmatrix}, \quad h_2 = \bar{b}_2 = \begin{bmatrix} 0 \\ 2 \end{bmatrix}. \quad (4.72)$$

Setting $\alpha_1 = \alpha_2 = 0.25$ and solving the LMIs from Corollary 4.1, a feasible solution is found and we get the following matrices used to construct the switching rule (4.12).

$$P_1 = P_2 = \begin{bmatrix} 0.6694 & 0.0875 \\ 0.0875 & 0.3350 \end{bmatrix}, \quad S_1 = \begin{bmatrix} 1.0762 \\ -0.4906 \end{bmatrix}, \quad S_2 = \begin{bmatrix} 0 \\ 0 \end{bmatrix} \quad (4.73)$$

Note that the knowledge of an equilibrium point was not necessary for the switching rule design, although the equilibrium point still needs to satisfy the condition from Lemma 4.1 to be considered as a ‘possible’ equilibrium for the switched system. Note from (4.7) that, for this particular system, we have

$$h_0 = \bar{A}_0 \bar{x} + \bar{b}_0 = \begin{bmatrix} \bar{x}_2 \\ -2\bar{x}_1 - 2\bar{x}_2 \end{bmatrix}, \quad (4.74)$$

and, recalling that $\bar{\psi} = \psi_x(\bar{x}_2)$, we get the following system of equations from (4.9).

$$\begin{cases} -2\bar{\theta}_1 + \bar{x}_2 = 0 \\ -\bar{\theta}_1 + 2\bar{\theta}_2 - 2\bar{x}_1 - 2\bar{x}_2 + \psi_x(\bar{x}_2) = 0 \end{cases} \quad (4.75)$$

As $0 \leq \bar{\theta}_1 \leq 1$, from the first equality of (4.75) we have that the possible equilibria must have $0 \leq \bar{x}_2 \leq 2$, and for this interval $\psi_x(\bar{x}_2) = \bar{x}_2$. As $\bar{\theta}_1 = \bar{x}_2/2$ from the first equality and $\bar{\theta}_2 = 1 - \bar{\theta}_1 = 1 - \bar{x}_2/2$, we have, for a given \bar{x}_2 , that $\bar{x}_1 = 1 - 5\bar{x}_2/4$ from the second equality. Therefore, the set of possible equilibria for this system is

$$\mathcal{X}_{eq} := \{\bar{x} : \bar{x}_1 = 1 - 5\bar{x}_2/4, 0 \leq \bar{x}_2 \leq 2\}. \quad (4.76)$$

Finally, simulation results showing the state trajectories for null initial conditions, $x(0) = [0 \ 0]'$, are presented in Figure 33. In order to show that the switching rule designed is robust to variations in the desired equilibrium, the simulation is started with the possible equilibrium $\bar{x} = [-7/8 \ 3/2]'$ and then changed to the possible equilibrium $\bar{x} = [3/8 \ 1/2]'$ in $t = 5s$ (after the previous equilibrium is achieved, according to Section 4.3.2). Notice that the state is correctly regulated to both equilibria. \square

The switching rule design proposed in the current chapter does not take into account information about the nonlinear function, therefore the switching rule designed can be applied to the same system for any nonlinear function contained inside the given sector bounds. For instance, if the nonlinear function (4.63) from the previous examples was replaced by the function

$$\psi_x(q_x(x(t))) = \tanh(x_2) \quad (4.77)$$

with $\bar{x}_2 = 0$, then the same switching rule could be applied for the new system, because (4.77) is also in sector $[l, u] = [0, 1.1]$, as shown in Figure 34.

4.6 Concluding remarks

The switching rule design technique proposed in this chapter can be extended in several directions, as to include performance requirements such as guaranteed cost and H_∞ attenuation, for instance. Another idea for future work is to extend the technique for a more general case with multiple sector-bounded nonlinearities.

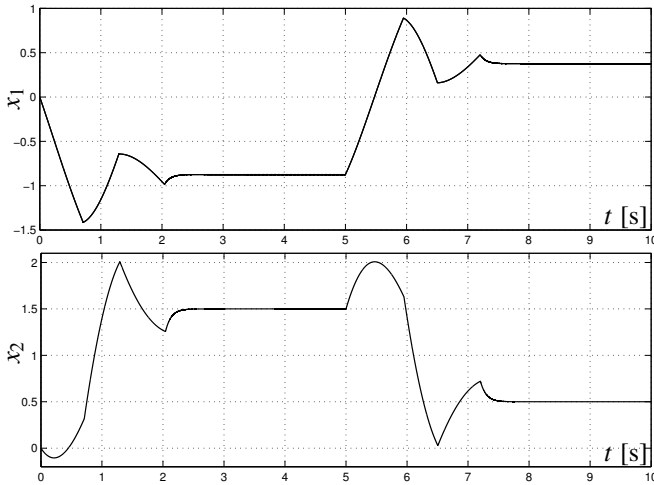


Figure 33: State trajectories for null initial conditions.

For the case of photovoltaic systems in particular, the nonlinear characteristic of the PV array may be modeled as a sector-bounded function. The application of the design technique for PV systems is presented in Chapter 5. When the PV system is connected to the grid, it also contains nonlinearities that are not state-dependent, but time-dependent (sinusoids), and thus an extension of design method to cover this type of system would be necessary in this case.

The derivation of LMI conditions for switching rule design with guarantee of stability for limited switching frequency is still an open problem. Some ideas to solve this problem are the introduction of dwell time constraints on the LMIs by using state-dependent dwell time as in (DE PERSIS; DE SANTIS; MORSE, 2003) or to use Lyapunov-Krassovskii functionals to consider the switching delay in the design, similarly to (MOARREF; RODRIGUES, 2014), (HETEL; DAAFOUZ; IUNG, 2008). Conditions based on the type of Lyapunov functions used in this thesis have shown to result in conservative LMIs in previous attempts to introduce dwell time into the switching rule, thus the modification of the Lyapunov function to also include the minimum dwell time variable may be an interesting approach for future work. Another idea to be investigated is to design a state-dependent switching surface without

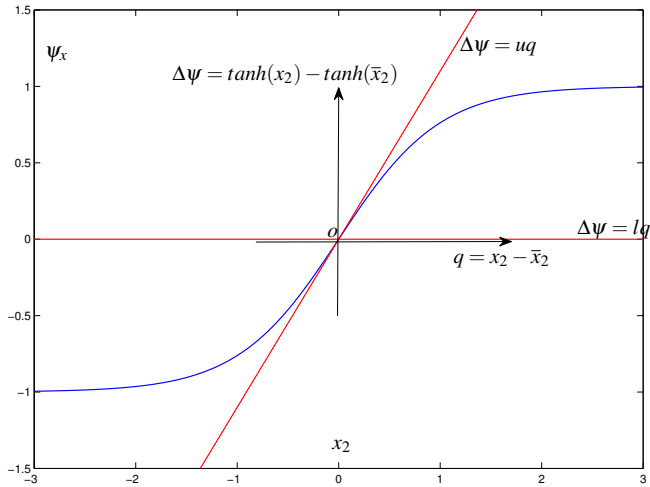


Figure 34: Sector bounds (red lines) for the nonlinear function (4.77) (blue curve).

considering a limited switching frequency and then analyzing the stability of the controlled system under limited switching frequency. Recall that in this last case the system trajectories do not converge to an equilibrium point, but to a region, as in (KUIAVA et al., 2013), where the stability of time-dependent switching rules is analyzed.

5 CONTROL OF PHOTOVOLTAIC SYSTEMS

5.1 Introduction

This chapter is dedicated to present the application of the control strategy proposed in Chapter 4 to PV systems, of which the operation was described in Chapter 2. As the nonlinear function in PV systems also depends on uncertain parameters, a formula for determining robust sector bounds for this system is also provided, allowing for the application of MPPT algorithms. The chapter is divided in two parts. The first part is devoted to the application of the method for stand-alone PV systems, starting by presenting the topology of the system to be controlled, the control objectives and some considerations about the system and ending with numerical simulations to show the effectiveness of the obtained results. The second part shows the modeling and control objectives for a grid-connected PV system to serve as a basis for the design of a switching rule to be presented in a future work.

5.2 Stand-alone PV system

This section deals with the application of the methodology for controlling a PV system feeding a local load through a Boost converter, without connection to the grid, starting the presentation from the system modeling and generation of references for maximizing the power generated (MPPT) to the design of the switching rule to be applied. A numerical example shows the effectiveness of the proposed method.

5.2.1 *Mathematical model of the PV-Boost system*

A PV array can be modeled as a current source, where the output current i_{pv} of the array is a nonlinear function of the voltage V_{pv} over the terminals of the array, represented by (2.7). Recall that it is not possible to isolate i_{pv} to determine its value algebraically. Moreover, i_{pv} is also a nonlinear function of the uncertain input parameters T and G .

The first stage consists of a PV array connected to a Boost converter with fixed output voltage as shown in Figure 35. This is the case for stand-alone systems with a battery bank or grid-connected systems with a constant DC link voltage. The objective considered here is to extract the maximum power of the array even under variations in T and G .

The PV system from Figure 35 has only one switching device (u_0)

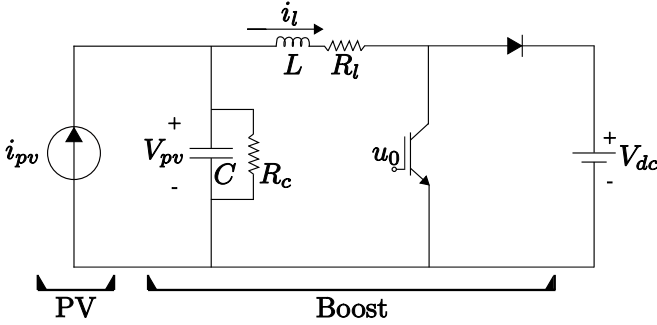


Figure 35: Topology of the DC/DC converter stage.

and, therefore, it is composed of two different subsystems ($m = 2$). The Table 4 shows the relation between the number of the active subsystem (mode of operation) and the binary command u_0 sent to switch s_0 of the Boost converter that enables the respective mode.

Mode (σ)	u_0
1	1
2	0

Table 4: Signal u_0 sent to the switch s_0 of the Boost converter, where $u_0 = 1$ puts the switch in the “closed” state (conducting) and $u_0 = 0$ in the “open” state (not conducting).

Consider the state vector $x = [i_l \ V_{pv}]'$, where i_l is the electric current through the inductor L and V_{pv} is the voltage over the capacitor C . Define the nonlinear function $\psi_x(q_x(x(t))) = i_{pv}(V_{pv})$. Therefore, $q_x(x(t)) = C_q x(t) = V_{pv}$ with $C_q = [0 \ 1]$. And the system matrices are

$$A_1 = A_2 = \begin{bmatrix} -R_l/L & 1/L \\ -1/C & -1/(R_c C) \end{bmatrix}, \quad b_1 = \begin{bmatrix} 0 \\ 0 \end{bmatrix}, \quad b_2 = \begin{bmatrix} -V_{dc}/L \\ 0 \end{bmatrix}, \quad B = \begin{bmatrix} 0 \\ 1/C \end{bmatrix}. \quad (5.1)$$

Considering the decomposition (4.6) and the definition (4.7), the sys-

tem matrices can be represented as in (4.10) with

$$\begin{aligned} \bar{A}_0 &= \begin{bmatrix} -R_l/L & 1/L \\ -1/C & -1/(R_c C) \end{bmatrix}, \quad \bar{A}_1 = \bar{A}_2 = 0_2, \\ \bar{b}_0 = \bar{b}_1 &= \begin{bmatrix} 0 \\ 0 \end{bmatrix}, \quad \bar{b}_2 = \begin{bmatrix} -V_{dc}/L \\ 0 \end{bmatrix}, \quad B = \begin{bmatrix} 0 \\ 1/C \end{bmatrix}. \end{aligned} \quad (5.2)$$

More details about modeling power electronic devices can be found in (MOHAN; UNDELAND; ROBBINS, 2003), for instance.

Finally, note in Figure 35 that a more realistic model of the capacitor C and of the inductor L was considered, with the presence of their parasitic resistances, which are, respectively, the resistance of the dielectric of the capacitor (R_c) and the intrinsic resistance of the conductive material of the inductor (R_l). These resistances are usually neglected, but they can be useful, as without them the dynamic matrices of the system models have eigenvalues on the imaginary axis and thus, no matter how small the influence of the resistances may be, they are already enough to make the system present stable eigenvalues. This point will be discussed in more detail during the project. Another study that consider the parasitic elements is (WILLMANN et al., 2007).

5.2.2 References generation for MPPT

Considering the Lemma 4.1, the equilibrium is defined by $\sum_{i=1}^m \bar{\theta}_i (h_o + h_i + B\bar{\psi}) = 0$, from which we get the following system of equations.

$$\begin{cases} \bar{i}_l = -\bar{V}_{pv}/R_c + \bar{i}_{pv} \approx \bar{i}_{pv} \\ \bar{V}_{pv} = R_l \bar{i}_{pv} + \bar{\theta}_2 V_{dc} \end{cases} \quad (5.3)$$

The approximation $\bar{i}_l \approx \bar{i}_{pv}$ in (5.3) takes into account that $1/R_c$ (the dielectric conductance of C) has very small values (around $n\Omega^{-1}$), (NETO, 2012). Therefore, in practice, the influence of the term $-\bar{V}_{pv}/R_c$ is negligible when compared to \bar{i}_{pv} .

There is no problem in doing the previous approximation, since, as it will be shown in the sequel, the equilibria are generated by the P&O MPPT algorithm, which may introduce a small inaccuracy in the references generated. However, note that the approximation is only possible for the definition of the equilibrium and not for the system model. If the model was built considering ideal elements, the dynamic matrix of the switched system in equilibrium

would be

$$A_{\bar{\theta}}^{ideal} = A_i^{ideal} = \begin{bmatrix} 0 & \frac{1}{L} \\ -\frac{1}{C} & 0 \end{bmatrix}, \quad (5.4)$$

which would have only eigenvalues on the imaginary axis and thus it would not be possible to find a solution for the LMIs proposed in this document, which require the system to have a stable convex combination for the $\bar{\theta}$ of equilibrium, according to the Remark 3.4.1. Moreover, the model considering the non-ideal components not only helps to introduce negative eigenvalue in A_{θ} , but it is also a more realistic approximation of the system.

Consider the objective of maximizing the power extracted from the PV array and note that we have $\bar{x} = [\bar{i}_{pv} \quad \bar{V}_{pv}]'$, according to (5.3). However, the values of \bar{i}_{pv} and \bar{V}_{pv} are coupled by the nonlinear equation (2.7), which depends on the uncertain parameters T and G , not known in real time. It means that if \bar{i}_{pv} is fixed, it is not possible to calculate \bar{V}_{pv} , and vice versa. Moreover, two MPPT algorithms simultaneously generating references cannot co-exist. This is because each algorithm operates independently of the other, although their outputs (\bar{i}_{pv} and \bar{V}_{pv}) must be coupled by the I - V characteristic of array so that the system can reach a feasible reference.

To overcome this difficulty, the switching rule is designed based on output feedback (Section 4.3.1), which requires the value of only one of the references in real time. In the case presented in this chapter, the output considered is the current state x_1 . Therefore, $y(t) = C_i x(t)$ with $C_i = \begin{bmatrix} 1 & 0 \end{bmatrix}$, $\forall i \in \mathbb{I}_m$. An alternative would be to measure only the voltage state x_2 , however, this case does not result in feasible LMIs.

In order to perform the MPPT, we consider the value of \bar{i}_{pv} as the output of an MPPT algorithm, such as the simple Perturb and Observe (P&O) algorithm. See (TAN; GREEN; HERNANDEZ-ARAMBURO, 2005) for details on the P&O algorithm considered. The algorithm will perform changes in the value of \bar{i}_{pv} to get as close as possible to the maximum power point even in case of changes in T and G . According to Section 4.3.2, \bar{i}_{pv} is allowed to change as a slowly varying piecewise constant function.

5.2.3 Robust sector bounds for PV systems

According to (4.4), in the system representation (4.10) we have $\Delta\psi = i_{pv}(q + \bar{V}_{pv}) - \bar{i}_{pv}$, where $q = C_q e = V_{pv} - \bar{V}_{pv}$ and $\bar{i}_{pv} = i_{pv}(\bar{V}_{pv})$. Note that $\Delta\psi = 0$ for $q = 0$, and therefore we are able to represent $\Delta\psi$ as a sector-bounded function of q as suggested in the Remark 4.2.1.

The Figure 36 shows the I - V characteristic curve of the array, obtained

by plotting (2.7) for fixed values of T and G . The Figure 36 also shows the q axis for the sector-bounded function $\Delta\psi$ as a function of q for specific values of \bar{i}_{pv} and \bar{V}_{pv} . Sector-bounding lines satisfying the sector condition for this case are also presented.

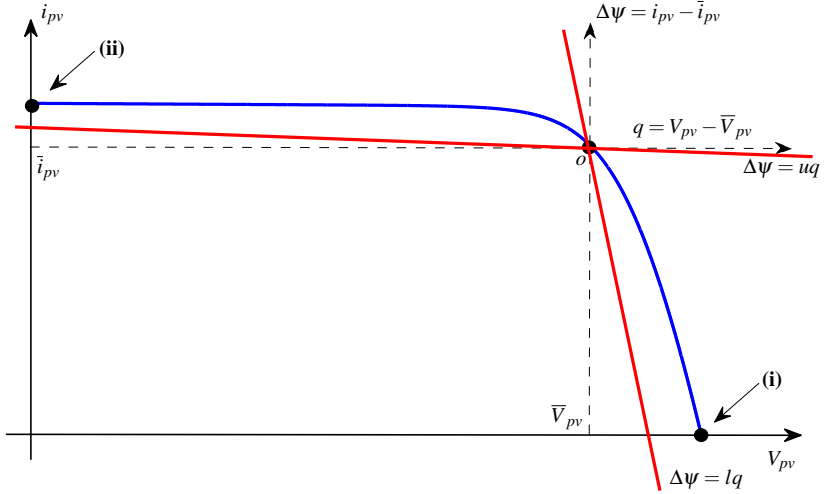


Figure 36: Example of I - V characteristic curve (blue curve) and sector bounds (red lines).

Note that the equilibrium point $(\bar{i}_{pv}, \bar{V}_{pv})$ can be any point on the I - V characteristic curve. In order to find sector bounds $[l, u]$ for the curve $\Delta\psi(q)$ for any value of $(\bar{i}_{pv}, \bar{V}_{pv})$ we must consider the following two worst case scenarios. **(i)** When $\bar{i}_{pv} = 0$ all the points of the curve are located in the second quadrant and the curve is limited above by a line with slope $l = \frac{d\Delta\psi}{dq}$ evaluated at the origin ($\Delta\psi = 0$ and $q = 0$ with $\bar{i}_{pv} = 0$). The value of $\frac{d\Delta\psi}{dq}$ at this point characterizes the most negative slope of the curve $\Delta\psi(q)$, as it can be seen in Figure 36. **(ii)** Analogously, when $\bar{V}_{pv} = 0$ all the points of the curve are located in the fourth quadrant and the curve is limited by a line with slope $u = \frac{d\Delta\psi}{dq}$ evaluated at the origin ($\Delta\psi = 0$ and $q = 0$ with $\bar{V}_{pv} = 0$). The value of $\frac{d\Delta\psi}{dq}$ at this point characterizes the least negative slope of the curve $\Delta\psi(q)$.

However, the slopes of the curve $\Delta\psi(q)$ in relation to q for the worst

cases are not known *a priori* because they depend on the uncertain parameters T and G , as shown in the sequence. Note that

$$\frac{d\Delta\psi}{dq} = \frac{di_{pv}}{dV_{pv}} = -\frac{M_p}{M_s N_s R_s (1 + f(T, G, V_{pv}, i_{pv}))}, \quad (5.5)$$

where

$$f(T, G, V_{pv}, i_{pv}) := \frac{\eta \kappa T}{\varepsilon R_s i_r \left(\exp \left(\frac{\varepsilon}{\eta \kappa T} \left(\frac{V_{pv}}{M_s N_s} + \frac{R_s i_{pv}}{M_p} \right) \right) - 1 \right)}. \quad (5.6)$$

In order to find a robust sector $[l, u]$, note in Equation (5.6) that f is always positive, independently of the values of (T, G, V_{pv}, i_{pv}) . Thus, the most negative (l) and the least negative (u) values of $\frac{d\Delta\psi}{dq}$ can be extracted from (5.5) as follows.

$$l = \lim_{f \rightarrow 0} \frac{d\Delta\psi}{dq} = -\frac{M_p}{M_s N_s R_s} \quad (5.7)$$

$$u = \lim_{f \rightarrow \infty} \frac{d\Delta\psi}{dq} = 0 \quad (5.8)$$

Therefore, the sector $[l, u]$ given by (5.7), (5.8) is robust in relation to T and G (it depends only on constant parameters of the system) and it is guaranteed to contain $\Delta\psi(q)$ for any reference $(\bar{i}_{pv}, \bar{V}_{pv})$ because these bounds contemplate the worst case scenarios corresponding to the points **(i)** and **(ii)** in Figure 36.

5.2.4 Switching rule design for the PV-Boost system

As the nonlinear function i_{pv} can be represented as a sector-bounded function according to Section 5.2.3, the switching rule design for the first stage will be based in the method presented in Chapter 4. Note in (5.1) that the matrices A_i are the same for all operation modes. Therefore, it is possible to use the results for switching rule design independent of the equilibrium point given by the Corollary 4.1, making it possible for the equilibrium to vary in order to perform the MPPT. In addition, the switching rule will be designed for a partial state measurement ($y = i_l$), as explained in Section 5.2.2, and thus the switching rule will be given by (4.52).

5.2.5 Results and simulations

The simulation data considered for the system from Figure 35 are presented in Table 5. Seeking only to exemplify the application of the control methodology, there was no concern with the optimal design of the electrical components of the converter circuits; for the design of the components the references (MARTINS; BARBI, 2008), (BARBI; MARTINS, 2008) are suggested, and for the particular application of grid-connected PV systems (DE SOUZA, 2009) is recommended. The PV array considered has $M_s = 10$ and $M_p = 2$, *i.e.* a total of 20 modules, where each module has the data presented in Table 1. This module and this configuration are the same used in (DE BRITO et al., 2010), (CASARO, 2009) and (COELHO; CONGER; MARTINS, 2009).

Parameter	Value
C	$100\mu\text{F}$
R_c	$1\text{G}\Omega$
L	50mH
R_l	$10\text{m}\Omega$
V_{dc}	350V

Table 5: Data of the PV system with a local load from Figure 35.

In the sequel, we have used the software Matlab, with the computational package SeDuMi (STURM, 2001), through the parser YALMIP (LÖFBERG, 2004), to solve the LMIs and Simulink to obtain the trajectories of the nonlinear switched systems. For the simulations that will be presented in the sequence, the tool Simulink with the toolbox SimPowerSystems from Matlab was used. This toolbox allows the construction of circuits directly from the connection of simulated electrical components, making it possible to validate the technique in a model closer to the real circuit, thus avoiding the application of the technique in the mathematical model from which it was designed.

Consider the sector $[l, u] = [-0.7407, 0]$ obtained with Equations (5.7)-(5.8) and the matrices P_i, S_i defined as in (3.42) with $Q_i = 0$ (according to Section 4.3.2) and $C_i = \begin{bmatrix} 1 & 0 \end{bmatrix}$, $\forall i \in \mathbb{I}_m$, as in Section 5.2.2. The LMIs of the Corollary 4.1 are satisfied and as a result we obtain the following coefficient matrices, from which Q_i, R_i , $i \in \mathbb{I}_m$, are used to compute the

switching rule (4.52).

$$\begin{aligned}
 P_0 &= \begin{bmatrix} 6.5852 & \star \\ -1.9675 \times 10^{-11} & 5.0115 \times 10^{-3} \end{bmatrix}, & S_0 &= \begin{bmatrix} 0 \\ 0 \end{bmatrix}, \\
 Q_1 &= -4.0794, & R_1 &= 0, \\
 Q_2 &= -4.0794, & R_2 &= 8.7702 \times 10^{-9},
 \end{aligned} \tag{5.9}$$

In the sequence, simulation results are presented. The simulation is initiated with $T = 10^\circ\text{C}$ and $G = 1000 \text{ W/m}^2$ and null initial conditions for all the states. To demonstrate the robustness of the technique with respect to the variation of the input parameters of the solar panel, T changes¹ from 10°C to 25°C in $t = 0.3\text{s}$, and G is changed from 1000 W/m^2 to 1200 W/m^2 in $t = 0.4\text{s}$.

In Figure 37(a) the plot of the power generated by the PV array is presented. It is possible to demonstrate, by plotting the P - V characteristic curves, that the MPP for each set of input parameters corresponds to the values of P_{pv} reached in steady state in Figure 37(a). Between $t = 0.3\text{s}$ and $t = 0.4\text{s}$ in particular, the system is in STC, therefore, it is easy to check that the MPP is achieved simply by multiplying the values of voltage and current in MPP from Table 1 between themselves and by the number of modules considered, which results in 4003W , the same obtained in simulation. The small oscillations in P_{pv} in steady state are due to the adjustments of the P&O algorithm, which has a compromise between speed of convergence and precision. A better response could be achieved by using an improved P&O algorithm such as in (KUMARI; BABU; BABU, 2012).

Figure 37(b) shows that the curve of i_{pv} converges to \bar{i}_{pv} (discretized output of an P&O algorithm²) due to the convergence of the state i_l to \bar{i}_{pv} as in (5.3). Figure 37(c) shows the convergence of the non-measured state V_{pv} to its reference (not known *a priori*). Recalling that these two variables are intrinsically connected by the I - V characteristic from Figure 6, when i_{pv} reaches the MPP it means that V_{pv} reached it as well, hence the need for using an MPPT algorithm for only one of these two variables. In this case, it is known that the current i_l is equal to i_{pv} when the system is in steady state and, therefore, it is sufficient for i_l to have as its equilibrium the value of i_{pv} of the

¹An extreme case is illustrated; in real situations the temperature does not undergo a step type of variation.

²An P&O algorithm for current control, as in (TAN; GREEN; HERNANDEZ-ARAMBURO, 2005), is used for MPPT. The algorithm is adjusted to perform steps of $\pm 0.8\text{A}$. The references are changed every $T_s = 0.01\text{s}$, according to Remark 4.3.2.

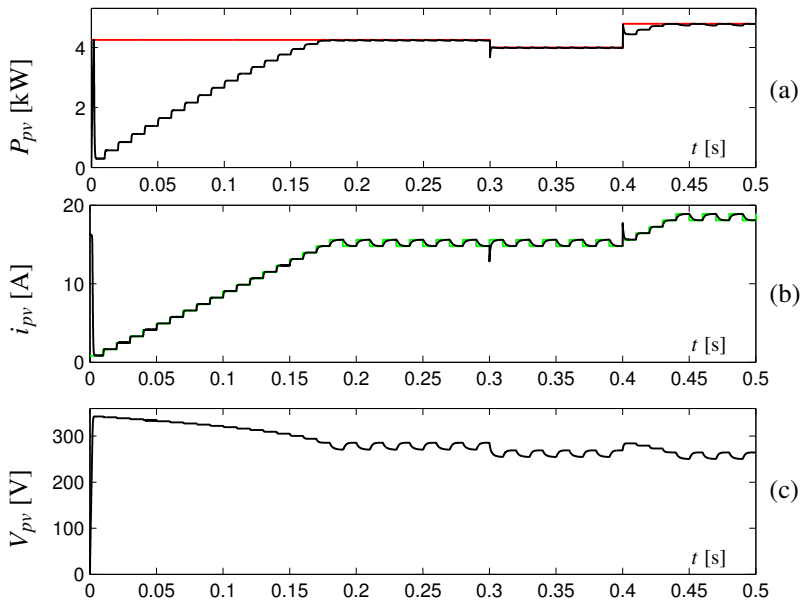


Figure 37: (a) $P_{pv} = V_{pv}i_{pv}$ (black curve) and the MPP for each values of T and G (red lines). (b) i_{pv} (black curve) and its reference \bar{i}_{pv} (green lines). (c) V_{pv} .

MPP in order for the system to achieve the maximum generation.

It is important to emphasize that the technique is designed considering the possibility of switching with infinite frequency, as there are no restrictions including a minimum residence time between switching instants. However, simulations similar to the one presented in Example 4.1 show that the designed switching rule works well for converters with limited switching frequency, since this frequency is high enough. By decreasing the maximum switching frequency, only an increase in the amplitude of the ripples and a small deviation of the average value of the states in steady state are observed, as expected according to Section 4.4. In the simulations presented it was assumed that all the switches can operate with a maximum frequency up to 1MHz, which is a frequency possible for switches of the MOSFET type (MOHAN; UNDELAND; ROBBINS, 2003), as shown in Table 3.

5.3 Grid-connected PV system

In order to illustrate the case of connection to the AC power grid, the system with two converter stages shown in Figure 38 will be used. It will be considered that the main control objective for this system is to generate and deliver to the grid the maximum power possible at unitary PF. The power circuit topology includes an L filter as interface between the inverter and the grid. Despite the advantages of the LCL filter described in Section 2.2.2.3, a single L filter is considered in order to simplify the exposition of the modeling process.

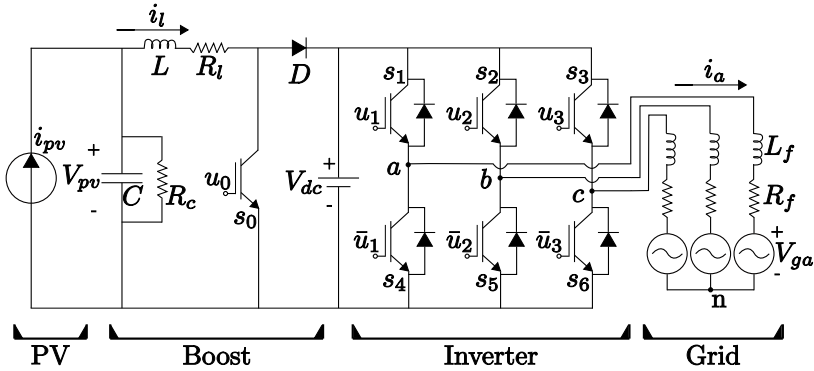


Figure 38: Topology considered for connection of the PV system with the grid.

The DC link voltage (V_{dc}) will be considered constant and with amplitude large enough to be able to reproduce in the output of the inverter a switching voltage with an average value similar in amplitude to the sinusoidal voltage of the grid. This case of DC link voltage kept constant by means of batteries, also known by the nomenclature *link-battery*, can be found in (NGE; MIDTGARD; NORUM, 2011), (DASGUPTA et al., 2011) and (GULES et al., 2008). The voltage V_{dc} is also applied to the output of the DC/DC converter of the first converter stage and we will consider a PV array for which the maximum operating voltage, even in the worst case T and G , will be less than V_{dc} , justifying the use of the Boost converter in this case.

Batteries with a high voltage value are not an impossibility. For instance, the electric vehicles developed by Itaipu Binacional contain batteries with voltages above 250 Volts (ITAIPU BINACIONAL, 2013). An alternative to

the use of high voltage batteries, but still with constant link voltage, would be to use a low battery voltage value, but with the system connected to the grid via a transformer, as shown in (LI; WOLFS, 2008), (TEODORESCU; LISERRE; RODRÍGUES, 2011, p.27). In this case, the whole system would operate with lower voltages, eventually forcing the use of converters of the type Buck-Boost (or similar) and the design of protection due to the higher current values.

A less expensive alternative to the use of batteries or transformers would be to replace the battery with a capacitor, enabling the regulation of the DC link voltage. However, the design of the control system becomes more complex due to the coupling of the two stages. The control strategy for this type of system will be addressed in a future work.

The control design can be performed independently for each converter stage, because the (constant) voltage V_{dc} decouples the dynamics of the state variables of the two stages. With this, there are two distinct systems: PV-Boost (stage 1) and inverter-grid (stage 2). As the output of the controller, there are the commands $u_0, u_1, u_2, u_3, \bar{u}_1, \bar{u}_2, \bar{u}_3$ to be applied to the opening or closing of each of 7 switches present in the structure of Figure 38.

The Table 4 shows the relation between the number of the active subsystem (mode of operation) and the binary command u_0 sent to switch s_0 of the Boost converter. The Table 6 shows the same relations, but for the case of the voltage inverter, where u_1, u_2, u_3 are the commands sent to the switches s_1, s_2, s_3 , respectively. The commands $\bar{u}_1, \bar{u}_2, \bar{u}_3$ sent to the switches s_4, s_5, s_6 are simply the binary complements of u_1, u_2, u_3 , because of a structural constraint (avoid short-circuit in V_{dc}), the two switches of a same leg of the inverter must be in a complementary position. Dead time will not be considered.

Because of the decoupling between the two converter stages, the control design for the first stage is exactly the same presented in Section 5.2. Therefore, only the inverter-grid stage will be considered in the sequel.

5.4 Stage 2: inverter-grid

This section deals with the application of the methodology for controlling the second converter stage (inverter-grid). First, note that the structure of this stage is the same presented in Figure 39. The presentation begins with a detailed system modeling and the generation of references to deliver the maximum active power to the grid, and ends with the design of the switching rule to be applied.

Mode (σ)	u_1	u_2	u_3
1	1	0	0
2	1	1	0
3	0	1	0
4	0	1	1
5	0	0	1
6	1	0	1
7	0	0	0

Table 6: Signals u_1, u_2, u_3 send to the switches s_1, s_2, s_3 of the inverter, where $u_j = 1$ puts the switch s_j in the “closed” state (conducting) and $u_j = 0$ in the “open” state (not conducting). The commands for s_4, s_5, s_6 are the binary complements $\bar{u}_1, \bar{u}_2, \bar{u}_3$, respectively.

5.4.1 Model

The dynamics of the inductor current in each filter between the inverter and the grid is given by the voltage difference in their terminals divided by the inductance value, that is

$$\begin{bmatrix} \dot{i}_a \\ \dot{i}_b \\ \dot{i}_c \end{bmatrix} = \frac{1}{L_f} \begin{bmatrix} V_{an} \\ V_{bn} \\ V_{cn} \end{bmatrix}_i - \frac{R_f}{L_f} \begin{bmatrix} i_a \\ i_b \\ i_c \end{bmatrix} - \frac{1}{L_f} \begin{bmatrix} V_{ga} \\ V_{gb} \\ V_{gc} \end{bmatrix}, \quad i \in \mathbb{I}_m = \{1, \dots, 7\}, \quad (5.10)$$

where the subscript i denotes the vector that varies according to the active operation mode.

Consider the Clarke’s transformation (2.10), the Park’s transformation (2.12) and their inverses (2.11) and (2.13), respectively, which deductions are presented in the Appendices B and C. Note that by taking the time derivative of both sides of (2.11) and (2.13) we get, in this order,

$$\begin{bmatrix} \dot{f}_a \\ \dot{f}_b \\ \dot{f}_c \end{bmatrix} = K_{\alpha\beta}^{\#} \begin{bmatrix} \dot{f}_\alpha \\ \dot{f}_\beta \end{bmatrix}, \quad (5.11)$$

$$\begin{bmatrix} \dot{f}_\alpha \\ \dot{f}_\beta \end{bmatrix} = K_{dq}^{-1} \begin{bmatrix} \dot{f}_d \\ \dot{f}_q \end{bmatrix} + \frac{d}{dt} \left(K_{dq}^{-1} \right) \begin{bmatrix} f_d \\ f_q \end{bmatrix}, \quad (5.12)$$

where $\phi = \omega t$ in the transformation matrices K_{dq} , with ω being the constant

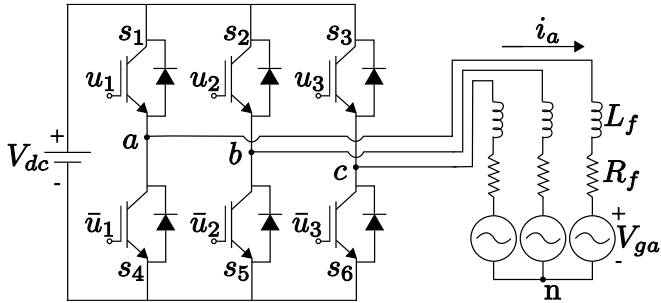


Figure 39: Three-phase inverter feeding a three-phase load (grid) through an L filter.

frequency of the grid and, therefore,

$$\frac{d}{dt} \left(K_{dq}^{-1} \right) = \omega \begin{bmatrix} -\sin(\omega t) & -\cos(\omega t) \\ \cos(\omega t) & -\sin(\omega t) \end{bmatrix}. \quad (5.13)$$

With the previous definitions, it is possible to rewrite (5.10) in $\alpha\beta$ coordinates³ as

$$K_{\alpha\beta}^{\#} \begin{bmatrix} \dot{i}_{\alpha} \\ \dot{i}_{\beta} \end{bmatrix} = -\frac{R_f}{L_f} K_{\alpha\beta}^{\#} \begin{bmatrix} i_{\alpha} \\ i_{\beta} \end{bmatrix} + \frac{1}{L_f} K_{\alpha\beta}^{\#} \begin{bmatrix} V_{\alpha n} \\ V_{\beta n} \end{bmatrix}_i - \frac{1}{L_f} K_{\alpha\beta}^{\#} \begin{bmatrix} V_{g\alpha} \\ V_{g\beta} \end{bmatrix} \quad (5.14)$$

and pre-multiplying both sides by $K_{\alpha\beta}$, we get

$$\begin{bmatrix} \dot{i}_{\alpha} \\ \dot{i}_{\beta} \end{bmatrix} = -\frac{R_f}{L_f} \begin{bmatrix} i_{\alpha} \\ i_{\beta} \end{bmatrix} + \frac{1}{L_f} \begin{bmatrix} V_{\alpha n} \\ V_{\beta n} \end{bmatrix}_i - \frac{1}{L_f} \begin{bmatrix} V_{g\alpha} \\ V_{g\beta} \end{bmatrix}. \quad (5.15)$$

Now consider the input/output voltage relation in the three-phase inverter given by⁴

$$\begin{bmatrix} V_{an} \\ V_{bn} \\ V_{cn} \end{bmatrix}_i = \frac{1}{3} \begin{bmatrix} 2 & -1 & -1 \\ -1 & 2 & -1 \\ -1 & -1 & 2 \end{bmatrix} \begin{bmatrix} u_1 \\ u_2 \\ u_3 \end{bmatrix}_i V_{dc}. \quad (5.16)$$

³The three-phase system is considered balanced here, thus the zero component is dismissed.

⁴Derived in Appendix A.

By using (2.10) it is possible to rewrite (5.16) in $\alpha\beta$ coordinates as

$$\begin{bmatrix} V_{an} \\ V_{bn} \\ V_{cn} \end{bmatrix}_i = V_{dc} \underbrace{\frac{1}{3} K_{\alpha\beta} \begin{bmatrix} 2 & -1 & -1 \\ -1 & 2 & -1 \\ -1 & -1 & 2 \end{bmatrix}}_{\begin{bmatrix} U_{\alpha i} \\ U_{\beta i} \end{bmatrix}} \begin{bmatrix} u_1 \\ u_2 \\ u_3 \end{bmatrix}_i, \quad (5.17)$$

where $U_{\alpha i}, U_{\beta i}$ are constants that are different for each of the 7 possible distinct operation modes and their values are shown in Table 7.

Mode i	$U_{\alpha i}$	$U_{\beta i}$	$\sqrt{U_{\alpha i}^2 + U_{\beta i}^2}$
1	2/3	0	2/3
2	1/3	$-\sqrt{3}/3$	2/3
3	$-1/3$	$-\sqrt{3}/3$	2/3
4	$-2/3$	0	2/3
5	$-1/3$	$\sqrt{3}/3$	2/3
6	1/3	$\sqrt{3}/3$	2/3
7	0	0	0

Table 7: Magnitudes of the elements $U_{\alpha i}$ and $U_{\beta i}$ and of the module of the vector $U_{\alpha\beta}$ for each operation mode.

By replacing (5.17) in (5.15), we get

$$\begin{bmatrix} \dot{i}_\alpha \\ \dot{i}_\beta \end{bmatrix} = -\frac{R_f}{L_f} \begin{bmatrix} i_\alpha \\ i_\beta \end{bmatrix} + \frac{V_{dc}}{L_f} \begin{bmatrix} U_{\alpha i} \\ U_{\beta i} \end{bmatrix} - \frac{1}{L_f} \begin{bmatrix} V_{g\alpha} \\ V_{g\beta} \end{bmatrix}. \quad (5.18)$$

Now it is possible to rewrite (5.18) in dq synchronous coordinates by

using the definitions of the Park's transformation and (5.12), as

$$\begin{aligned} & \begin{bmatrix} \cos(\omega t) & -\sin(\omega t) \\ \sin(\omega t) & \cos(\omega t) \end{bmatrix} \begin{bmatrix} \dot{i}_d \\ \dot{i}_q \end{bmatrix} + \omega \begin{bmatrix} -\sin(\omega t) & -\cos(\omega t) \\ \cos(\omega t) & -\sin(\omega t) \end{bmatrix} \begin{bmatrix} i_d \\ i_q \end{bmatrix} = \\ & -\frac{R_f}{L_f} \begin{bmatrix} \cos(\omega t) & -\sin(\omega t) \\ \sin(\omega t) & \cos(\omega t) \end{bmatrix} \begin{bmatrix} i_d \\ i_q \end{bmatrix} + \frac{V_{dc}}{L_f} \begin{bmatrix} U_{\alpha i} \\ U_{\beta i} \end{bmatrix} \\ & - \begin{bmatrix} \cos(\omega t) & -\sin(\omega t) \\ \sin(\omega t) & \cos(\omega t) \end{bmatrix} \frac{1}{L_f} \begin{bmatrix} V_{gd} \\ V_{gq} \end{bmatrix}. \quad (5.19) \end{aligned}$$

Observe the following relations.

$$\begin{aligned} & -\omega \begin{bmatrix} \cos(\omega t) & -\sin(\omega t) \\ \sin(\omega t) & \cos(\omega t) \end{bmatrix}^{-1} \begin{bmatrix} -\sin(\omega t) & -\cos(\omega t) \\ \cos(\omega t) & -\sin(\omega t) \end{bmatrix} = \\ & \omega \begin{bmatrix} \cos(\omega t) & \sin(\omega t) \\ -\sin(\omega t) & \cos(\omega t) \end{bmatrix} \begin{bmatrix} \cos(\omega t) & \sin(\omega t) \\ -\sin(\omega t) & \cos(\omega t) \end{bmatrix} = \begin{bmatrix} 0 & \omega \\ -\omega & 0 \end{bmatrix} \quad (5.20) \end{aligned}$$

$$\begin{aligned} & \begin{bmatrix} \cos(\omega t) & -\sin(\omega t) \\ \sin(\omega t) & \cos(\omega t) \end{bmatrix}^{-1} \begin{bmatrix} U_{\alpha i} \\ U_{\beta i} \end{bmatrix} = \\ & \begin{bmatrix} \cos(\omega t) & \sin(\omega t) \\ -\sin(\omega t) & \cos(\omega t) \end{bmatrix} \begin{bmatrix} U_{\alpha i} \\ U_{\beta i} \end{bmatrix} = \\ & \begin{bmatrix} U_{\beta i} & U_{\alpha i} \\ -U_{\alpha i} & U_{\beta i} \end{bmatrix} \begin{bmatrix} \sin(\omega t) \\ \cos(\omega t) \end{bmatrix} \quad (5.21) \end{aligned}$$

$$\begin{bmatrix} \cos(\omega t) & -\sin(\omega t) \\ \sin(\omega t) & \cos(\omega t) \end{bmatrix}^{-1} \begin{bmatrix} \cos(\omega t) & -\sin(\omega t) \\ \sin(\omega t) & \cos(\omega t) \end{bmatrix} = \begin{bmatrix} 1 & 0 \\ 0 & 1 \end{bmatrix} \quad (5.22)$$

By replacing (5.20)-(5.22) in (5.19), we get the following state space

representation in synchronous coordinates.

$$\begin{aligned} \begin{bmatrix} \dot{i}_d \\ \dot{i}_q \end{bmatrix} &= \underbrace{\begin{bmatrix} -\frac{R_f}{L_f} & \omega \\ -\omega & -\frac{R_f}{L_f} \end{bmatrix}}_{A_i} \underbrace{\begin{bmatrix} i_d \\ i_q \end{bmatrix}}_x - \frac{1}{L_f} \underbrace{\begin{bmatrix} V_{gdq} \\ V_{gq} \end{bmatrix}}_{b_i} \\ &+ \underbrace{\begin{bmatrix} \frac{V_{dc}}{L_f} & 0 \\ 0 & \frac{V_{dc}}{L_f} \end{bmatrix}}_B \underbrace{\begin{bmatrix} U_{\beta i} & U_{\alpha i} \\ -U_{\alpha i} & U_{\beta i} \end{bmatrix}}_{U_i} \underbrace{\begin{bmatrix} \sin(\omega t) \\ \cos(\omega t) \end{bmatrix}}_z \end{aligned} \quad (5.23)$$

In (5.23), note that the matrices A_i , $i \in \{1, 7\}$, are the same for all the operation modes, however, the subscript i was maintained to avoid confusion with the notation adopted in (3.12). Also note that the real part of the eigenvalues of A_i is strictly negative if $R_f \neq 0$.

By representing the switched system (5.23) as a function of the error between the state x and its desired constant reference \bar{x} , that is $e = x - \bar{x}$, we have

$$\dot{e} = A_i e + A_i \bar{x} + b_i + B U_i z(t) \quad (5.24)$$

Assuming the sliding mode dynamics of the system can be represented as convex combinations of the subsystems as in Definition 3.1, according to (FILIPPOV, 1988), the global switched system, that includes the subsystem dynamics and the sliding mode dynamics that may eventually occur in any switching surface, is represented by

$$\begin{aligned} \dot{e}(t) &= \sum_{i \in \sigma(e(t), z(t))} \theta_i(e(t), z(t)) (A_i e(t) + A_i \bar{x} + b_i + B U_i z(t)) \quad (5.25) \\ &= \sum_{i \in \mathbb{L}_m} \theta_i(e(t), z(t)) (A_i e(t) + A_i \bar{x} + b_i + B U_i z(t)), \quad \theta(e(t), z(t)) \in \Theta, \end{aligned} \quad (5.26)$$

where $\theta(e(t), z(t))$ is the vector with entries $\theta_i(e(t), z(t))$ and Θ is the unitary simplex defined in (3.7).

In order to achieve the tracking objective, the origin must be an asymptotically stable equilibrium point of (5.26). Define $\bar{\theta}(z(t)) = \theta(0, z(t))$. Hence, the following lemma is established.

Lemma 5.1 *The origin is an equilibrium point of (5.26) iff there exists*

$\bar{\theta}(z(t)) \in \Theta$ such that

$$\sum_{i=1}^m \bar{\theta}_i(z(t)) (A_i \bar{x} + b_i + BU_i z(t)) = 0. \quad (5.27)$$

□

Proof: Set $\dot{e}(t) = 0$ and $e(t) = 0$ in (5.26). □

Taking into account the Lemma 5.1, the equilibrium of the system is defined by solving $\sum_{i=1}^m \bar{\theta}_i(z(t)) (A_i \bar{x} + b_i + BU_i z(t)) = 0$, from which we get the following system of equations for the system (5.23).

$$\bar{i}_{dq} = A_i^{-1} \frac{1}{L_f} \left(V_{dc} \sum_{i=1}^m \bar{\theta}_i(z(t)) U_i z(t) - V_{gdq} \right) \quad (5.28)$$

Knowing that $A_i, L_f, V_{dc}, V_{gdq}$ are constant and equal for all modes, $z(t) \in \mathbb{R}^{n_z}$ contains sinusoidal variables and the switching alters only the value of U_i , thus the term $\sum_{i=1}^m \bar{\theta}_i(z(t)) U_i$ must be commuted in order to generate a sinusoidal behavior that annuls the influence of $z(t)$ in steady state, since \bar{i}_{dq} must be constant, because a constant equilibrium in synchronous coordinates represents a sinusoidal waveform in three-phase abc coordinates. Observing the values in Table 7, one way to get that result is to commute in the sequence from 1 to 6 and restart the cycle, as it is traditionally performed in the vector control techniques existing in the literature. However, several other sequences including sliding modes may occur.

Another observation is that $\bar{\theta}(z(t))$ is unknown and not constant. This differs from the case of Boost converter from Section 5.2, because in that case $\bar{\theta}$ was unknown, but constant. Finding a relation that provides the values of $\bar{\theta}(z(t))$ in this case is not a trivial task, perhaps not even possible in some cases.

5.4.2 References generation

For the equilibrium of the currents in the output of the inverter (grid side) two criteria will be used: **(i)** obtaining unitary PF; **(ii)** power balance. The first criterion has the goal of delivering only active power to the grid and the second criterion is intended to deliver power generated by the PV array only, resulting in a null average power entering or leaving the battery V_{dc} , making the presence of the battery only necessary to maintain the DC link voltage constant and not to feed the system or the grid.

With the use of the synchronization of the reference frame of the system with the grid presented in Section 2.2.6, the grid voltages in synchronous coordinates are established as $V_{gd} = V_g^{peak}$ and $V_{gq} = 0$. Therefore, in order to deliver the currents in phase with the voltages, it is sufficient to impose $\bar{i}_d = i_g^{peak}$ and $\bar{i}_q = 0$ as the references for the currents. With that, criterion (i) is satisfied. The value of i_g^{peak} , which is the amplitude of the sinusoidal output current, will be designed in order to satisfy the criterion (ii). This can be accomplished through the following power balance, where P_g is the power delivered to the grid, P_{pv} is the power generated by the PV array, and P_{Rc} , P_{Rl} and P_{Rf} are the power losses in the resistive elements R_c , R_l and R_f , respectively.

$$P_g = P_{pv} - P_{Rc} - P_{Rl} - P_{Rf} \quad (5.29)$$

$$3V_g^{rms}i_g^{rms}\cos(\phi) = V_{pv}i_{pv} - \frac{V_{pv}^2}{R_c} - R_l i_l^2 - 3R_f i_g^{rms2} \quad (5.30)$$

Note that the power balance (5.29) is performed without considering “commutation” (switching) losses, which occur on every switching instant and, therefore, the losses depend on the number of switchings. It is assumed that the DC link will feed/absorb the unbalanced power.

As by the criterion (i) we have unitary PF, then $\cos(\phi) = 1$. Thus, (5.30) can be rewritten as

$$i_g^{rms2} + \frac{V_g^{rms}}{R_f} i_g^{rms} + \frac{1}{3R_f} \left(\frac{V_{pv}^2}{R_c} + R_l i_l^2 - V_{pv} i_{pv} \right) = 0. \quad (5.31)$$

The solution of the quadratic equation (5.31) for i_g^{rms} results in

$$i_g^{rms} = -\frac{V_g^{rms}}{2R_f} \pm \sqrt{\left(\frac{V_g^{rms}}{2R_f} \right)^2 - \frac{1}{3R_f} \left(\frac{V_{pv}^2}{R_c} + R_l i_l^2 - V_{pv} i_{pv} \right)}. \quad (5.32)$$

Knowing that a negative Root Mean Square (RMS) value for the current does not have physical meaning, the negative signal at the left of the root can be eliminated. Finally, as i_g is a sinusoidal current, $i_g^{peak} = \sqrt{2} i_g^{rms}$, and thus the desired equilibria for the state variables of the output currents of the

inverter are the following.

$$\bar{i}_d = -\frac{\sqrt{2}V_g^{rms}}{2R_f} + \sqrt{\left(\frac{\sqrt{2}V_g^{rms}}{2R_f}\right)^2 - \frac{2}{3R_f}\left(\frac{V_{pv}^2}{R_c} + R_l i_l^2 - V_{pv} i_{pv}\right)} \quad (5.33)$$

$$\bar{i}_q = 0 \quad (5.34)$$

Note in (5.33)-(5.34) that the references adopted for the control of the inverter depend on variables that are controlled by the Boost converter stage. As the design of the switching rules for the two stages are done separately, without this coupling in the references (updating the reference of the inverter based in the values of the variables in the Boost in real time) the power delivered to the grid would be always the same, regardless of how much power was being generated by the array. Thus, the battery V_{dc} (responsible for the decoupling) would bear with the unbalance by generating the lacking power or consuming the excess, which are undesirable situations.

5.4.3 Perspectives for the switching rule design for the stage 2

The content presented in Sections 5.4.1 and 5.4.2 about the modeling of the system and the generation of the desired references is intended to be a basis for the switching rule design, to be presented in a future work.

We are interested in designing a switching rule that drives the switched error system (5.26) to the origin. Note that θ is a function of z , and therefore the switching rule σ must also be a function of z . For this purpose consider the switching rule given by

$$\sigma(e, z) := \arg \max_{i \in \mathbb{I}_m} \{v_i(e, z)\}. \quad (5.35)$$

where $v_i(e, z)$ are auxiliary functions to be determined. According to previous studies, such as the one presented in (SCHARLAU et al., 2013), a promising structure for the auxiliary functions in this case is

$$v_i(e, z) = e' P_u e + 2e' Y k_i(z), \quad (5.36)$$

where $P_u = P'_u \in \mathbb{R}^{n \times n}$ and $Y \in \mathbb{R}^{n \times n}$ are matrices to be determined. This is the same switching rule presented in Equation (3.3), but with a particular structure for the matrices P_i and S_i , with the latter depending on the nonlinear function z . This particular structure has some interesting properties for making the stability conditions independent of $\bar{\theta}$, that is unknown and not

constant. However, more work has to be done in order to obtain feasible LMI conditions.

5.4.4 Analysis of the complete system

A block diagram representation of the control structure applied to the system of Figure 38 is presented in Figure 40, comprising since the measured variables until the command signals to be imposed to the switches.

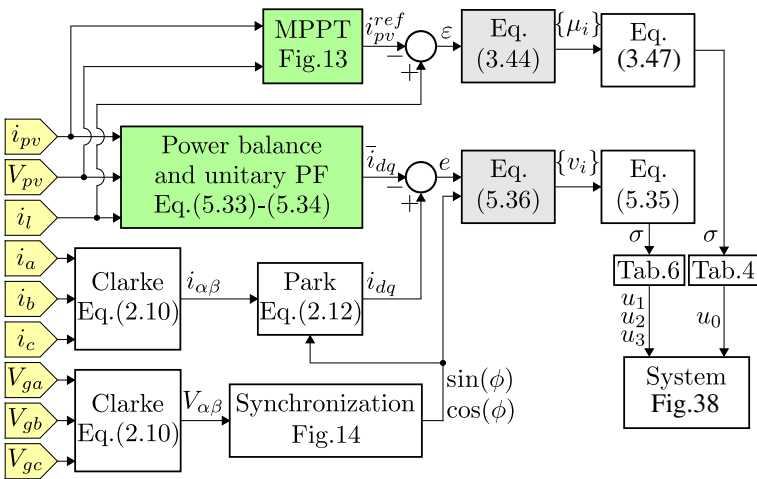


Figure 40: Complete control structure. The highlighted blocks are: the measured variables (in yellow), reference generation blocks (in green) and blocks for calculation of the Lyapunov functions (in gray).

All the measured variables necessary for the solution of the problem are presented in Figure 40 (in yellow color). These variables are only voltages and currents, all accessible and easy to obtain through measurement. The number of measuring devices could be reduced by eliminating one current measurement and one voltage measurement when the system is perfectly balanced, as considered in this work. This is possible because the sum of the three-phase currents or three-phase voltages is null in balanced systems, thus it is enough to measure the variables of two of the phases and calculate the

variables of the third phase by using the relations

$$i_c = -i_a - i_b, \quad (5.37)$$

$$V_c = -V_a - V_b. \quad (5.38)$$

It is noteworthy that the measurement of V_{pv} is not required for the switching rule designed for the stage 1, because this is accomplished with partial state measurement, however, its measurement is still necessary to calculate the references for both stages (green blocks in Figure 40). The design using partial state information was not performed with the objective of reducing the number of measuring devices, but to avoid problems in the references generation, as shown in Section 5.2.2.

A prerequisite for the operation of this control structure is to find a solution to the LMI problems of switching rule design. The solution of the LMIs is done offline, *i.e.* out of the control structure, and the coefficients Q_1, Q_2, R_1, R_2 obtained from Corollary 4.1 and P_u, Y (assuming the structure (5.36) for which the conditions for design are not presented in this thesis) are stored and then used to calculate the auxiliary functions $\mu_i, i = \{1, 2\}$, and $v_i, i = \{1, \dots, 7\}$ (grey blocks in Figure 40). It is worth to mention that the switching rules proposed in this thesis have low complexity and thus easy implementation and fast real-time computability.

For the control of the inverter, the values of v_i are compared with each other and the index of the function with the highest value determines the operation mode to be active at that instant, that is, σ . If σ is the same of the previous iteration, then there is no switching. Knowing σ , Table 6 is used to determine the commands for the position of the switches u_1, u_2, u_3 to be applied to the inverter, switching if needed. The control of the Boost is performed in a similar manner, by determining the active mode from the comparison between the values of μ_i and using the Table 4 to define u_0 .

Finally, the references of the states must pass through a ZOH, due to the consideration that these variables must be piecewise constant.

5.5 Concluding remarks

This chapter presented an application of the switching rule design technique for PV systems, where two particular topologies were used to demonstrate the procedure: a stand-alone PV system and a PV array connected to the utility grid through two converter stages. The mathematical models of the DC/DC converter (Boost) and of the DC/AC converter (in-

verter) present in the topologies were presented. The model of the voltage inverter took into account transformations to the synchronous two-phase coordinate system, specially to simplify the synchronization with the variables of the grid.

For the grid-connected topology, a decoupling between the models of the DC/DC and DC/AC converters, due to the constant DC link voltage, allows the switching rule design for each converter to be performed independently. This makes it possible to divide the two main control objectives between the two stages: the Boost achieves the MPPT while the inverter delivers power to the grid with unitary PF. With respect to the equilibrium of the system, the proposed technique performs a reference tracking, whose dynamics (unknown) are neglected with the assumption that the references are piecewise constant. A result that accomplishes reference tracking based on the (known) model of the reference dynamics can be seen in (TROFINO et al., 2009c).

As a result, the LMIs presented for the switching rule design applied for the PV-Boost system proved to be feasible and simulations were performed for the stand-alone case. From these simulations, the correct system operation could be verified, even under variations on the input parameters of the PV array, which alter both the dynamics of the system and its references. The simulated system accomplished the desired objectives in all cases, always reaching the MPP in steady state. The control design for the inverter-grid case will be considered in future works. Another idea to be explored in the future is to design observer-based switching rules. Note that the partial state information used for the DC/DC converter requires the measurement of the current state, and current sensors are more expensive and fragile than voltage sensors (YOSHIMURA et al., 2013).

As already mentioned, the development of a new MPPT technique via LMIs to be embedded into the switching rule design is also an interesting problem to be addressed in a future work. Accomplishing this task, there would be no more need to use other MPPT techniques existing in the literature for generating references to reach the MPP. A possible way to address the problem is to consider the dynamics of the power variable in the LMIs and to use a maximization criterion, as the H_∞ for instance, in a similar manner to the performed in (XU; YANG, 2010), where the objective is to maximize the sensitivity to faults in the system. Another idea is to consider the derivative of the power with respect to i_{pv} or V_{pv} , as in (2.9), as an additional state to the system to be controlled and by driving this new state to zero, the maximum power point would be reached. The main difficulty in both cases is the neces-

sity of dealing with the nonlinearities present in Equation (2.8), which makes the problem challenging to be expressed in terms of LMIs.

6 STABILITY ANALYSIS OF PIECEWISE AFFINE SYSTEMS WITH SLIDING MODES

6.1 Introduction

In continuous-time systems, the sliding mode phenomenon (UTKIN, 1992) plays an important theoretical role as a mathematical model of complex dynamics found in many practical applications (FILIPPOV, 1988). The analysis of sliding modes can be quite complex, and for this reason, it is rare to find methodologies considering the cases where sliding modes exist. Important exceptions for stability analysis of PWA systems with attractive sliding modes are found in (BRANICKY, 1998), (JOHANSSON, 2003), (SAMADI; RODRIGUES, 2011). It is proposed in (BRANICKY, 1998) to add the sliding dynamics to the modes of the system. However, this needs *a priori* information about the sliding modes, which is typically hard to get. In (JOHANSSON, 2003, p.64), an extra condition is introduced to extend the analysis to systems with attractive sliding modes. However, the conditions are never satisfied for the case where the origin belongs to a boundary between affine subsystems. In (SAMADI; RODRIGUES, 2011), stability is verified without the need of *a priori* information about the sliding modes. However, systems containing sliding modes are treated only by using common Lyapunov functions and the conservativeness introduced by not using PWQ Lyapunov functions requires the use of common Lyapunov functions of higher degree. Furthermore, the case where the equilibrium point is located at a boundary between affine subsystems has not been considered for PWA systems before in the literature, excluding important classes of systems as, for instance, applications where state-dependent surfaces are designed for tracking references that are not the equilibrium point of any of the subsystems (TROFINO et al., 2011), and power electronic converters.

This chapter presents new sufficient conditions for stability of PWA systems considering the presence of sliding modes. The results guarantee global exponential stability of the state dynamics even if attractive sliding modes occur along any switching surface of the system and even if the origin is located in a boundary between affine subsystems. The conditions are based on a convex combination of PWQ Lyapunov function and are formulated as LMIs. The method can handle PWA systems with discontinuous vector fields, which may lead to the existence of sliding modes involving any number of subsystems. Moreover, there is no need for *a priori* information about the sliding modes. If the conditions are satisfied for a system that con-

tains sliding modes, then these sliding modes are guaranteed to be stable. As a by-product, sufficient conditions for stability for any possible switching surfaces are derived as a corollary, allowing to check stability independently of the complexity of the boundary. The contributions are illustrated through four numerical examples.

The new method combines ideas from two approaches, stability analysis of PWA systems in (SAMADI; RODRIGUES, 2011) and stabilization of switched affine systems with sliding modes (TROFINO et al., 2011), providing a unified theory for both classes.

6.2 Preliminaries

This section presents the background and notation used in the rest of the chapter. First, the dynamics of a PWA system can be written as

$$\dot{x} = f_i(x) = A_i x + b_i, \quad x \in \mathcal{R}_i, \quad (6.1)$$

where $x(t) \in \mathcal{R}_i \subset \mathbb{R}^n$ is the state vector with initial condition $x(0) = x_0$, $A_i \in \mathbb{R}^{n \times n}$, $b_i \in \mathbb{R}^n$. The state space is partitioned into m open regions \mathcal{R}_i , $i \in \mathbb{I}_m := \{1, \dots, m\}$, such that

$$\bigcup_{i=1}^m \overline{\mathcal{R}_i} = \mathbb{R}^n, \quad \mathcal{R}_i \cap \mathcal{R}_j = \emptyset, \quad i \neq j. \quad (6.2)$$

where $\overline{\mathcal{R}_i}$ denotes the closure of \mathcal{R}_i . The dependence of x with respect to the time will be omitted throughout the chapter.

Considering the Filippov definition of trajectories (FILIPPOV, 1988) for solutions of (6.1), based on Definition 3.1, we get the following more general system representation of (6.1), which includes any possible sliding mode dynamics

$$\dot{x} = A_\theta x + b_\theta, \quad \theta \in \Theta, \quad x \in \mathbb{R}^n, \quad (6.3)$$

where Θ is the unit simplex defined in (3.7) and

$$A_\theta = \sum_{i=1}^m \theta_i(x) A_i, \quad b_\theta = \sum_{i=1}^m \theta_i(x) b_i. \quad (6.4)$$

The description (6.3) is general enough to represent the system dynamics at a boundary that is the intersection between any number of regions.

For stability of the origin of (6.3) we must have $\dot{x} = 0$ and $x = 0$. Therefore the following assumption is necessary.

$$\exists \theta(0) \in \Theta \quad \text{such that} \quad \sum_{i \in \sigma(0)} \theta_i(0) b_i = 0 \quad (6.5)$$

Remark 6.2.1 When $b_i \neq 0$ for some $i \in \sigma(0)$, assumption (6.5) implies that if the PWA system is stable, the equilibrium is maintained by an intermittent switching. The assumption (6.5) is more general than the assumption available in the current literature, where it is assumed that $b_i = 0$ if $i \in \sigma(0)$. \square

The subsystem i is active when $x \in \bar{\mathcal{R}}_i$. When $x \in \mathcal{R}_i$, then $\theta_i(x) = 1$, $\theta_j(x) = 0$, $\forall j \neq i$. When $x \in \bar{\mathcal{R}}_i \cap \bar{\mathcal{R}}_j \neq \emptyset$, then $\theta(x)$ assumes a specific value in Θ for that point x . The dependence of θ with respect to x can be nonlinear and difficult to take into account to formulate convex problems. For this reason, the dependence will be omitted and we will use a (possibly) more conservative approach where θ is treated as a free parameter that can assume any value inside the simplex Θ .

Finally, note that system (6.3) can be rewritten using the following more compact notation.

$$\dot{\tilde{x}} = \sum_{i=1}^m \theta_i \tilde{A}_i \tilde{x}, \quad \tilde{A}_i = \begin{bmatrix} A_i & b_i \\ 0_{1 \times n} & 0 \end{bmatrix}, \quad \tilde{x} = \begin{bmatrix} x \\ 1 \end{bmatrix} \quad (6.6)$$

6.3 Main results

This section presents the main results for the stability analysis of PWA systems, where the regions can be described by

$$\mathcal{R}_i = \{x : E_i x + e_i \succ 0\}, \quad (6.7)$$

with $E_i \in \mathbb{R}^{p_i \times n}$ and $e_i \in \mathbb{R}^{p_i}$, where p_i is the number of hyperplanes enclosing the region \mathcal{R}_i . Stability of Filippov solutions in (6.3) will be proved using a Lyapunov function. The candidate Lyapunov function considered in this chapter is a convex combination of PWQ functions with the following structure.

$$V(x) = \sum_{i=1}^m \theta_i \tilde{x}' \tilde{P}_i \tilde{x}, \quad \tilde{P}_i = \begin{bmatrix} P_i & \star \\ q'_i & r_i \end{bmatrix} \quad (6.8)$$

Before presenting the theorem for stability, consider the following definitions, auxiliary notation and LMI conditions.

Let $\mathcal{S}_k \subset \mathbb{R}^n$ be the set of points x belonging to the k -th surface between any number of adjacent regions and let \mathbb{S}_k be the set of all regions i sharing the k -th surface, where $k \in \mathbb{I}_g$ and g is the total number of surfaces.

Note that $\text{row}_j(E_i)x + \text{row}_j(e_i) = 0$, $j \in \mathbb{I}_{p_i}$, represents each of the p_i surfaces surrounding $\bar{\mathcal{R}}_i$. For all $k \in \mathbb{I}_g$, define l_k as one (it can be any) of the integers in \mathbb{S}_k . Therefore, if $i = l_k$, then $i \in \mathbb{S}_k$. Define for all $k \in \mathbb{I}_g$, $E_k := \text{row}_j(E_{l_k})$ and $e_k := \text{row}_j(e_{l_k})$, where j is such that $\text{row}_j(E_{l_k})x + \text{row}_j(e_{l_k}) = 0 \forall x \in \mathcal{S}_k$. Therefore, $E_k x + e_k = 0$, $\forall x \in \mathcal{S}_k$.

Consider the following auxiliary notation.

$$C_{a_k} = E_k, \quad \tilde{C}_{a_k} = [E_k \quad e_k], \quad \tilde{E}_i = \begin{bmatrix} E_i & e_i \\ 0_{1 \times n} & 1 \end{bmatrix} \quad (6.9)$$

$$P = [P_1 \quad \dots \quad P_m], \quad q = [q_1 \quad \dots \quad q_m], \quad r = [r_1 \quad \dots \quad r_m] \quad (6.10)$$

$$A = [A_1 \quad \dots \quad A_m] \quad , \quad b = [b_1 \quad \dots \quad b_m] \quad (6.11)$$

$$\tilde{\alpha} = [\alpha_1 \quad \dots \quad \alpha_m] \quad , \quad \alpha = \tilde{\alpha} \otimes I_n \quad (6.12)$$

$$C_t = \mathfrak{K}_\theta \otimes I_n \quad , \quad \tilde{C}_t = \begin{bmatrix} \mathfrak{K}_\theta \otimes I_n & 0_{dn \times m} \\ 0_{d \times nm} & \mathfrak{K}_\theta \end{bmatrix} \quad (6.13)$$

$$\mathfrak{K}_\theta \in \mathbb{R}^{d \times m} \quad , \quad M = [1 \quad \dots \quad 1] \in \mathbb{R}^{1 \times m} \quad (6.14)$$

$$C_{b_k} = C_{a_k} (M \otimes I_n) \quad , \quad \tilde{C}_{b_k} = \tilde{C}_{a_k} \begin{bmatrix} M \otimes I_n & 0_{n \times m} \\ 0_{1 \times nm} & M \end{bmatrix} \quad (6.15)$$

$$\Upsilon = \begin{bmatrix} A'P + P'A + \alpha'P + P'\alpha & \star \\ b'P + q'A + 2q'\alpha & b'q + q'b + \alpha'_m r + r'\alpha_m \end{bmatrix} \quad (6.16)$$

where \mathfrak{K}_θ is the linear annihilator of θ as defined in (2.20).

1) LMI conditions for positivity of $\mathbf{V}(\mathbf{x})$ with $\mathbf{V}(\mathbf{0}) = \mathbf{0}$:

$$r_i = 0, \quad \text{if } i \in \sigma(0) \quad (6.17)$$

$$q_i = 0, \quad \text{if } b_i = 0 \quad (6.18)$$

$$q'_i = \sum_{j=1}^{p_i} \gamma_{ij} \text{row}_j(E_i), \quad \text{if } b_i \neq 0 \quad (6.19)$$

$$P_i \geq \varepsilon I_n, \quad \text{if } b_i = 0 \text{ and } e_i \neq 0 \quad (6.20)$$

$$\begin{cases} Z_i \succeq 0 \\ P_i - E'_i Z_i E_i \geq \varepsilon I_n \end{cases}, \quad \text{if } e_i = 0 \quad (6.21)$$

$$\begin{cases} \tilde{Z}_i \succeq 0 \\ \tilde{P}_i - \tilde{E}'_i \tilde{Z}_i \tilde{E}_i \geq \varepsilon \begin{bmatrix} I_n & \star \\ 0_{1 \times n} & 0 \end{bmatrix} \end{cases}, \quad \text{if } b_i \neq 0 \text{ and } e_i \neq 0 \quad (6.22)$$

$$Q'_{a_k} (P_i - \varepsilon I_n) Q_{a_k} \geq 0, \quad \text{if } e_i = 0 \quad (6.23)$$

$$\tilde{Q}'_{a_k} \left(\tilde{P}_i - \varepsilon \begin{bmatrix} I_n & \star \\ 0_{1 \times n} & 0 \end{bmatrix} \right) \tilde{Q}_{a_k} \geq 0, \quad \text{if } b_i \neq 0 \text{ and } e_i \neq 0 \quad (6.24)$$

where $\varepsilon > 0$, $\gamma_{ij} > 0$, $\forall i \in \mathbb{I}_m$, $\forall j \in \mathbb{I}_{p_i}$, and Q_{a_k}, \tilde{Q}_{a_k} are given matrix basis for the null spaces of C_{a_k}, \tilde{C}_{a_k} , respectively.

2) LMI conditions for decay of $\mathbf{V}(\mathbf{x})$:

$$P_i A_i + A'_i P_i + \alpha_i P_i < 0, \quad \text{if } b_i = 0 \text{ and } e_i \neq 0 \quad (6.25)$$

$$\begin{cases} \Lambda_i \succeq 0 \\ P_i A_i + A'_i P_i + \alpha_i P_i + E'_i \Lambda_i E_i < 0 \end{cases}, \quad \text{if } b_i = 0 \text{ and } e_i = 0 \quad (6.26)$$

$$\begin{cases} \tilde{\Lambda}_i \succeq 0 \\ \tilde{P}_i \tilde{A}_i + \tilde{A}'_i \tilde{P}_i + \alpha_i \tilde{P}_i + \tilde{E}'_i \tilde{\Lambda}_i \tilde{E}_i < 0 \end{cases}, \quad \text{if } b_i \neq 0 \quad (6.27)$$

$$P'A + A'P + \alpha'P + P'\alpha + L_t C_t(\theta) + C_t(\theta)' L'_t < 0, \quad \forall \theta \in \vartheta(\Theta), \\ \text{if } b_i = 0 \forall i \in \mathbb{I}_m \text{ and } \exists i : e_i \neq 0 \quad (6.28)$$

$$Q'_{b_k} (P'A + A'P + \alpha'P + P'\alpha + L_t C_t(\theta) + C_t(\theta)' L'_t) Q_{b_k} < 0, \quad \forall \theta \in \vartheta(\Theta), \\ \text{if } (b_i = 0 \text{ and } e_i = 0) \forall i \in \mathbb{I}_m \quad (6.29)$$

$$\tilde{Q}'_{b_k} (\Upsilon + \tilde{L}_t \tilde{C}_t(\theta) + \tilde{C}_t(\theta)' \tilde{L}'_t) \tilde{Q}_{b_k} < 0, \quad \forall \theta \in \vartheta(\Theta), \quad \text{if } \exists i : b_i \neq 0 \quad (6.30)$$

where L_t has the dimensions of $C_t(\theta)'$ and Q_{b_k}, \tilde{Q}_{b_k} are given matrix basis for the null spaces of C_{b_k}, \tilde{C}_{b_k} , respectively.

3) LMI conditions for continuity of $\mathbf{V}(\mathbf{x})$:

$$\tilde{Q}'_{a_k} (\tilde{P}_i - \tilde{P}_j) \tilde{Q}_{a_k} = 0 \quad , \quad \forall i, j \in \mathbb{S}_k, i \neq j \quad (6.31)$$

Taking into account all possible pairs $i, j \in \mathbb{S}_k$ for $i \neq j$ without repetition, *i.e.* $\forall i, j \in \mathbb{S}_k$ with $j > i$, we avoid declaring redundant LMIs in (6.31).

The result for global stability analysis is formalized in the following theorem.

Theorem 6.1 Consider the system (6.3) with assumption (6.5) and regions described by (6.7). With the auxiliary notation (6.9)-(6.16), let $Q_{a_k}, \tilde{Q}_{a_k}, Q_{b_k}, \tilde{Q}_{b_k}$ be given matrix basis for the null space of $C_{a_k}, \tilde{C}_{a_k}, C_{b_k}, \tilde{C}_{b_k}$, respectively, and L_t, \tilde{L}_t be matrices to be determined with the dimensions of $C_t(\theta)'$, $\tilde{C}_t(\theta)'$. Suppose $\exists \tilde{P}_i, Z_i, \tilde{Z}_i, \Lambda_i, \tilde{\Lambda}_i, L_t, \tilde{L}_t, \varepsilon > 0, \gamma_i > 0$ and given decay rates $\alpha_i > 0$ solving the LMIs (6.17)-(6.31) for all $i \in \mathbb{I}_m$ and for all $k \in \mathbb{I}_g$. Then (6.8) is a Lyapunov function for the system (6.3) and the origin is globally exponentially stable. \square

Proof: The proof is structured as follows. First, continuity of $V(x)$ is ensured $\forall x \in \mathbb{R}^n$, followed by positivity of $V(x), \forall x \in \mathbb{R}^n$. Next, the proof for decreasing of $V(x), \forall x \in \mathbb{R}^n$ is divided in two parts, $\forall x \in \mathcal{R}_i, \forall i \in \mathbb{I}_m$ and $\forall x \in \mathcal{S}_k, \forall k \in \mathbb{I}_g$ (note that the union of \mathcal{R}_i for all $i \in \mathbb{I}_m$ and \mathcal{S}_k for all $k \in \mathbb{I}_g$ results in \mathbb{R}^n). At the end, the results are summarized and the conclusion about stability is presented.

Consider the Lyapunov function candidate (6.8) rewritten as $V(x) = \sum_{i=1}^m \theta_i v_i(x)$, where $v_i(x) = \tilde{x}' \tilde{P}_i \tilde{x}$. Noticing that $\tilde{C}_{a_k} \tilde{x} = 0$ and then using the Finsler's Lemma, it follows from (6.31) that for any $x \in \mathcal{S}_k, \forall k \in \mathbb{I}_g, v_i(x) = v_j(x), \forall i, j \in \mathbb{S}_k$. Therefore, $V(x)$ is continuous $\forall x \in \mathbb{R}^n$. In addition, constraint (6.17) implies that $V(0) = 0$. Note in Definition 3.1 that if $x \in \mathcal{R}_i$, then $\theta_i = 1, \theta_j = 0, \forall j \neq i$, therefore $V(x) = v_i(x), \forall x \in \mathcal{R}_i$.

The proof that positivity of $V(x)$ is ensured $\forall x \in \mathbb{R}^n$ is subdivided in three parts, contemplating all cases of e_i and b_i :

1. If $e_i \neq 0$ and $b_i = 0$, we conclude from (6.17), (6.18), (6.20) that for all $x \neq 0 \in \overline{\mathcal{R}}_i$ (including $\forall x \in \mathcal{S}_k$), $v_i(x) = x' P_i x \geq \varepsilon \|x\|^2 > 0$, therefore

$$V(x) = \sum_{i=1}^m \theta_i v_i(x) \geq \min_{i \in \mathbb{I}_m} \{v_i(x)\} \geq \varepsilon \|x\|^2 > 0, \quad \forall \theta \in \Theta.$$

2. If $e_i = 0$, we have $\mathcal{R}_i = \{x \mid E_i x \succ 0\}$, then for any Z_i with appropriate dimensions and non-negative entries, for all $x \in \mathcal{R}_i$, $x' E_i' Z_i E_i x \geq 0$. Also note that (6.19) with $\gamma_j \succ 0$ implies $q_i' x = \sum_{j=1}^{P_i} \gamma_j \text{row}_j(E_i) x \succeq 0$ for all $x \in \overline{\mathcal{R}}_i$. In this case, (6.17), (6.18), (6.19), (6.21) yield

$$\begin{aligned} V(x) = v_i(x) &= x' P_i x + 2q_i' x \geq x' P_i x \geq \\ & x' E_i' Z_i E_i x + \varepsilon \|x\|^2 \geq \varepsilon \|x\|^2 > 0. \end{aligned} \quad (6.32)$$

for all $x \neq 0 \in \mathcal{R}_i$. To ensure positiveness of $V(x)$, $\forall x \in \mathcal{S}_k$, $\forall k \in \mathbb{I}_g$, the condition is

$$\begin{aligned} V(x) &= \sum_{i=1}^m \theta_i \tilde{x}' \tilde{P}_i \tilde{x} \geq \sum_{i=1}^m \theta_i x' P_i x \geq \varepsilon x' x = \varepsilon \|x\|^2 > 0, \\ & \forall \theta \in \vartheta(\Theta), \forall x \in \mathbb{R}^n : C_{a_k} x = 0. \end{aligned} \quad (6.33)$$

Evaluating θ_i in $\sum_{i=1}^m \theta_i x' P_i x \geq \varepsilon x' x$ for all vertices of Θ and noticing that C_{a_k} is an annihilator of x with constant entries only, we get (6.23) by using the Finsler's Lemma.

3. If $e_i \neq 0$ and $b_i \neq 0$, we have $\mathcal{R}_i = \{x \mid \tilde{E}_i \tilde{x} \succ 0\}$ and similarly to the previous case, condition (6.22) yields

$$V(x) = v_i(x) = \tilde{x}' \tilde{P}_i \tilde{x} \geq \tilde{x}' \tilde{E}_i' \tilde{Z}_i \tilde{E}_i \tilde{x} + \varepsilon \|x\|^2 \geq \varepsilon \|x\|^2 > 0. \quad (6.34)$$

for all $x \neq 0 \in \mathcal{R}_i$. To ensure positiveness of $V(x)$, $\forall x \in \mathcal{S}_k$, $\forall k \in \mathbb{I}_g$, the condition is

$$\begin{aligned} V(x) &= \sum_{i=1}^m \theta_i \tilde{x}' \tilde{P}_i \tilde{x} \geq \varepsilon x' x = \varepsilon \|x\|^2 > 0, \\ & \forall \theta \in \vartheta(\Theta), \forall x \in \mathbb{R}^n : \tilde{C}_{a_k} \tilde{x} = 0. \end{aligned} \quad (6.35)$$

Evaluating θ_i for the vertices of Θ in condition (6.35) and noticing that \tilde{C}_{a_k} is an annihilator of \tilde{x} with constant entries only, we get (6.24) by using the Finsler's Lemma.

It has been shown that $V(x)$ is positive for $x \in \mathbb{R}^n$. Also $V(x)$ is radially unbounded since $V(x) \geq \varepsilon \|x\|^2$, which is a positive definite quadratic form. Moreover, $v_i(x) \leq \beta_i(\|x\|)$ where $\beta_i(\|x\|) := \|P_i\| \|x\|^2 + 2\|q_i\| \|x\| + \|r_i\|$. As

$V(x)$ is a convex combination of the active functions $v_i(x)$, we have $V(x) \leq \max_{i \in \sigma(x)} \{v_i(x)\}$. This shows that

$$\varepsilon \|x\|^2 \leq V(x) \leq \max_{i \in \sigma(x)} \{\beta_i(\|x\|)\}, \quad (6.36)$$

where the lower and upper bounds are class \mathcal{K}_∞ functions, as in Definition 2.3.

The proof that $V(x)$ is decreasing $\forall x \in \mathcal{R}_i$ is also divided in three parts, contemplating all cases of b_i and e_i :

1. If $b_i = 0$ and $e_i \neq 0$, we conclude from (6.25) that for all $x \neq 0 \in \mathcal{R}_i$,

$$\begin{aligned} \nabla V(x)' A_\theta x &= \nabla v_i(x)' A_i x = 2x' P_i A_i x = x' (P_i A_i + A_i' P_i) x \\ &< -\alpha_i x' P_i x = -\alpha_i v_i(x) = -\alpha_i V(x) < 0. \end{aligned} \quad (6.37)$$

2. If $b_i = 0$ and $e_i = 0$, we have $\mathcal{R}_i = \{x \mid E_i x \succ 0\}$, then for any Λ_i with appropriate dimensions and non-negative entries, for all $x \in \mathcal{R}_i$, $x' E_i' \Lambda_i E_i x \geq 0$. In this case, (6.26) yields

$$\begin{aligned} \nabla V(x)' A_\theta x &= \nabla v_i(x)' A_i x < -\alpha_i x' P_i x - x' E_i' \Lambda_i E_i x \\ &\leq -\alpha_i x' P_i x = -\alpha_i v_i(x) = -\alpha_i V(x) < 0 \end{aligned} \quad (6.38)$$

for all $x \neq 0 \in \mathcal{R}_i$.

3. If $b_i \neq 0$, we have $\mathcal{R}_i = \{x \mid \tilde{E}_i \tilde{x} \succ 0\}$ and similarly to the previous case, condition (6.27) yields

$$\begin{aligned} \nabla V(x)' (A_\theta x + b_\theta) &= \nabla v_i(x)' (A_i x + b_i) = 2\tilde{x}' \tilde{P}_i \tilde{A}_i \tilde{x} \\ &< -\alpha_i \tilde{x}' \tilde{P}_i \tilde{x} - \tilde{x}' \tilde{E}_i' \tilde{\Lambda}_i \tilde{E}_i \tilde{x} \leq -\alpha_i \tilde{x}' \tilde{P}_i \tilde{x} \\ &= -\alpha_i v_i(x) = -\alpha_i V(x) < 0 \end{aligned} \quad (6.39)$$

for all $x \neq 0 \in \mathcal{R}_i$.

The next steps show how to obtain the conditions for $V(x)$ decreasing for $x \in \mathcal{S}_k$, $\forall k \in \mathbb{I}_g$. Consider the compact notation $P_\theta := \sum_{i=1}^m \theta_i P_i$ and $q_\theta, r_\theta, A_\theta, b_\theta, \alpha_\theta$ defined in a similar way.

1. If $b_i = 0, \forall i \in \mathbb{S}_k$, this condition can be characterized by

$$\begin{aligned} \nabla V(x)' A_\theta x &= 2x' P_\theta A_\theta x = x' (P_\theta A_\theta + A'_\theta P_\theta) x < \\ &- 2\alpha_\theta x' P_\theta x = -2\alpha_\theta V(x) < 0. \end{aligned} \quad (6.40)$$

See (TROFINO et al., 2011) for details on the equivalence in the first equality of (6.40). Using the auxiliary notation (6.10)-(6.16), the condition (6.40) can be rewritten as

$$x' (P_\theta A_\theta + A'_\theta P_\theta) x - 2\alpha_\theta x' P_\theta x = x'_\theta (PA + A'P + P\alpha + \alpha'P) x_\theta < 0, \quad (6.41)$$

where $x_\theta = \theta \otimes x = [\theta_1 x' \quad \dots \quad \theta_m x']' \in \mathbb{R}^{mn}$. Noticing that $C_t(\theta)$ is a linear annihilator of x_θ (i.e. $C_t(\theta)x_\theta = 0$), we insert it in condition (6.41) by using the Finsler's Lemma and obtain the LMI (6.28). Moreover, if $e_i = 0, \forall i \in \mathbb{I}_m$, it is possible to use the annihilator $C_{b_k} x_\theta = 0$, along with the Finsler's Lemma, to reduce the conservativeness of (6.28), obtaining (6.29).

2. If $\exists i \in \mathbb{S}_k : b_i \neq 0$, the condition for $V(x)$ decreasing for $x \in \mathcal{S}_k, \forall k \in \mathbb{I}_g$, can be characterized by

$$\begin{aligned} \nabla V(x)' (A_\theta x + b_\theta) &= \tilde{x}' \begin{bmatrix} P_\theta A_\theta + A'_\theta P_\theta & \star \\ b'_\theta P_\theta + q'_\theta A_\theta & b'_\theta q_\theta + q'_\theta b_\theta \end{bmatrix} \tilde{x} \\ &< -2\alpha_\theta \tilde{x}' \begin{bmatrix} P_\theta & \star \\ q'_\theta & r_\theta \end{bmatrix} \tilde{x} = -2\alpha_\theta V(x) < 0. \end{aligned} \quad (6.42)$$

See (TROFINO et al., 2011) for details on the first equality of (6.42). Using (6.10)-(6.16), the condition (6.42) can be rewritten as

$$\tilde{x}'_\theta \Upsilon \tilde{x}_\theta < 0, \quad \tilde{x}_\theta = \begin{bmatrix} \theta \otimes x \\ \theta \end{bmatrix}. \quad (6.43)$$

As in the previous case, note that $\tilde{C}_t(\theta)\tilde{x}_\theta = 0$ and $\tilde{C}_{b_k}\tilde{x}_\theta = 0$. By using the Finsler's Lemma to insert these annihilators to relax the condition (6.43), we get the LMI condition (6.30).

The last situation that needs to be considered is when $V(x)$ is not differentiable at a point x . As $V_i(x)$ are continuously differentiable functions, $V(x)$ is locally Lipschitz. Keeping in mind that θ and σ are piecewise continuous and piecewise constant, respectively, the points of discontinuity of the

vector field are isolated points of the system trajectory and thus $V(x)$ cannot increase at the points where $V(x)$ is not differentiable. Furthermore, θ may be discontinuous at the boundaries but $V(x)$ is guaranteed to be decreasing because the conditions (6.28)-(6.30) hold $\forall \theta \in \Theta$.

In summary, $V(x)$ is continuous, positive definite and satisfies the bounds (6.36). Moreover, $V(x)$ is globally strictly decreasing for the dynamics of the system (6.3), that includes the subsystem dynamics and the sliding mode dynamics that may eventually occur at any switching surface, and global exponential stability follows from (FILIPPOV, 1988, p.155). \square

Remark 6.3.1 *Compared to the current literature, conditions (6.19), (6.23), (6.24), (6.28)-(6.30) are new. Condition (6.19) allows feasibility when the origin is located in a boundary between affine subsystems and (6.23), (6.24), (6.28)-(6.30) guarantee stability of any sliding mode dynamics that may occur.* \square

The following interesting corollary is derived from Theorem 6.1.

Corollary 6.1 (Stability independent of the boundaries) *If it is possible to find a solution for Theorem 6.1 by replacing the variables $Z_i, \tilde{Z}_i, \Lambda_i, \tilde{\Lambda}_i, \gamma_{ij}$ by zeros and $Q_{a_k}, \tilde{Q}_{a_k}, Q_{b_k}, \tilde{Q}_{b_k}$ by identity matrices, all with appropriate dimensions, then this system is globally exponentially stable for any boundaries.* \square

Proof: Follows trivially as a particular case of the proof of Theorem 6.1, noticing that by fixing the decision variables as suggested in Corollary 6.1, the LMIs are now checked without inserting any information about any specific surface to relax the conditions. \square

Remark 6.3.2 *Note that in Corollary 6.1, the continuity condition (6.31) is replaced by*

$$\tilde{P}_i - \tilde{P}_j = 0 \quad , \quad \forall i, j \in \mathbb{I}_m, i \neq j, \quad (6.44)$$

which is satisfied only if it is possible to force all Lyapunov functions to be equal, reducing the problem to the one of finding a single quadratic Lyapunov function. This may be more conservative than Theorem 6.1, but a stronger result is obtained as stability is guaranteed even if the boundaries change. \square

Remark 6.3.3 (Discontinuous Lyapunov functions) *It is known that a continuous Lyapunov function is not a requirement for stability analysis of PWA*

systems as long as it decreases along the trajectories, as shown and exemplified in (MIGNONE; FERRARI-TRECCATE; MORARI, 2000). However, discontinuous Lyapunov functions are only possible where the state trajectory crosses the switching surfaces without entering in a sliding mode, thus a priori knowledge about the existence and location of sliding modes is required. For instance, consider a point located at a switching surface between regions \mathcal{R}_i and \mathcal{R}_j . If a sliding mode is occurring, then the crossing may occur both from \mathcal{R}_i to \mathcal{R}_j and from \mathcal{R}_j to \mathcal{R}_i at that point. If there is a decreasing discontinuity in the Lyapunov function in one direction, then it is increasing in the other direction. Thus, continuity of the Lyapunov function is required at the given point. \square

6.4 Numerical examples

In the examples that follow we have used SeDuMi (STURM, 2001) and SDPT3 (TOH; TODD; TÜTÜNCÜ, 1996) with Yalmip interface (LÖFBERG, 2004) to solve the LMIs and Simulink to obtain the state trajectories. Example 6.1 shows a systems with unstable sliding modes. Example 6.2 illustrates the case where the origin is located at a boundary between affine subsystems. Example 6.3 shows the application of Corollary 6.1.

Example 6.1 (Unstable sliding mode) Consider the system

$$\begin{cases} \dot{x} = A_1x + b_1, & \text{if } x_2 \geq 0 \\ \dot{x} = A_2x + b_2, & \text{if } x_2 \leq 0 \end{cases} \quad (6.45)$$

with the following matrices A_1 , A_2 , b_1 , b_2 , respectively (SAMADI; RODRIGUES, 2011).

$$\begin{bmatrix} 1 & -2 \\ 2 & -2 \end{bmatrix}, \begin{bmatrix} 1 & 2 \\ -2 & -2 \end{bmatrix}, \begin{bmatrix} 0 \\ 0 \end{bmatrix}, \begin{bmatrix} 0 \\ 0 \end{bmatrix} \quad (6.46)$$

Although this system has both A_1 and A_2 Hurwitz, it presents an unstable sliding mode (SAMADI; RODRIGUES, 2011), as shown in Figure 41.

The regions \mathcal{R}_i can be expressed as in (6.7) with

$$E_1 = \begin{bmatrix} 0 & 1 \end{bmatrix}, E_2 = \begin{bmatrix} 0 & -1 \end{bmatrix}, e_1 = e_2 = 0. \quad (6.47)$$

The LMIs to be solved in this case are (6.17), (6.21), (6.23), (6.26), (6.29), (6.31). It is not possible to find a feasible solution, which is consistent

with the expected result. Without the condition (6.29) for inclusion of sliding modes dynamics, the LMI problem would be feasible, providing a wrong conclusion about the stability of the system. Reference (SAMADI; RODRIGUES, 2011) gets the same infeasible result by using a more conservative approach with a common quadratic Lyapunov function. \square

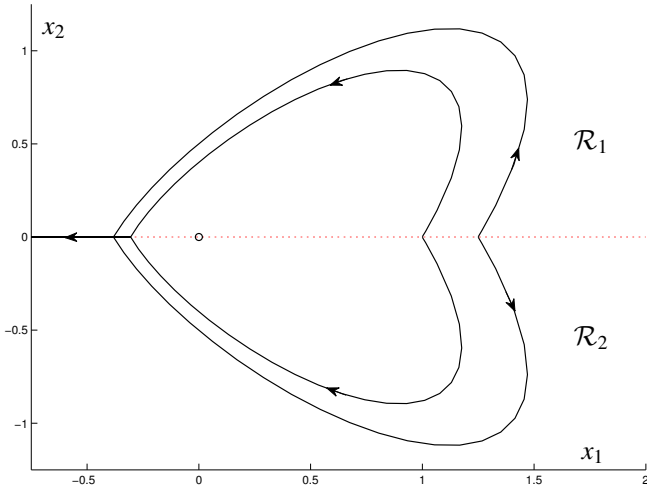


Figure 41: Some state trajectories for the system in Example 6.1 (solid black curves) and the switching surface (red dotted line).

Example 6.2 (Origin at the surface between affine subsystems) Consider the system (6.45), with the regions parameterized by (6.47), with the matrices A_1, A_2, b_1, b_2 given by, respectively,

$$\begin{bmatrix} -2 & -2 \\ 4 & 1 \end{bmatrix}, \begin{bmatrix} -2 & 2 \\ -4 & 1 \end{bmatrix}, \begin{bmatrix} 0 \\ -\delta \end{bmatrix}, \begin{bmatrix} 0 \\ \delta \end{bmatrix}, \quad (6.48)$$

where δ is a given fixed parameter. This system presents only stable sliding modes for $\delta \geq 0$. First, consider the case where $\delta = 0$. According to (JOHANSSON, 2003, p. 84), it is not possible to find a quadratic or class C^1 PWQ function for this system. However, Theorem 6.1 does not require a class C^1 function to be satisfied. Solving the same LMIs of Example 6.1, a feasible

solution is found. Reference (SAMADI; RODRIGUES, 2011) solves this case by using a sixth order C^1 polynomial Lyapunov function.

For the case where $\delta > 0$, note that the system satisfies assumption (6.5) with $\theta_i(0) = 1/2, \forall i \in \mathbb{I}_m$. In this case the LMIs to be solved are (6.17), (6.19), (6.21), (6.23), (6.26), (6.30), (6.31). Consider $\delta = 2$ as an example, for which some trajectories are shown in Figure 42. If an initial condition is outside the blue dot-dashed curve, then it converges to the origin through the sliding mode $\dot{x} = f_\theta = [x_1 \ 0]'$. Otherwise, through the sliding mode $\dot{x} = f_\theta = [-x_1 \ 0]'$. The conditions are tested and a feasible solution is found. Note that the origin is located at a boundary between affine subsystems, for which case there is no other stability analysis method available in the current literature. \square

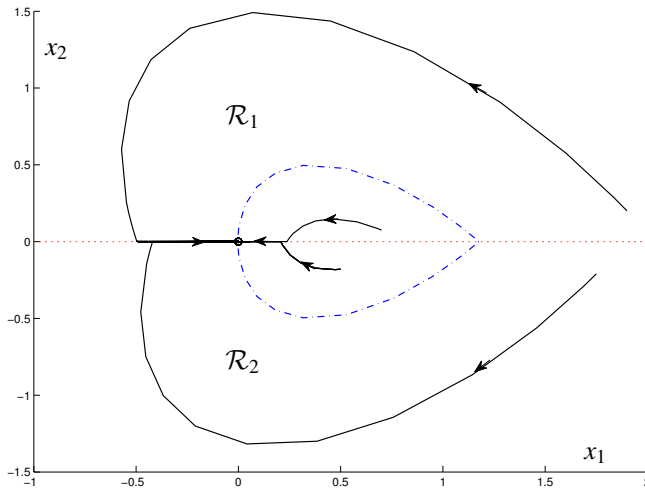


Figure 42: Some state trajectories for the system in Example 6.2 with $\delta = 2$ (black solid curves), the switching surface (red dotted line) and trajectories that touch the surface only at the origin (blue dot-dashed curve).

Example 6.3 Consider the system

$$\begin{cases} \dot{x} = A_1x + b_1, & \text{if } x_2 + 1 \geq 0 \\ \dot{x} = A_2x + b_2, & \text{if } x_2 + 1 \leq 0 \end{cases} \quad (6.49)$$

with the matrices A_1, A_2, b_1, b_2 given by, respectively,

$$\begin{bmatrix} -1 & -2 \\ 2 & -2 \end{bmatrix}, \begin{bmatrix} -1 & 2 \\ -2 & -2 \end{bmatrix}, \begin{bmatrix} 0 \\ 0 \end{bmatrix}, \begin{bmatrix} \delta \\ 0 \end{bmatrix}, \quad (6.50)$$

where δ is a given fixed parameter. The regions \mathcal{R}_i are parameterized as in (6.7) with

$$E_1 = \begin{bmatrix} 0 & 1 \end{bmatrix}, \quad E_2 = \begin{bmatrix} 0 & -1 \end{bmatrix}, \quad e_1 = 1, \quad e_2 = -1. \quad (6.51)$$

For the case of $\delta = 0$, the LMIs to be solved are the same as in Example 6.1. A feasible solution is found, showing that the system (6.49) is stable for the given surface, even with the occurrence of a sliding mode. Moreover, it is possible to prove that the system (6.49) is stable for any possible surfaces by fixing the matrices Z_i, Λ_i equal to zero and $Q_{a_k}, Q_{a_k}, Q_{b_k}$ equal to identity matrices, as mentioned in the Corollary 6.1, then solving the same set of LMIs, which is feasible.

For the case of $\delta \neq 0$, subsystem 2 is affine and Corollary 6.1 is not feasible because the equilibrium point of this subsystem, given by

$$\bar{x}|_{i=2} = -A_2^{-1}b_2 = \frac{1}{3} \begin{bmatrix} \delta \\ -\delta \end{bmatrix}, \quad (6.52)$$

is not the origin. Recalling that A_2 is Hurwitz, it is easy to realize that for boundaries that let $\bar{x}|_{i=2} \in \mathcal{R}_2$, the system is not globally stable. Therefore, for the boundary given in (6.49), the origin of the PWA system is not globally stable for $\delta \geq 3$. For this case, the LMIs to be solved to analyze stability are (6.17), (6.20), (6.25) for $i = 1$, (6.22), (6.24), (6.27) for $i = 2$, and (6.30), (6.31). As expected, it is not possible to find a solution when $\delta \geq 3$, but it is possible when $\delta < 3$. In the latter case, the closer δ gets to 3, the closer α_2 must get to 0. Figure 43 shows the occurrence of a stable sliding mode for the particular case of $\delta = 1$. \square

Example 6.4 (Switching rule stability) The objective of this example is to check the stability of a previously designed switching rule method for a real application. Consider the Buck converter presented in Figure 44 with a linear

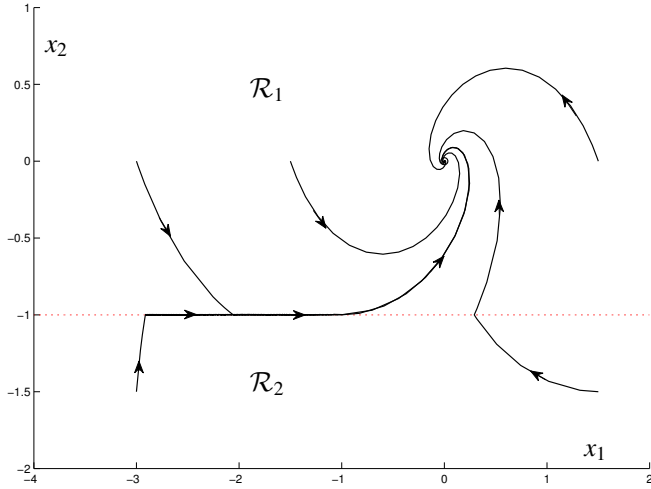


Figure 43: Some state trajectories for the system in Example 6.3 for $\delta = 1$ (black solid curves) and the switching surface (red dotted line).

load (resistor).

Considering as system states the error between the current in the inductor and its desired reference ($x_1 = i_L - \bar{i}_L$) and the error between the voltage over the output capacitor and its desired reference ($x_2 = V_{out} - \bar{V}_{out}$), we have the system representation (6.3) with two different subsystems ($m = 2$), where

$$A_1 = \begin{bmatrix} 0 & -\frac{1}{L} \\ \frac{1}{C} & -\frac{1}{RC} \end{bmatrix}, A_2 = \begin{bmatrix} 0 & -\frac{1}{L} \\ \frac{1}{C} & -\frac{1}{RC} \end{bmatrix}, b_1 = \begin{bmatrix} \frac{V_{in} - \bar{V}_{out}}{L} \\ 0 \end{bmatrix}, b_2 = \begin{bmatrix} -\frac{\bar{V}_{out}}{L} \\ 0 \end{bmatrix}. \quad (6.53)$$

The following relation can be established based on the assumption (6.5).

$$\theta_1(0) = \frac{\bar{V}_{out}}{V_{in}} \quad (6.54)$$

This shows that the desired equilibrium is always maintained by an intermittent switching, except for the trivial cases $\bar{V}_{out} = 0$ (switch constantly open) and $\bar{V}_{out} = V_{in}$ (switch constantly closed).

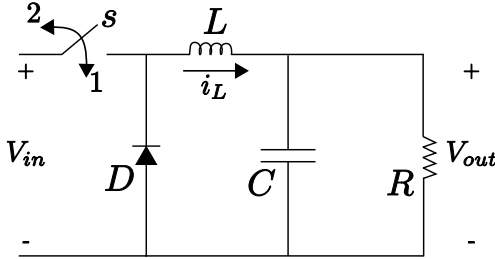


Figure 44: Structure of the Buck converter.

Parameter	Value
V_{in}	15V
L	10^{-3}H
C	10^{-6}F
R	30Ω
\bar{V}_{out}	9V
\bar{i}_L	$\frac{\bar{V}_{out}}{R}$

Table 8: Parameters of the Buck converter from Figure 44.

Let us consider the switching rule design method proposed in Chapter 3 (TROFINO *et al.*, 2011), where the state space is partitioned into two regions and in each region the switch s is in one position. As the objective is to make the states converge to a given reference, the origin of the error system must be stable. The constant parameters of the system are given in Table 8. Let us inspect the switching rule (3.3). Note that by forcing the matrices to be determined in the quadratic term to be equal $\forall i \in \mathbb{I}_m$, the quadratic term does not influence the index given by the max function in the switching rule. Thus, the switching rule (3.3) can be rewritten as

$$\sigma(x(t)) := \arg \max_{i \in \mathbb{I}_m} \{2S'_i x(t)\} = \begin{cases} 1 & \text{if } (S'_1 - S'_2)x(t) > 0 \\ 2 & \text{if } (S'_2 - S'_1)x(t) > 0 \end{cases} \quad (6.55)$$

Solving the LMIs of Theorem 3.1 for the given Buck system, we get the switch-

ing rule (6.55) with the matrices S_i given by

$$S_1 = \begin{bmatrix} -1.4284 \times 10^{-3} \\ -1.5579 \times 10^{-4} \end{bmatrix}, \quad S_2 = \begin{bmatrix} 2.1426 \times 10^{-3} \\ 2.3369 \times 10^{-4} \end{bmatrix}. \quad (6.56)$$

This results in a PWA system where the regions can be expressed as in (6.7) with

$$E_1 = S'_1 - S'_2 = \begin{bmatrix} -3.5711 \times 10^{-3} & -3.8949 \times 10^{-4} \end{bmatrix}, \\ E_2 = -E_1, \quad e_1 = e_2 = 0. \quad (6.57)$$

The LMIs from Theorem 6.1 to be solved in this case are (6.17), (6.19), (6.21), (6.23), (6.26), (6.30), (6.31), and a feasible solution is found. This shows that the origin of the error system is stable, i.e. the desired equilibrium point is achieved by the given switching rule. \square

6.5 Concluding remarks

In this chapter, sufficient conditions for stability of PWA systems were formulated as convex problems. The conditions are sufficient for checking the stability of systems even in the occurrence of sliding modes and there is no need to know *a priori* in which switching surfaces a sliding mode happens, if it does. Besides that, a relaxation to the equilibrium assumption is presented, allowing the stability analysis of systems where the origin is located at the boundary between affine subsystems. With this result, it is possible to check the stability of the switching rule design technique proposed in Chapter 3 for affine systems, provided that the switching surface is a hyperplane. As a by-product, sufficient conditions for stability for any switching surfaces are derived at the expense of some additional conservatism. Examples were used to illustrate the application and the advantages of the proposed method.

Some ideas for future works are discussed in the sequel. First, the extension for the case where the surfaces are characterized by quadratic equations, not hyperplanes, in which the stability analysis could include systems such as the one in Example 3.2. This theory is already under development and will be published soon. Second, control design for mixed systems of the type switched affine and piecewise affine, *e.g.* systems containing controllable switches and switchings with predefined behavior, such as a security switch that opens when a voltage (state) reaches a certain level, for instance. Third, the stability analysis of systems with overlapping regions. Concerning

this last idea, it may be possible to force a dwell time or hysteresis between switches in a previously designed switching rule, which would result in a system with overlapping regions, then analyze its stability.

7 CONCLUSIONS AND PROSPECTS

7.1 General concluding remarks

This thesis presented the main aspects involved in the analysis and development of control techniques for switched systems with application in photovoltaic power generation, although all the methods were presented in a manner that is general enough to be applied in systems other than PV. The objectives, the applications that are being studied, the requirements of the proposed control techniques and the resulting contributions were specified.

For a better understanding of the aspects surrounding the topic under investigation in this work, Chapter 2 presented a survey of the main features and properties of photovoltaic systems. The research topics presented in this chapter provide an overview of the topologies and techniques for control and achievement of the maximization of the power generated that exist in the current literature. Additionally, we presented the basic results that are necessary for the development of control techniques for this type of system, the main control objectives, as well as all the basic tools that would be used throughout the document. Therefore, this chapter contains the theoretical background necessary for the subsequent chapters.

Next, a new methodology for controlling switched systems, published in (TROFINO et al., 2011), was presented in Chapter 3. This methodology allows for the design of a switching rule with guaranteed asymptotic convergence of the states of the system to a desired equilibrium point, ensuring stability of the system even under the occurrence of sliding modes. The use of this new technique has been illustrated in two examples of control design, one applied to a Buck-Boost converter and the other applied to a system with three modes of operation. The simulation results demonstrated the possibility of including requirements for robustness to parameter variation and uncertain equilibrium points. A requirement for the application of the technique is that the system must have a stable convex combination in the equilibrium.

One of the main contributions of this thesis was presented in Chapter 4, also published in (DEZUO; TROFINO; SCHARLAU, 2014). This chapter presented a switching rule design technique for a class of nonlinear systems. To summarize, the results from the preceding chapter were extended to include sector-bounded nonlinearities and the applicability of the new method was illustrated through some numerical examples. The new design procedure has shown to have special importance for the design of a switching rule for PV systems, as the panel can be modeled as a sector-bounded current source. An-

other important requirement for PV systems achieved in this chapter was the possibility of designing the control without knowing *a priori* the value of the constant reference, allowing it to undergo step variations.

In Chapter 5, the study was directed to the application of the new design methodologies for the control of photovoltaic generation systems. Two cases were studied, each one representing a common topology of photovoltaic systems. The first case is the stand-alone connection containing a static DC/DC converter (of the Boost type), and in the second case a DC/AC converter (of the VSI type) was included for connection of the PV array to the three-phase grid. For this application, the main control objectives were assumed to be the maximization of the power generated by the PV array through the use of an MPPT technique and the delivery of only active power to the grid, that is, obtaining unitary power factor via synchronization with the grid. Due to an electrical decoupling present between the two converter stages, the design of the switching rules for the Boost and for the inverter could be carried out separately and with the previously specified goals respectively divided between them. In the case of grid-connection, the system contains a time-dependent external signal, which makes it challenging for obtaining LMI conditions, thus the design for this case was left as a future work.

The technique designed for the stand-alone case proved to be robust with respect to the value of the current generated by the PV array, which is a nonlinear variable that is difficult to treat and would require a great effort to representation via LMIs. The feasibility of the problem has been verified and the results obtained were tested in simulation. Through these tests, it was possible to verify that the results were satisfactory and objectives were met, even under variation of the input parameters of the panel (temperature and solar radiation). The applicability of the technique in real systems depends only on the inclusion of conditions to guarantee stability under limitation of the switching frequency, which are currently under development. Although, simulation results show that imposing a dwell time for the current techniques may not be an issue for stability if the dwell time is small enough. Other works to be performed in the future are: the development of an MPPT technique that can be included in the switching rule design method via LMIs, the control of switched systems without stable convex combination and battery charging, as well as improving the results already obtained.

Inspired by the lack of a method for stability analysis of piecewise affine systems with sliding modes, a novel methodology was proposed in Chapter 6. The new results were particularly interesting for allowing the sta-

bility analysis of the switching rule designed for affine switched systems in the third chapter, however, it may also be applied for the class of piecewise affine systems. The contents of this chapter were also published in (DEZUO; RODRIGUES; TROFINO, 2014). The technique can be used to check the stability of piecewise affine systems with hyperplanes as switching surfaces. Therefore, a relevant improvement to be made is to treat the case of switching surfaces expressed as polynomial functions of higher degree.

7.2 Prospects

As prospects for continuation of the work, the following activities are proposed:

1. To conduct a study to improve the results already obtained. In this direction, it is possible to include performance guarantees, to consider uncertainties in different parameters of the system, among other actions;
2. To investigate the development of an MPPT technique to be implemented in the switching rule design via LMIs, thus eliminating the dependence on other MPPT techniques from the literature;
3. To consider the application of charging batteries using the PV system;
4. To develop a switching rule design technique for DC/AC converters, allowing the connection to the grid;
5. To include conditions for limited switching frequency, thus avoiding the occurrence of chattering and ensuring stability in the experimental implementation of the control methodologies proposed;
6. To perform the extension of the obtained results for the case of control of switched systems without a stable convex combination of its subsystems;
7. To publish the results yet unpublished in relevant international journals and conferences.

7.3 Activities abroad

An internship abroad with duration of twelve months was carried out as part of the activities planned for the Ph.D. program. The activities were

conducted at the Department of Electrical & Computer Engineering at Concordia University in Montreal, Canada, in collaboration with the faculty members of this department and under the guidance of Professor Luis Rodrigues. Professor Rodrigues has done work with significant contributions in the area of control systems of high complexity (switched, hybrid and nonlinear control systems), optimal control and convex optimization methods applied the control using LMIs as a tool (SAMADI; RODRIGUES, 2011), (SAMADI; RODRIGUES, 2008), (RODRIGUES, 2003), and also having experience with variable structure systems and discrete-time dynamics (RODRIGUES, 2007). Among the results generated by the cooperation, we can cite the stability analysis technique presented in Chapter 6 as an important contribution for this thesis.

7.4 Publications related to the work

The activities performed during the Ph.D. program led to results that gave rise to the following papers already published (see Appendix D for the abstract of each paper):

- A. Trofino, C. C. Scharlau, T. J. M. Dezuo, M. C. de Oliveira. **“Stabilizing switching rule design for affine switched systems”**. *Proceedings of 50th IEEE Conference on Decision and Control*, 2011.
- A. Trofino, C. C. Scharlau, T. J. M. Dezuo, M. C. de Oliveira. **“Switching rule design for affine switched systems with \mathcal{H}_∞ performance”**. *Proceedings of 51th IEEE Conference on Decision and Control*, 2012.
- C. C. Scharlau, T. J. M. Dezuo, A. Trofino, R. Reginatto. **“Switching rule design for inverter-fed induction motors”**. *Proceedings of 52nd IEEE Conference on Decision and Control*, 2013.
- C. C. Scharlau, M. C. de Oliveira, A. Trofino, T. J. M. Dezuo. **“Switching rule design for affine switched systems using a max-type composition rule”**. *Systems & Control Letters*, 2014.
- T. Dezuo, L. Rodrigues, A. Trofino. **“Stability analysis of piecewise affine systems with sliding modes”**. *Proceedings of 2014 American Control Conference*, 2014.
- T. Dezuo, A. Trofino, C. C. Scharlau. **“Switching rule design for sector-bounded nonlinear switched systems”**. *Proceedings of 19th*

International Federation of Automatic Control (IFAC) World Congress, 2014.

The author also worked on the development of other papers not directly related to the content of this thesis, but to the stability analysis and observer design for nonlinear systems (vide abstracts in Appendix D), which are:

- A. Trofino, T. J. M. Dezuo. “**Global stability of uncertain rational nonlinear systems with some positive states**”. *Proceedings of 50th IEEE Conference on Decision and Control*, 2011.
- A. Trofino, T. J. M. Dezuo. “**LMI stability conditions for uncertain rational nonlinear systems**”. *International Journal of Robust and Nonlinear Control*, 2013. DOI: 10.1002/rnc.3047, pages 1-46.
- T. Dezuo, A. Trofino. “**LMI conditions for designing rational nonlinear observers**”. *Proceedings of 2014 American Control Conference*, 2014.
- T. Dezuo, A. Trofino. “**LMI conditions for designing rational nonlinear observers with guaranteed cost**”. *Proceedings of 19th International Federation of Automatic Control (IFAC) World Congress*, 2014.

REFERENCES

- ANEEL. *Atlas de Energia Elétrica do Brasil*. 2. ed. Brasília, Brazil: Agência Nacional de Energia Elétrica (ANEEL), 2005.
- ARIYUR, K. B.; KRSTIC, M. Multivariable extremum seeking feedback: analysis and design. In: *15th International Symposium on Mathematical Theory of Networks and Systems*. Notre Dame, USA, 2000. p. 12–19.
- ARMSTRONG, S.; HURLEY, W. G. Self-regulating maximum power point tracking for solar energy systems. In: *39th International Universities Power Engineering Conference*. Bristol, United Kingdom, 2004. v. 2, p. 604–609.
- ASSMANN, D. *Estratégias de comutação para controle de sistemas de estrutura variável*. Thesis (Master) — Federal University of Santa Catarina, Florianópolis, Brazil, 2008.
- ATTIVISSIMO, F.; DI NISIO, A.; SAVINO, M.; SPADAVECCHIA, M. Uncertainty analysis in photovoltaic cell parameter estimation. *IEEE Transactions on Instrumentation and Measurement*, v. 61, n. 5, p. 1334–1342, May 2012.
- BALAGUER, I. J.; KIM, H.; PENG, F. Z.; ORTIZ, E. I. Survey of photovoltaic power systems islanding detection methods. In: *34th Annual Conference of IEEE Industrial Electronics*. Orlando, USA, 2008. p. 2247–2252.
- BARBI, I. *Teoria Fundamental do Motor de Indução*. Florianópolis, Brazil: Editora da UFSC, 1985.
- BARBI, I. *Eletrônica de Potência*. 5. ed. Florianópolis, Brazil: Editora da UFSC, 2006.
- BARBI, I.; MARTINS, D. C. *Conversores CC-CC Básicos Não Isolados*. Florianópolis, Brazil: Author's Edition, 2008.
- BEN-BRAHIM, L. On the compensation of dead time and zero-current crossing for a PWM-inverter-controlled AC servo drive. *IEEE Transactions on Industrial Electronics*, v. 51, n. 5, p. 1113–1118, October 2004.

- BENAVIDES, C. M. *Analysis and control of a single-phase single-stage grid-connected photovoltaic inverter*. Thesis (Ph.D.) — Universitat Politècnica de Catalunya, Barcelona, Spain, 2007.
- BLAABJERG, F.; IOV, F.; TEREKES, T.; TEODORESCU, R.; MA, K. Power electronics - key technology for renewable energy systems. In: *2nd Power Electronics, Drive Systems and Technologies Conference*. Tehran, Iran, 2011. p. 445–466.
- BOLZERN, P.; SPINELLI, W. Quadratic stabilization of a switched affine system about a nonequilibrium point. In: *Proceedings of the 2004 American Control Conference*. Boston, USA, 2004. p. 3890–3895.
- BOSE, B. K. (Ed.). *Power Electronics and Variable Frequency Drives: Technology and Applications*. Michigan, USA: Wiley-IEEE Press, 1996.
- BOSE, B. K. *Modern Power Electronics and AC Drives*. Upper Saddle River, USA: Prentice-Hall, 2002.
- BOYD, S.; EL GHAOU, L.; FERON, E.; BALAKRISHNAN, V. *Linear Matrix Inequalities in System and Control Theory*. Philadelphia, USA: SIAM, 1994.
- BRANICKY, M. S. Multiple Lyapunov functions and other analysis tools for switched and hybrid systems. *IEEE Transactions on Automatic Control*, v. 43, n. 4, p. 475–482, April 1998.
- BUSQUETS-MONGE, S.; ROCABERT, J.; RODRÍGUES, P.; ALEPUZ, S.; BORDONAU, J. Multilevel diode-clamped converter for photovoltaic generators with independent voltage control of each solar array. *IEEE Transactions on Industrial Electronics*, v. 55, n. 7, p. 2713–2723, July 2008.
- CARDIM, R.; TEIXEIRA, M. C. M.; ASSUNÇÃO, E.; COVACIC, M. R. Variable structure control design of switched systems with an application to a DC-DC power converter. *IEEE Transactions on Industrial Electronics*, v. 56, n. 9, p. 3505–3513, September 2009.
- CASARO, M. M. *Inversor trifásico de dois estágios modificado aplicado no processamento da energia solar fotovoltaica em sistemas conectados à rede elétrica*. Thesis (Ph.D.) — Federal University of Santa Catarina, Florianópolis, Brazil, 2009.

- CHEN, L.; PENG, F. Z. Elimination of dead-time in PWM controlled inverters. In: *Proceedings of the 22nd Annual IEEE Applied Power Electronics Conference (APEC)*. Anaheim, USA, 2007. p. 306–309.
- CHEN, Y.; CHEN, K. Prediction maximum power point tracking method for PV-battery micro-satellite systems with body mounted solar panels. In: *International Power Electronics Conference*. Sapporo, Japan, 2010. p. 2585–2590.
- CHIU, C.; OUYANG, Y. Robust maximum power tracking control of uncertain photovoltaic systems: a unified T-S fuzzy model-based approach. *IEEE Transactions on Control Systems Technology*, v. 19, n. 6, p. 1516–1526, November 2011.
- CIOBOTARU, M.; TEODORESCU, R.; BLAAJBERG, F. Control of single-stage single-phase PV inverter. In: *European Conference on Power Electronics Application*. Dresden, Germany, 2005.
- COELHO, R. F.; CONGER, F.; MARTINS, D. C. A study of the basic DC-DC converters applied in maximum power point tracking. In: *Brazilian Power Electronics Conference*. Bonito, Brazil, 2009. p. 673–678.
- COLANERI, P.; GEROMEL, J. C.; ASTOLFI, A. Stabilization of continuous-time nonlinear switched systems. In: *IEEE Conference on Decision and Control and European Control Conference (CDC-ECC)*. Seville, Spain, 2005. p. 3309–3314.
- COUTINHO, M. S. *Projeto via LMI de sistemas de controle comutado para um motor de indução*. Thesis (Master) — Federal University of Santa Catarina, Florianópolis, Brazil, 2006.
- DA SILVA, N. A. V. M. *Controlo das potências activa e reactiva fornecidas à rede eléctrica por conversores CC/CA fontes de tensão*. Thesis (Master) — University of Porto, Porto, Portugal, 2004.
- DASGUPTA, S.; MOHAN, S. N.; SAHOO, S. K.; PANDA, S. K. A Lyapunov function based current controller to control active and reactive power flow in a three phase grid connected PV inverter under generalized grid voltage conditions. In: *8th IEEE International Conference on Power Electronics and ECCE Asia (ICPE & ECCE)*. Jeju, South Korea, 2011. p. 1110–1117.

- DE BRITO, M. A. G.; LUIGI, G.; SAMPAIO, L. P.; CANESIN, C. A. Avaliação das principais técnicas para obtenção de MPPT de painéis fotovoltaicos. In: *9th IEEE/IAS International Conference on Industry Applications (INDUSCON)*. São Paulo, Brazil, 2010. p. 1–6.
- DE OLIVEIRA, M. C.; SKELTON, R. E. Stability tests for constrained linear systems. In: MOHEIMANI, S. O. R. (Ed.). *Perspectives in Robust Control Design*. London, United Kingdom: Springer-Verlag, 2001, (Lecture Notes in Control and Information Sciences, v. 268). p. 241–257.
- DE PERSIS, C.; DE SANTIS, R.; MORSE, A. S. Switched nonlinear systems with state-dependent dwell-time. *System & Control Letters*, v. 50, n. 4, p. 291–302, November 2003.
- DE SOUZA, K. C. A. *Estudo e otimização de conversores estáticos utilizados em sistemas fotovoltaicos conectados à rede elétrica comercial*. Thesis (Ph.D.) — Federal University of Santa Catarina, Florianópolis, Brazil, 2009.
- DEAECTO, G. S.; GEROMEL, J. C.; GARCIA, F. S.; POMILIO, J. A. Switched affine systems control design with application to DC-DC converters. *IET Control Theory & Applications*, v. 4, n. 7, p. 1201–1210, July 2010.
- DECARLO, R. A.; BRANICKY, M. S.; PETTERSSON, S.; LENNARTSON, B. Perspectives and results on the stability and stabilizability of hybrid systems. *Proceedings of the IEEE*, v. 88, n. 7, p. 1069–1082, 2000.
- DECARLO, R. A.; ZAK, S. H.; MATTHEWS, G. P. Variable structure control of nonlinear multivariable systems: a tutorial. *Proceedings of the IEEE*, v. 76, n. 3, p. 212–232, March 1988.
- DEMASSA, T. A. The prediction of tunnel diode voltage-current characteristics. *Solid-State Electronics*, v. 13, n. 2, p. 131–138, February 1970.
- DEZUO, T. J. M. *Estabilidade de sistemas não lineares e controle de sistemas chaveados*. Thesis (Master) — Federal University of Santa Catarina, Florianópolis, Brazil, 2010.
- DEZUO, T. J. M.; RODRIGUES, L.; TROFINO, A. Stability analysis of piecewise affine systems with sliding modes. In: *Proceedings of the*

- 2014 American Control Conference. Portland, USA, 2014. p. 2005–2010.
- DEZUO, T. J. M.; TROFINO, A. LMI conditions for designing rational nonlinear observers. In: *Proceedings of the 2014 American Control Conference*. Portland, USA, 2014. p. 5343–5348.
- DEZUO, T. J. M.; TROFINO, A. LMI conditions for designing rational nonlinear observers with guaranteed cost. In: *Proceedings of 19th International Federation of Automatic Control (IFAC) World Congress*. Cape Town, South Africa, 2014. p. 67–72.
- DEZUO, T. J. M.; TROFINO, A.; SCHARLAU, C. C. Switching rule design for sector-bounded nonlinear switched systems. In: *Proceedings of 19th International Federation of Automatic Control (IFAC) World Congress*. Cape Town, South Africa, 2014. p. 4074–4079.
- DIAKAKI, C.; PAPAGEORGIOU, M.; ABOUDOLAS, K. A multivariable regulator approach to traffic-responsive network-wide signal control. *Control Engineering Practice*, v. 10, n. 2, p. 183–195, 2002.
- DURGADEVI, A.; ARUSELVI, S.; NATARAJAN, S. P. Photovoltaic modeling and its characteristics. In: *International Conference on Emerging Trends in Electrical and Computer Technology*. Tamil Nadu, India, 2011. p. 469–475.
- EGIZIANO, L.; FEMIA, N.; LISI, G.; PETRONE, G.; SPAGNUOLO, G.; VITELLI, M. Design and optimization of a maximum power point tracking controller for a PV battery charger. In: *IEEE International Symposium on Industrial Electronics*. Vigo, Spain, 2007. p. 2426–2431.
- EL-FARRA, N. H.; MHASKAR, P.; CHRISTOFIDES, P. D. Output feedback control of switched nonlinear systems using multiple Lyapunov functions. *Systems & Control Letters*, v. 54, n. 12, p. 1163–1182, 2005.
- ESRAM, T.; CHAPMAN, P. L. Comparison of photovoltaic array maximum power point tracking techniques. *IEEE Transactions on Energy Conversion*, v. 22, n. 2, p. 439–449, June 2007.
- EUROPEAN PHOTOVOLTAIC INDUSTRY ASSOCIATION (EPIA). *Global market outlook for photovoltaics 2013-2017*. Brussels, Belgium: , May 2013. Available in: <http://www.epia.org>.

- EUROPEAN PHOTOVOLTAIC INDUSTRY ASSOCIATION (EPIA). *Global market outlook for photovoltaics 2014-2018*. Brussels, Belgium: , June 2014. Available in: <http://www.epia.org>.
- EUROPEAN PHOTOVOLTAIC INDUSTRY ASSOCIATION (EPIA). *Market Report 2013*. Brussels, Belgium: , March 2014. Available in: <http://www.epia.org>.
- FERON, E. *Quadratic stabilizability of switched systems via state and output feedback*. Center for Intelligent Control Systems, MIT Publication CICS-P 468, 1996.
- FERREIRA, S. B. *Estudo e avaliação do desempenho de estratégias de controle direto do torque em máquinas de indução*. Thesis (Master) — PUCRS, Porto Alegre, Brazil, 2004.
- FILIPPOV, A. F. *Differential Equations with Discontinuous Righthand Sides*. Dordrecht, Netherlands: Kluwer Academic Publishers, 1988.
- GOETZBERGER, A.; HOFFMANN, V. U. *Photovoltaic Solar Energy Generation*. Berlin, Germany: Springer, 2005.
- GULES, R.; PACHECO, J. P.; HEY, H. L.; IMHOFF, J. A maximum power point tracking system with parallel connection for PV stand-alone applications. *IEEE Transactions on Industrial Electronics*, v. 55, n. 7, p. 2674–2683, July 2008.
- HAEBERLIN, H. Evolution of inverters for grid-connected PV-systems from 1989 to 2000. In: *17th European Photovoltaic Solar Energy Conference*. Munich, Germany, 2001. p. 426–430.
- HESPANHA, J. P. Uniform stability of switched linear systems: extensions of LaSalle's invariance principle. *IEEE Transactions on Automatic Control*, v. 49, n. 4, p. 470–482, April 2004.
- HETEL, L.; DAAFOUZ, J.; IUNG, C. Equivalence between the Lyapunov-Krasovskii functionals approach for discrete delay systems and that of the stability conditions for switched systems. *Nonlinear Analysis: Hybrid Systems*, v. 2, n. 3, p. 697–705, 2008.
- HU, T.; MA, L.; LIN, Z. On several composite quadratic Lyapunov functions for switched systems. In: *Proceedings of the 45th IEEE Conference on Decision and Control*. San Diego, USA, 2006. p. 113–118.

- HU, T.; MA, L.; LIN, Z. Stabilization of switched systems via composite quadratic functions. *IEEE Transactions on Automatic Control*, v. 53, n. 11, p. 2571–2585, 2008.
- HUANG, Y.; PENG, F. Z.; WANG, J.; YOO, D. Survey of the power conditioning system for PV power generation. In: *37th IEEE Power Electronics Specialists Conference*. Jeju, South Korea, 2006. p. 1–6.
- HWANG, S.; KIM, J. Dead time compensation method for voltage-fed PWM inverter. *IEEE Transactions on Energy Conversion*, v. 25, n. 1, p. 1–10, March 2010.
- IEEE STANDARDS. *IEEE recommended practice for utility interface of photovoltaic (PV) systems*. New York, USA, January 2000.
- ITAIPU BINACIONAL. *VE project - technical chart*. 2013. http://www2.itaipu.gov.br/ve/english/ficha_tecnica.html. Accessed in: 11/18/2013.
- JAIN, S.; AGARWAL, V. A new algorithm for rapid tracking of approximate maximum power point photovoltaic systems. *IEEE Power Electronics Letters*, v. 2, n. 1, p. 16–19, 2004.
- JAMRI, M. S.; WEI, T. C. Modeling and control of a photovoltaic energy system using the state-space averaging technique. *American Journal of Applied Sciences*, v. 7, n. 5, p. 682–691, 2010.
- JOHANSSON, M. *Piecewise Linear Control Systems*. Berlin, Germany: Springer, 2003.
- KHALIL, H. K. *Nonlinear Systems*. 3. ed. Upper Saddle River: Prentice Hall, 2002.
- KJAER, S. B.; PEDERSEN, J. K.; BLAAJBERG, F. Power inverter topologies for photovoltaic modules - a review. In: *37th IAS Annual Meeting*. Pittsburgh, USA, 2002. v. 2, p. 782–788.
- KJAER, S. B.; PEDERSEN, J. K.; BLAAJBERG, F. A review of single-phase grid-connected inverters for photovoltaic modules. *IEEE Transactions on Industry Applications*, v. 41, n. 5, p. 1292–1306, September 2005.
- KUIAVA, R.; RAMOS, R. A.; POTA, H. R.; ALBERTO, L. F. C. Practical stability of switched systems without a common equilibria and

- governed by a time-dependent switching signal. *European Journal of Control*, v. 19, n. 3, p. 206–213, May 2013.
- KUMARI, J. S.; BABU, D. C. S.; BABU, A. K. Design and analysis of P&O and IP&O MPPT technique for photovoltaic system. *International Journal of Modern Engineering Research*, v. 2, n. 4, p. 2174–2180, July 2012.
- LASDON, L. S. *Optimization Theory for Large Systems*. New York, USA: Macmillan, 1970.
- LAUB, A. J. *Matrix Analysis for Scientists & Engineers*. Philadelphia, USA: SIAM, 2005.
- LI, Q.; WOLFS, P. A review of the single phase photovoltaic module integrated converter topologies with three different DC link configurations. *IEEE Transactions on Power Electronics*, v. 23, n. 3, p. 1320–1333, May 2008.
- LIBERZON, D. *Switching in Systems and Control*. Boston, USA: Birkhäuser, 2003.
- LIBERZON, D. Switched systems. In: *Handbook of Networked and Embedded Control Systems*. 1. ed. [S.l.]: Birkhäuser, 2005. p. 559–574.
- LIBERZON, D.; MORSE, A. S. Basic problems in stability and design of switched systems. *IEEE Control Systems Magazine*, v. 19, n. 5, p. 59–70, 1999.
- LIN, H.; ANTISAKLIS, P. J. A necessary and sufficient condition for robust asymptotic stabilizability of continuous-time uncertain switched linear systems. In: *Proceedings of the 43rd IEEE Conference on Decision and Control*. Paradise Islands, Bahamas, 2004. v. 4, p. 3690–3695.
- LIN, H.; ANTSAKLIS, P. J. Stability and stabilizability of switched linear systems: a short survey of recent results. In: *Proceedings of the IEEE International Symposium on Intelligent Control*. Limassol, Cyprus, 2005. p. 24–29.
- LIN, H.; ANTSAKLIS, P. J. Stability and stabilizability of switched linear systems: a survey of recent results. *IEEE Transactions on Automatic Control*, v. 54, n. 2, p. 308–322, February 2009.

- LÖFBERG, J. Yalmip: a toolbox for modeling and optimization in MATLAB. In: *International Symposium on Computer Aided Control Systems Design*. Taipei, Taiwan, 2004. p. 284–289. Yalmip home page <<http://control.ee.ethz.ch/~joloef/yalmip.php>>.
- LUQUE, A.; HEGEDUS, S. *Handbook of Photovoltaic Science and Engineering*. Chichester, England: John Wiley & Sons, 2003.
- MAINARDI JÚNIOR, E. I.; TEIXEIRA, M. C. M.; CARDIM, R.; MOREIRA, M. R.; ASSUNÇÃO, E.; YOSHIMURA, V. L. On the control of switched affine systems with application to DC-DC converters. In: *Frontiers in Advanced Control Systems*. [S.l.]: InTech, 2012. cap. 5, p. 101–116.
- MARANDI, D.; SOWMYA, T. N.; BABU, B. C. Comparative study between unipolar and bipolar switching scheme with LCL filter for single-phase grid connected inverter system. In: *Proceedings of the 2012 IEEE Students' Conference on Electrical, Electronics and Computer Science (SCEECS)*. Bhopal, India, 2012. p. 1–4.
- MARTINS, D. C.; BARBI, I. *Introdução ao Estudo dos Conversores CC-CA*. 2. ed. Florianópolis, Brazil: Instituto de Eletrônica de Potência (INEP), 2008.
- MHASKAR, P.; EL-FARRA, N. H.; CHRISTOFIDES, P. D. Predictive control of switched nonlinear systems with scheduled mode transitions. *IEEE Transactions on Automatic Control*, v. 50, n. 11, p. 1670–1680, 2005.
- MIGNONE, D.; FERRARI-TRECCATE, G.; MORARI, M. Stability and stabilization of piecewise affine and hybrid systems: an LMI approach. In: *Proceedings of the 39th IEEE Conference on Decision and Control*. Sydney, Australia, 2000. v. 1, p. 504–509.
- MOARREF, M.; RODRIGUES, L. On exponential stability of linear networked control systems. *International Journal of Robust and Nonlinear Control*, v. 24, n. 7, p. 1221–1240, May 2014.
- MOHAN, N.; UNDELAND, T. M.; ROBBINS, W. P. *Power Electronics: Converters, Applications and Design*. 3. ed. [S.l.]: John Wiley & Sons, 2003.

- MORSE, A. S. (Ed.). *Control Using Logic Based Switching*. London, England: Springer, 1997.
- NETO, L. P. S. *Caracterização de dielétricos para sistemas de armazenamento de alta energia e de geração de RF em aplicações aeroespaciais*. Thesis (Master) — Instituto Nacional de Pesquisas Espaciais (INPE), São José dos Campos, Brazil, 2012.
- NG, K. Tunnel diode. In: *Complete Guide to Semiconductor Devices*. 1. ed. [S.l.]: Wiley-IEEE Press, 2002. cap. 6, p. 57–63.
- NGE, C. L.; MIDTGARD, O. M.; NORUM, L. Power management of grid-connected photovoltaic inverter with storage battery. In: *IEEE Trondheim Powertech*. Trondheim, Norway, 2011. p. 1–6.
- PAPAGEORGIOU, M.; DIAKAKI, C.; DINOPOULOU, V.; KOTSIALOS, A.; WANG, Y. Review of road traffic control strategies. *Proceedings of the IEEE*, v. 91, n. 12, p. 2043–2067, 2003.
- PATEL, M. R. *Wind and Solar Power Systems*. Boca Raton, USA: CRC Press, 1999.
- PETER, P. K.; AGARWAL, V. Switched capacitor dc-dc converter based maximum power point tracking of a PV source for nano satellite application. In: *35th IEEE Photovoltaic Specialists Conference (PVSC)*. Honolulu, USA, 2010. p. 2604–2609.
- PETTERSSON, S. Synthesis of switched linear systems. In: *42nd IEEE Conference on Decision and Control*. Maui, USA, 2003. p. 5283–5288.
- PINTO, L. P. G.; TROFINO, A. State and parameter estimation based on switched observers - an LMI approach. In: *Proceedings of the 2014 American Control Conference*. Portland, USA, 2014. p. 3249–3254.
- RADWAN, H.; ABDELKAREM, E.; AHMED, M.; ORABI, M. The non ideality effect of optimizing the P&O MPPT algorithm for PV battery charger applications. In: *IEEE 33rd International Telecommunications Energy Conference*. Amsterdam, Netherlands, 2011. p. 1–8.
- RODRIGUES, L. Stability analysis using controlled invariant sets for piecewise-affine systems. In: *Proceedings of 4th International Conference on Control and Automation*. Montreal, Canada, 2003. p. 198–202.

- RODRIGUES, L. Stability of sampled-data piecewise-affine systems under state feedback. *Automatica*, v. 43, n. 7, p. 1249–1256, 2007.
- SAMADI, B.; RODRIGUES, L. Extension of local linear controllers to global piecewise affine controllers for uncertain non-linear systems. *International Journal of Systems Science*, v. 39, n. 9, p. 867–879, September 2008.
- SAMADI, B.; RODRIGUES, L. A unified dissipativity approach for stability analysis of piecewise smooth systems. *Automatica*, v. 47, n. 12, p. 2735–2742, 2011.
- SANDEEP, N.; MURTHY, M. K.; KULKAMI, P. S. Single-phase grid-connected photovoltaic system based on ripple correlation control maximum power point tracking. In: *Proceedings of the 2014 IEEE Students' Conference on Electrical, Electronics and Computer Science (SCEECS)*. Bhopal, India, 2014. p. 1–6.
- SCHARLAU, C. C. *Controle de Sistemas Chaveados e Aplicações*. Thesis (Ph.D.) — Federal University of Santa Catarina, Florianópolis, Brazil, 2013.
- SCHARLAU, C. C.; DE OLIVEIRA, M. C.; TROFINO, A.; DEZUO, T. J. M. Switching rule design for affine switched systems using a max-type composition rule. *Systems & Control Letters*, v. 68, p. 1–8, June 2014.
- SCHARLAU, C. C.; DEZUO, T. J. M.; TROFINO, A.; REGINATTO, R. Switching rule design for inverter-fed induction motors. In: *Proceedings of 52nd IEEE Conference on Decision and Control*. Firenze, Italy, 2013. p. 4662–4667.
- SHELLEKENS, J. M.; DUARTE, J. L.; HUISMAN, H.; HENDRIX, M. A. M. High-precision current control through opposed current converters. In: *Proceedings of the 14th European Conference on Power Electronics and Applications*. Birmingham, England, 2011. v. 1, p. 1–10.
- SCHIMPF, F.; NORUM, L. E. Grid connected converters for photovoltaic, state of the art, ideas for improvement of transformerless inverters. In: *Nordic Workshop on Power and Industrial Electronics*. Espoo, Finland, 2008. p. 1–6.

- SENGER, G. A.; TROFINO, A. Switching rule design for a class of switched systems with uncertain equilibrium. In: *Proceedings of 53rd IEEE Conference on Decision and Control*. Los Angeles, USA, 2014.
- SHIEH, H.; SHYU, K. Nonlinear sliding-mode torque control with adaptive backstepping approach for induction motor drive. *IEEE Transactions on Industrial Electronics*, v. 46, n. 2, p. 380–389, 1999.
- SHTESSEL, Y. B.; ZINOBER, A. S. I.; SHKOLNIKOV, I. A. Boost and buck-boost power converters control via sliding modes using method of stable system centre. In: *Proceedings of the 41st IEEE Conference Decision and Control*. Las Vegas, USA, 2002. v. 1, p. 340–345.
- SIRA-RAMÍREZ, H. Sliding mode- Δ modulation control of a “buck” converter. In: *Proceedings of the 42nd IEEE Conference Decision and Control*. Lahaina, USA, 2003. v. 3, p. 2999–3004.
- SKAFIDAS, E.; EVANS, R. J.; SAVKIN, A. V.; PETERSEN, I. R. Stability results for switched controller systems. *Automatica*, v. 35, n. 4, p. 553–564, 1999.
- STURM, J. F. Using SeDuMi 1.02, a Matlab[®] toolbox for optimization over symmetric cones. Tilburg, Netherlands, October 2001.
- SUN, Z. Combined stabilizing strategies for switched linear systems. *IEEE Transactions on Automatic Control*, v. 51, n. 4, p. 666–674, 2006.
- SUN, Z.; GE, S. S.; LEE, T. H. Controllability and reachability criteria for switched linear systems. *Automatica*, v. 38, n. 5, p. 775–786, 2002.
- SVENSSON, J. Synchronisation methods for grid-connected voltage source converters. *IEE Proceedings - Generation, Transmission and Distribution*, v. 148, n. 3, p. 229–235, May 2001.
- TAN, C. W.; GREEN, T. C.; HERNANDEZ-ARAMBURO, C. A. An improved maximum power point tracking algorithm with current-mode control for photovoltaic applications. In: *International Conference on Power Electronics and Drives Systems*. Kuala Lumpur, Malaysia, 2005. v. 1, p. 489–494.
- TASDIGHI, M.; SALAMATI, P. J.; RAHIMIKIAN, A.; GHASEMI, H. Energy management in a smart residential building. In: *11th International Conference on Environment and Electrical Engineering*. Venice, Italy, 2012. p. 128–133.

- TEODORESCU, R.; LISERRE, M.; RODRÍGUES, P. Photovoltaic inverter structures. In: *Grid Converters for Photovoltaic and Wind Power Systems*. 1. ed. [S.l.]: Wiley-IEEE Press, 2011. cap. 2, p. 5–29.
- TOH, K. C.; TODD, M. J.; TÛTÛNCÛ, R. H. SDPT3 - a MATLAB® package for semidefinite programming. *Technical Report, Cornell University*, Ithaca, USA, 1996.
- TORRES, M.; LOPES, L. Inverter-based diesel generator emulator for the study of frequency variations in a laboratory-scale autonomous power system. *Energy and Power Engineering*, v. 5, n. 3, p. 274–283, May 2013.
- TROFINO, A.; ASSMANN, D.; SCHARLAU, C. C.; COUTINHO, D. F. Switching rule design for switched dynamic systems with affine vector fields. *IEEE Transactions on Automatic Control*, v. 54, n. 9, p. 2215–2222, September 2009.
- TROFINO, A.; ASSMANN, D.; SCHARLAU, C. C.; COUTINHO, D. F. Switching rule design for switched dynamic systems with affine vector fields. In: *Proceedings of the IEEE Conference on Decision and Control*. Shanghai, China, 2009.
- TROFINO, A.; DEZUO, T. J. M. Global stability of uncertain rational nonlinear systems with some positive states. In: *50th IEEE Conference on Decision and Control and European Control Conference*. Orlando, USA, 2011. p. 7337–7342.
- TROFINO, A.; DEZUO, T. J. M. LMI stability conditions for uncertain rational nonlinear systems. *International Journal of Robust and Nonlinear Control, Published online in Wiley InterScience (www.interscience.wiley.com)*. DOI: 10.1002/rnc.3047, p. 1–46, April 2013.
- TROFINO, A.; REGINATTO, R.; DE OLIVEIRA, J.; SCHARLAU, C. C.; COUTINHO, D. F. A reference tracking strategy for affine switched systems. In: *IEEE International Conference on Control and Automation*. Christchurch, New Zealand, 2009. p. 1744–1750.
- TROFINO, A.; SCHARLAU, C. C.; COUTINHO, D. F. Corrections to “Switching rule design for switched dynamic systems with affine vector fields”. *IEEE Transactions on Automatic Control*, v. 57, n. 4, p. 1080–1082, April 2012.

- TROFINO, A.; SCHARLAU, C. C.; DEZUO, T. J. M.; DE OLIVEIRA, M. C. Stabilizing switching rule design for affine switched systems. In: *50th IEEE Conference on Decision and Control and European Control Conference*. Orlando, USA, 2011. p. 1183–1188.
- TROFINO, A.; SCHARLAU, C. C.; DEZUO, T. J. M.; DE OLIVEIRA, M. C. Switching rule design for affine switched systems with H_∞ performance. In: *51th IEEE Conference on Decision and Control*. Maui, USA, 2012. p. 1923–1928.
- UTKIN, U. I. *Sliding Modes in Control and Optimization*. Berlin, Germany: Springer-Verlag, 1992.
- VILLALVA, M. G.; GAZOLI, J. R.; FILHO, E. R. Modeling and circuit-based simulation of photovoltaic arrays. In: *Brazilian Power Electronics Conference*. Bonito, Brazil, 2009. p. 1244–1254.
- WALKER, D. K.; COAKLEY, K. J.; SPLETT, J. D. Nonlinear modeling of tunnel diode detectors. In: *Proceedings of the 2004 IEEE International Geoscience and Remote Sensing Symposium (IGARSS)*. Anchorage, USA, 2004. v. 6, p. 3969–3972.
- WANG, L.; LIN, T. Stability and performance of an autonomous hybrid wind-PV-battery system. In: *International Conference on Intelligent Systems Applications*. Toki Messe, Japan, 2007. p. 1–6.
- WILLMANN, G.; COUTINHO, D. F.; PEREIRA, L. F. A.; LIBANO, F. B. Multiple-loop H-infinity control design for uninterruptible power supplies. *IEEE Transactions on Industrial Electronics*, v. 54, n. 3, p. 1591–1602, June 2007.
- XU, S.; YANG, Y. Global robust $\mathcal{H}_2/\mathcal{H}_\infty$ synchronization for a class of dynamical networks. In: *Proceedings of the 2010 American Control Conference*. Baltimore, USA, 2010. p. 4480–4485.
- XU, X.; ZHAI, G.; HE, S. On practical asymptotic stabilizability of switched affine systems. *Nonlinear Analysis: Hybrid Systems*, v. 2, n. 1, p. 196–208, March 2008.
- YAN, W.; UTKIN, V.; XU, L. Sliding mode pulse width modulation. In: *Proceedings of the 2007 American Control Conference*. New York, USA, 2007. p. 4530–4535.

- YAZDANI, A.; DASH, P. P. A control methodology and characterization of dynamics for a photovoltaic (PV) system interfaced with a distribution network. *IEEE Transactions on Power Delivery*, v. 24, n. 3, p. 1538–1551, July 2009.
- YOSHIMURA, V. L.; ASSUNÇÃO, E.; DA SILVA, E. R. P.; TEIXEIRA, M. C. M.; MAINARDI JÚNIOR, E. I. Observer-based control design for switched affine systems and applications to DC-DC converters. *Journal of Control, Automation and Electrical Systems*, v. 24, n. 4, p. 535–543, August 2013.
- YOUNG, K. D. *Variable Structure Control for Robotics and Aerospace Applications*. New York, USA: Elsevier, 1993.
- YUAN, K. D.; ZHANG, Y. Status and opportunities of photovoltaic inverters in grid-tied and micro-grid systems. In: *5th International Power Electronics and Motion Control Conference*. Shanghai, China, 2006. p. 1–4.
- ZHENG, S.; WANG, L. Research on charging control for battery in photovoltaic system. In: *6th IEEE Conference on Industrial Electronics and Applications*. Beijing, China, 2011. p. 2321–2325.

APPENDIX A – INPUT/OUTPUT VOLTAGES RELATION IN A THREE-PHASE INVERTER

Consider the inverter shown in Figure 45, where the point o is a virtual point inserted just to simplify the analysis. The output of the inverter (points a, b, c) is connected to the point n in a star¹ configuration.

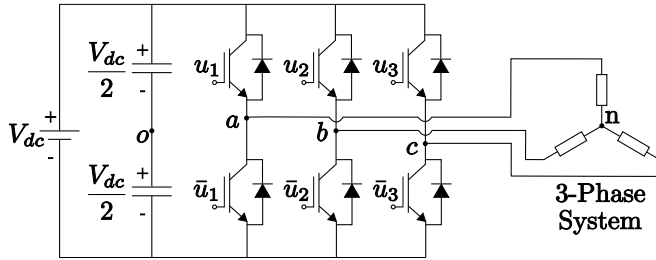


Figure 45: Three-phase inverter with output connected in a star configuration.

Recalling that the input command of the two switches of an arm of the inverter must be complementary, *i.e.* \bar{u}_i is the binary complement of u_i for $i = 1, 2, 3$, the following relations can be verified:

$$V_a - V_o = \frac{V_{dc}}{2} (u_1 - \bar{u}_1) = \frac{V_{dc}}{2} (2u_1 - 1) \quad (\text{A.1})$$

$$V_b - V_o = \frac{V_{dc}}{2} (u_2 - \bar{u}_2) = \frac{V_{dc}}{2} (2u_2 - 1) \quad (\text{A.2})$$

$$V_c - V_o = \frac{V_{dc}}{2} (u_3 - \bar{u}_3) = \frac{V_{dc}}{2} (2u_3 - 1) \quad (\text{A.3})$$

Summing $-V_n + V_n$ to the left of the equalities in (A.1-A.3), we get, respectively:

$$V_a - V_n + V_n - V_o = V_{an} + V_{no} = \frac{V_{dc}}{2} (2u_1 - 1) \quad (\text{A.4})$$

$$V_b - V_n + V_n - V_o = V_{bn} + V_{no} = \frac{V_{dc}}{2} (2u_2 - 1) \quad (\text{A.5})$$

$$V_c - V_n + V_n - V_o = V_{cn} + V_{no} = \frac{V_{dc}}{2} (2u_3 - 1) \quad (\text{A.6})$$

¹Also known as "Y" configuration.

Summing the three Equations (A.4)-(A.6) and taking into account that the system is balanced, *i.e.* $V_{an} + V_{bn} + V_{cn} = 0$, we get

$$3V_{no} = \frac{V_{dc}}{2}(2u_1 + 2u_2 + 2u_3 - 3) \quad (\text{A.7})$$

and isolating V_{no} :

$$V_{no} = \frac{1}{3} \left(u_1 + u_2 + u_3 - \frac{3}{2} \right) V_{dc} \quad (\text{A.8})$$

Finally, replacing (A.8) in (A.4)-(A.6) and isolating the variables V_{an}, V_{bn}, V_{cn} , we get

$$\begin{bmatrix} V_{an} \\ V_{bn} \\ V_{cn} \end{bmatrix} = V_{dc} \frac{1}{3} \begin{bmatrix} 2 & -1 & -1 \\ -1 & 2 & -1 \\ -1 & -1 & 2 \end{bmatrix} \begin{bmatrix} u_1 \\ u_2 \\ u_3 \end{bmatrix}. \quad (\text{A.9})$$

APPENDIX B – CLARKE'S TRANSFORMATION

Consider the reference frames abc and $\alpha\beta$ with the orientations indicated in Figure 46, from which we can deduce that the projections f_α and f_β of the vectors f_a, f_b, f_c are:

$$f_\alpha = 1f_a - \cos(60^\circ)f_b - \cos(60^\circ)f_c \quad (\text{B.1})$$

$$f_\beta = 0f_a + \sin(60^\circ)f_b - \sin(60^\circ)f_c \quad (\text{B.2})$$

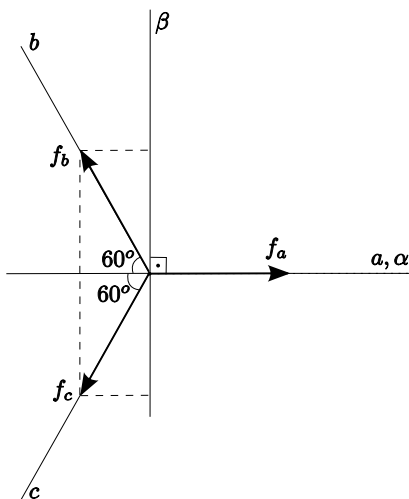


Figure 46: Transformation from abc to $\alpha\beta$.

Recalling that, if the system is balanced, $f_b + f_c = -f_a$, (B.1) can be rewritten as

$$f_\alpha = 1f_a + \cos(60^\circ)f_a = \frac{3}{2}f_a. \quad (\text{B.3})$$

Due to the relation (B.3), if it is of interest to keep f_α with the same amplitude

as f_α , (B.1)-(B.2) are multiplied by $2/3$, that is,

$$f_\alpha = \frac{2}{3} \left(1f_a - \frac{1}{2}f_b - \frac{1}{2}f_c \right), \quad (\text{B.4})$$

$$f_\beta = \frac{2}{3} \left(0f_a + \frac{\sqrt{3}}{2}f_b - \frac{\sqrt{3}}{2}f_c \right), \quad (\text{B.5})$$

which can be rewritten in a matrix form as

$$\begin{bmatrix} f_\alpha \\ f_\beta \end{bmatrix} = \frac{2}{3} \underbrace{\begin{bmatrix} 1 & -\frac{1}{2} & -\frac{1}{2} \\ 0 & \frac{\sqrt{3}}{2} & -\frac{\sqrt{3}}{2} \end{bmatrix}}_{K_{\alpha\beta}} \begin{bmatrix} f_a \\ f_b \\ f_c \end{bmatrix}. \quad (\text{B.6})$$

The inverse transformation can be obtained by calculating the pseudo-inverse of $K_{\alpha\beta}$, although it is deduced here step by step as a confirmation of the previously obtained transformation. Consider the Figure 47. In this case, the projections f_a, f_b, f_c of f_α, f_β in the abc axis are, respectively:

$$f_a = 1f_\alpha + 0f_\beta \quad (\text{B.7})$$

$$f_b = -\cos(60^\circ)f_\alpha + \cos(30^\circ)f_\beta \quad (\text{B.8})$$

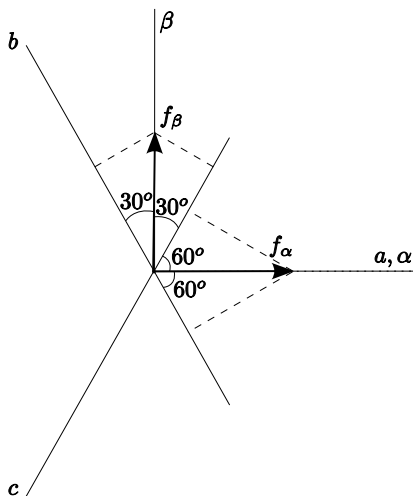
$$f_c = -\cos(60^\circ)f_\alpha - \cos(30^\circ)f_\beta \quad (\text{B.9})$$

Note in (B.7) that this deduction already results in f_a and f_α to have equal amplitudes.

Finally, rewriting (B.7-B.9) in a matrix form, we get

$$\begin{bmatrix} f_a \\ f_b \\ f_c \end{bmatrix} = \underbrace{\begin{bmatrix} 1 & 0 \\ -\frac{1}{2} & \frac{\sqrt{3}}{2} \\ -\frac{1}{2} & -\frac{\sqrt{3}}{2} \end{bmatrix}}_{K_{\alpha\beta}^\#} \begin{bmatrix} f_\alpha \\ f_\beta \end{bmatrix}. \quad (\text{B.10})$$

It is possible to verify that $K_{\alpha\beta}^\#$ is the pseudo-inverse of $K_{\alpha\beta}$ from Equation (B.6), hence its nomenclature. Transformations between three-phase and two-phase variables with different Cartesian axis orientations and that consider the 0 component can be found in (BARBI, 1985) and (FERREIRA, 2004), for instance. Also, note in the Figure 46 that the transformation described here

Figure 47: Transformation from $\alpha\beta$ to abc .

has the β axis in advance in relation to the α axis (BARBI, 1985).

APPENDIX C – PARK'S TRANSFORMATION

Consider the reference frames $\alpha\beta$ and dq (synchronous) as shown in the Figure 48, where the reference frame dq is synchronized with the grid and, therefore, it rotates with the constant angular velocity ω , and thus

$$\phi = \int \omega dt = \omega t. \quad (\text{C.1})$$

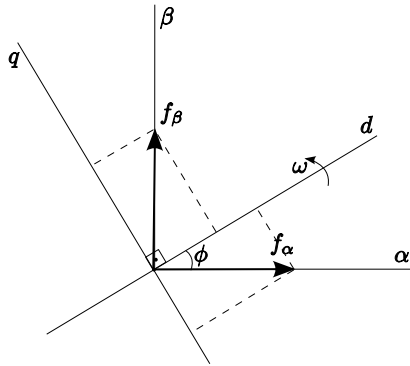


Figure 48: Transformation from $\alpha\beta$ to dq .

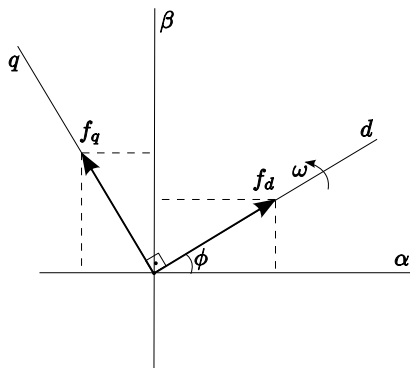


Figure 49: Transformation from dq to $\alpha\beta$.

Observing the Figure 48, we can infer that

$$\begin{bmatrix} f_d \\ f_q \end{bmatrix} = \underbrace{\begin{bmatrix} \cos(\phi) & \sin(\phi) \\ -\sin(\phi) & \cos(\phi) \end{bmatrix}}_{K_{dq}} \begin{bmatrix} f_\alpha \\ f_\beta \end{bmatrix}. \quad (\text{C.2})$$

The deduction of the inverse transformation can be obtained simply by calculating the inverse of the matrix K_{dq} , or as shown in the sequence to confirm the previously obtained transformation. Consider the Figure 49, from which we get the following relations.

$$\begin{bmatrix} f_\alpha \\ f_\beta \end{bmatrix} = \underbrace{\begin{bmatrix} \cos(\phi) & -\sin(\phi) \\ \sin(\phi) & \cos(\phi) \end{bmatrix}}_{K_{dq}^{-1}} \begin{bmatrix} f_d \\ f_q \end{bmatrix}. \quad (\text{C.3})$$

It is possible to verify that K_{dq}^{-1} is the inverse of K_{dq} , hence its nomenclature.

APPENDIX D – ABSTRACTS OF PUBLISHED PAPERS

In this appendix, the abstracts of each publication mentioned in Section 7.4 are presented.

- A. Trofino, C. C. Scharlau, T. J. M. Dezuo, M. C. de Oliveira. **“Stabilizing switching rule design for affine switched systems”**. *Proceedings of 50th IEEE Conference on Decision and Control*, 2011.

We propose a method for designing switching rules that can drive the state of the switched dynamic system to a desired equilibrium point. The method deals with the class of switched systems where each subsystem has an affine vector field. The results are given in terms of linear matrix inequalities and they guarantee global asymptotic stability of the tracking error dynamics even if sliding motion occurs along a switching surface of the system. The switching rules are based on complete and partial state measurements. Two examples are used to illustrate the approach.

- A. Trofino, C. C. Scharlau, T. J. M. Dezuo, M. C. de Oliveira. **“Switching rule design for affine switched systems with \mathcal{H}_∞ performance”**. *Proceedings of 51th IEEE Conference on Decision and Control*, 2012.

In this paper we consider the class of affine switched systems subject to \mathcal{L}_2 disturbances and we propose a method for switching rule design such that an upper bound on the disturbance gain, in the \mathcal{H}_∞ sense, is minimized. In the absence of disturbances the switching rule drives the state of the switched system to a desired equilibrium point. The results are given in terms of linear matrix inequalities and they guarantee global asymptotic stability of the tracking error dynamics even if sliding motion occurs on any switching surface of the system. An example is used to illustrate the approach.

- C. C. Scharlau, T. J. M. Dezuo, A. Trofino, R. Reginatto. **“Switching rule design for inverter-fed induction motors”**. *Proceedings of 52nd IEEE Conference on Decision and Control*, 2013.

This paper presents a method for designing switching rules that drive the state of a class of nonlinear switched system to a desired constant reference. The proposed method is focused on an application of a three-phase squirrel-cage induction motor fed by an inverter and considers a

switching rule using ‘max’ composition of auxiliary functions. The results are given in terms of linear matrix inequalities and they guarantee local asymptotic stability of the closed-loop system even if sliding modes occur on any switching surface of the system.

- C. C. Scharlau, M. C. de Oliveira, A. Trofino, T. J. M. Dezuo. “**Switching rule design for affine switched systems using a max-type composition rule**”. *Systems & Control Letters*, 2014.

This paper presents conditions for designing a switching rule that drives the state of the switched dynamic system to a desired equilibrium point. The proposed method deals with the class of switched systems where each subsystem has an affine vector field and considers a switching rule using ‘max’ composition. The results guarantee global asymptotic stability of the tracking error dynamics even if sliding mode occur at any switching surface of the system. In addition, the method does not require a Hurwitz convex combination of the dynamic matrices of the subsystems. Two numerical examples are used to illustrate the results.

- T. Dezuo, L. Rodrigues, A. Trofino. “**Stability analysis of piecewise affine systems with sliding modes**”. *Proceedings of 2014 American Control Conference*, 2014.

This paper proposes new sufficient conditions for stability analysis of PWA systems. The conditions are based on a convex combination of PWQ Lyapunov functions and are given in terms of LMIs, which can be solved efficiently using available software packages. There are three contributions of the new conditions presented in this paper. First, the conditions guarantee exponential stability of the state dynamics even in the presence of non-destabilizing sliding modes of all possible dimensions smaller than the dimension of the state space. Second, the conditions can handle the important case where the equilibrium point is located at a boundary between affine subsystems. Third, sufficient conditions for stability of systems independently of the parametrization of the boundary surfaces are derived as a corollary. The new method presented in this paper leads to a unified methodology for stability analysis of switched affine systems and piecewise affine systems with sliding modes.

- T. Dezuo, A. Trofino, C. C. Scharlau. “**Switching rule design for sector-bounded nonlinear switched systems**”. *Proceedings of 19th*

International Federation of Automatic Control (IFAC) World Congress, 2014.

This paper presents a technique for designing switching rules that drive the state of a class of nonlinear switched system to a desired constant reference. The system may contain state-dependent sector-bounded nonlinear functions. The proposed method considers a switching rule using the ‘max’ composition of auxiliary functions. The results are given in terms of LMIs and they guarantee global asymptotic stability of the closed-loop system even if sliding modes occur on any switching surface of the system. The application of the method is illustrated through a numerical example based on a PV system and important requirements are achieved, such as the MPPT and robustness with respect to the uncertain parameters of the PV array.

- A. Trofino, T. J. M. Dezuo. “**Global stability of uncertain rational nonlinear systems with some positive states**”. *Proceedings of 50th IEEE Conference on Decision and Control*, 2011.

This paper presents LMI conditions for local and global asymptotic stability of rational uncertain nonlinear systems where some or all the state variables are constrained by the model to have definite signal. The uncertainties are modeled as real time varying parameters with magnitude and rate of variation bounded by given polytopes. The stability conditions are based on a rational Lyapunov function with respect to the states and uncertain parameters. A numerical example is used to illustrate the potential of the proposed results.

- A. Trofino, T. J. M. Dezuo. “**LMI stability conditions for uncertain rational nonlinear systems**”. *International Journal of Robust and Nonlinear Control*, 2013. DOI: 10.1002/rnc.3047, pages 1-46.

This paper presents LMI conditions for local, regional and global robust asymptotic stability of rational uncertain nonlinear systems. The uncertainties are modeled as real time varying parameters with magnitude and rate of variation bounded by given polytopes and the system vector field is a rational function of the states and uncertain parameters. Sufficient LMI conditions for asymptotic stability of the origin are given through a rational Lyapunov function of the states and uncertain parameters. The case where the time derivative of the Lyapunov function is negative semi-definite is also considered and connections with the well known LaSalle’s invariance conditions are established. In

regional stability problems an algorithm to maximize the estimate of the region of attraction is proposed. The algorithm consists of maximizing the estimate for a given target region of initial states. The size and shape of the target region are recursively modified in the directions where the estimate can be enlarged. The target region can be taken as a polytope (convex set) or union of polytopes (non-convex set). The estimates of the region of attraction are robust with respect to the uncertain parameters and their rate of change. The case of global and orthant stability problems are also considered. Connections with some results found in SOS based methods and other related methods found in the literature are established. The LMIs in this paper are obtained by using the Finsler's Lemma and the notion of annihilators. The LMIs are characterized by affine functions of the state and uncertain parameters and they are tested at the vertices of a polytopic region. It is also shown that, with some additional conservatism, the use of the vertices can be avoided by modifying the LMIs with the *S*-Procedure. Several numerical examples found in the literature are used to compare the results and illustrate the advantages of the proposed method.

- T. Dezuo, A. Trofino. “**LMI conditions for designing rational nonlinear observers**”. *Proceedings of 2014 American Control Conference*, 2014.

This paper presents a technique for designing rational nonlinear observers for rational nonlinear systems. The approach is based on a Lyapunov function that is quadratic in the estimation error and rational in the system states. The design conditions are formulated as LMIs. If the conditions are satisfied, then the estimation error is guaranteed to asymptotically converge to zero for initial conditions on an estimated region of attraction. An optimization procedure for enlarging the region of attraction is also provided. An example is used to illustrate the results.

- T. Dezuo, A. Trofino. “**LMI conditions for designing rational nonlinear observers with guaranteed cost**”. *Proceedings of 19th International Federation of Automatic Control (IFAC) World Congress*, 2014.

This paper presents a technique for designing rational nonlinear observers for rational nonlinear systems with guaranteed cost performance. The approach is based on a Lyapunov function that is quadratic in the estimation error and rational in the system states. The design

conditions are formulated as LMIs. If the conditions are satisfied, then the estimation error is guaranteed to asymptotically converge to zero for initial conditions on an estimated region of attraction. An optimization procedure for enlarging the region of attraction is also provided. An example is used to illustrate the results.